Fundamentals of Electric Machine Drives

Marko Hinkkanen, Lennart Harnefors, and Jarno Kukkola

March 11, 2024

Preface

These lecture notes are prepared for the course *ELEC-E8405 Electric Drives* lectured at the Aalto University, Espoo, Finland. The course is taught during the first autumn of a Master's program as the first course on electric machine drives. The prerequisites for the course are the basics of circuit theory and the basics of control engineering, in addition to fundamental university mathematics and physics. In addition to lectures, the course contains exercises and assignments, which are not included in these notes.

Marko Hinkkanen
Aalto University, Espoo, Finland

Lennart Harnefors
ABB Corporate Research, Västerås, Sweden / Aalto University

Jarno Kukkola
ABB Drives, Helsinki, Finland / Aalto University

Contents

Chapter 1

Introduction

This chapter gives a brief overview of the field of electric machine drives and power converters. A general introduction to electrical energy is first made.

1.1 Role of Electrical Energy

To mitigate the climate change, the use of fossil fuels (coal, oil, and natural gas) should be abandoned in the coming years. Figure 1.1(a) shows the total energy supply in Europe by primary energy source. The share of fossil fuels was about 70% in 2019. Electrical energy (electricity) is a secondary energy source, generated from primary energy sources. Figure 1.1(b) shows electricity generation in Europe by source. About 20% of the total energy was converted to electricity in 2019. The share of fossil fuels in electricity generation was about 40%. To meet the climate targets, power generation should be solely based on renewable sources (mainly wind, solar, and hydro) and nuclear power in the future.

Electrical energy has several advantages. First, it can be produced from carbon-free sources. Second, it can be efficiently transmitted and distributed. Third, it can be efficiently and flexibly converted to other useful forms of energy, such as motion, light, and heat. Due to these advantages, electrical energy has a key role in climate change mitigation. The target is to decarbonize power generation as well as to electrify all processes that now require fossil fuels. For example, transportation still depends to more than 90% on fossil fuels, but electrification is currently advancing fast. As another example, buildings can be efficiently heated using heat pumps. Many industrial processes currently relying on fossil fuels can also be electrified, a steel production process being one remarkable example. Due to this electrification trend, the consumption of electrical energy is expected to increase, even if the total energy consumption may level off and start to decrease in the future. These trends are also visible in Figure 1.1.

1.2 Electricity Generation

A vast majority of electrical energy is generated using rotating electric generators in thermal power stations, illustrated in Figure 1.2(a). Heat is typically
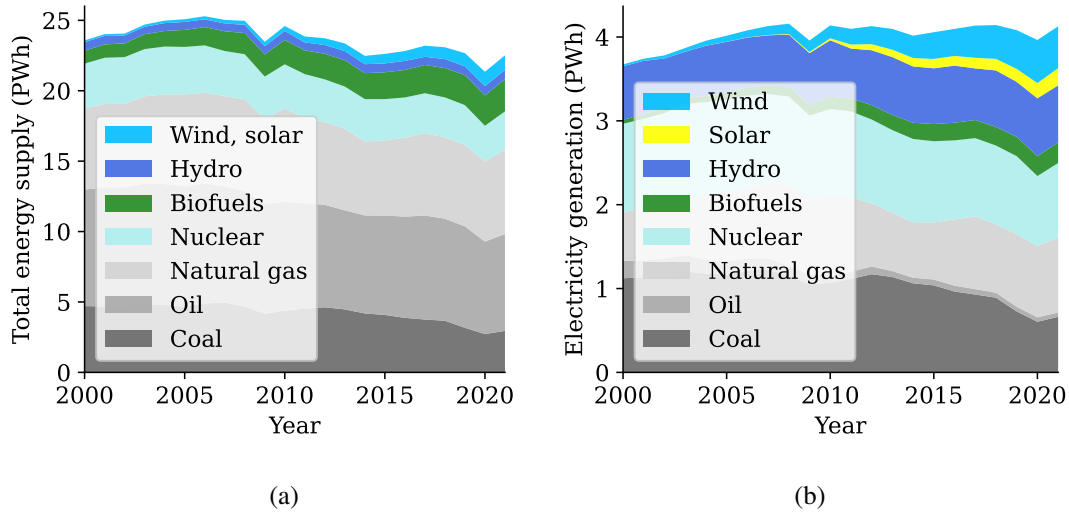
Figure 1.1: Energy statistics by source, Europe: (a) total energy supply; (b) electricity generation. Note that 1 PWh = 10^9 MWh and 1 Wh = 3 600 J. Data source: https://www.iea.org/data-and-statistics.

produced by fossil fuels, bio fuels or nuclear power. Solar thermal and geothermal power plants operate in a similar manner. Heat energy drives a steam turbine (or alternatively a gas turbine), which is connected to a synchronous generator. Since the generator is directly connected to the AC grid, its rotor has to rotate in synchronism with the grid and its other generators. The kinetic energy stored in the generator rotor acts as an energy buffer and thus contributes to the power balance of the grid together with other generators. Typical capacities of thermal power stations are hundreds of megawatts, in the case of nuclear power even above 1 000 MW.

Wind turbines also use rotating electric generators, see Figure 1.2(b). Since modern wind-turbine generators are connected to the AC grid through an AC-AC converter (frequency converter), their rotation speed can be individually optimized in real time according to the wind conditions. Large wind turbines rotate slowly, around 10–20 r/min. A fixed-ratio gearbox can be used, in which case the generator rotates at much higher speed. The gear ratios around 100 are typical. Direct-driven wind turbines without gearbox are also used. Their advantage is a simpler mechanical transmission, but, on the other hand, the physical size of the generator becomes larger. Large wind turbines have rated powers in the range of 2–10 MW. Large wind farms may contain tens of turbines.

Figure 1.2(c) illustrates a solar photovoltaic (PV) plant. Solar panels consist of PV cells that generate DC electricity directly without intermediate mechanical motion. To increase the generated voltage, the panels can be connected in series as strings. To increase the output current, such strings can be further connected in parallel, resulting in a solar array. One or more arrays can be connected to a DC-AC converter (inverter), which converts the generated DC voltage to the three-phase AC grid voltage. To maximize the energy yield, the inverter adjusts the DC voltage in real time in order to track the maximum power point according to the varying solar irradiation conditions. Utility-scale solar PV plants can be based on central inverters whose rated power is typically in the range of 1–5 MW.
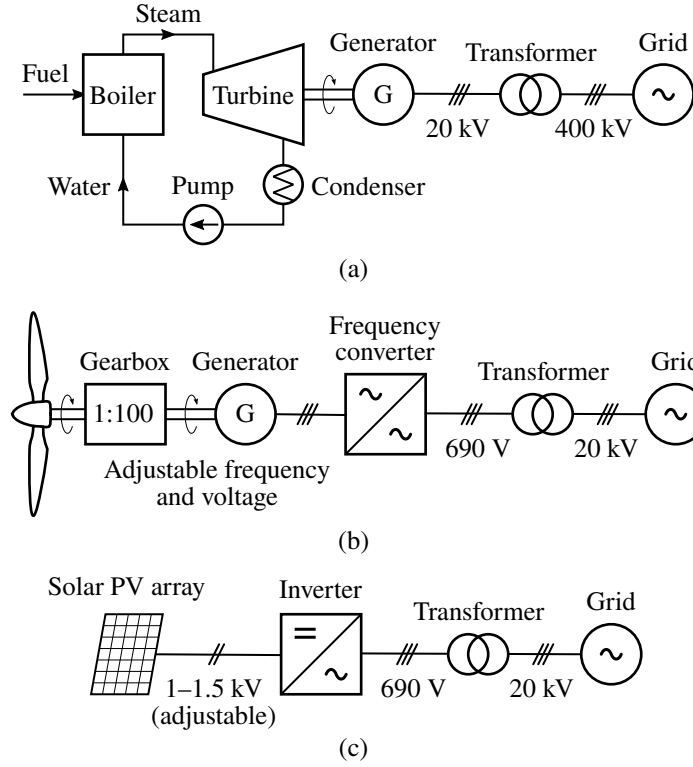
Figure 1.2: Simplified schematics of power plants: (a) thermal power station; (b) wind turbine; (c) utility-scale solar PV. The generator in (a) has to rotate in synchronism with the AC grid while the rotor speed of the converter-connected generator in (b) is adjusted according to the wind speed. In (c), a single inverter station of a large solar PV plant is shown. A wind turbine in (b) and a central inverter in (c) could have their rated powers in the range of 2–10 MW (and big power plants may contain tens of such units). The given values for voltage levels and a gearbox ratio are exemplary.

Large plants may contain tens or hundreds of such inverters. Alternatively, solar plants can be built using string inverters, whose rated power is typically a few tens of kilowatts. The converter technologies used in wind turbines and in solar inverters are similar.

1.3 Energy Conversion

The energy has to be converted into different forms both in generation and consumption. Figure 1.3 illustrates power balance of an energy conversion process. According to the first law of thermodynamics, energy can be converted from one form to another, but it cannot be created or destroyed. The efficiency η of a conversion device can be defined as

$$\eta = \frac{\text{useful output power}}{\text{input power}} \tag{1.1}$$

According to the second law of thermodynamics, the efficiency is less than 100% (unless the useful output power is heat). In the steady-state conditions, the input and output powers in (1.1) can be equivalently replaced with the input and output energies over some time period. It is worth noticing that the efficiency of many energy-conversion devices (such as electric machines) depends strongly on the

3
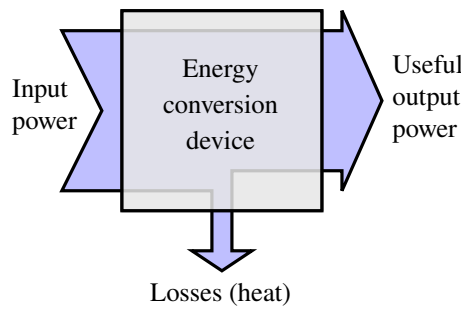
Figure 1.3: Power balance of an energy conversion process.

operating point. If a single value for an efficiency is given, it typically refers to the rated operating point of a device or a system.

Let us first consider electricity generation as an example. A typical thermal power station has the following conversion stages: 1) a power plant boiler generates steam at high temperature and at high pressure, thus converting chemical energy of fuel into heat energy; 2) steam spins the turbine, converting heat energy into mechanical work; 3) the electrical generator connected to the turbine converts the mechanical work into the electrical energy. Assuming a large thermal power station, efficiencies could be around 90% for a boiler, 45% for a turbine, and 98% for a generator, resulting in the total efficiency of 40%. The higher is the efficiency, the less fuel is needed to generate the power.

A solar PV plant converts solar energy directly to the DC electricity. The efficiency of a PV cell is the portion of energy in the sunlight that is converted into electricity. Typical efficiencies of silicon-based PV cells are around 20–25%. The generated DC electricity has to be further converted into grid-compatible AC power by means of a power converter, typically having efficiency in the range of 95–98%. The total efficiency of about 20% might look low. However, compared to fossil-fuel-based generation, the efficiency is a less important factor, since sunlight is free, clean, and abundant. The situation is the same also for wind power. However, improving the efficiencies of renewable generation is important since the land area and materials needed to produce power can be reduced.

On the consumption side, electrical energy is converted to useful forms such as mechanical work, light, and heat. In some processes, significant energy savings can be reached by switching from conventional to modern technologies. For example, the efficiency of LED lights is more than ten times that of incandescent light bulbs. As another example, let us consider pumps and fans that are needed for moving various fluids (liquids and gases) in heating, ventilation, and air-conditioning (HVAC) systems as well as in many industrial processes. Constant-speed pumps and fans are common in old installations. A mechanical throttling valve has to be used to adjust fluid flow, which results in poor efficiencies at lower flow rates. The process efficiency can be improved significantly (even more than 20%) using a variable-speed pump or fan.

Due to losses in energy production, transmission, and distribution, much more primary energy is needed than the amount of consumed final energy. Consequently, improving the efficiency of the final energy use is an effective way to decrease greenhouse gas emissions. As an example, consider a thermal power station having the efficiency of 40% and the transmission and distribution
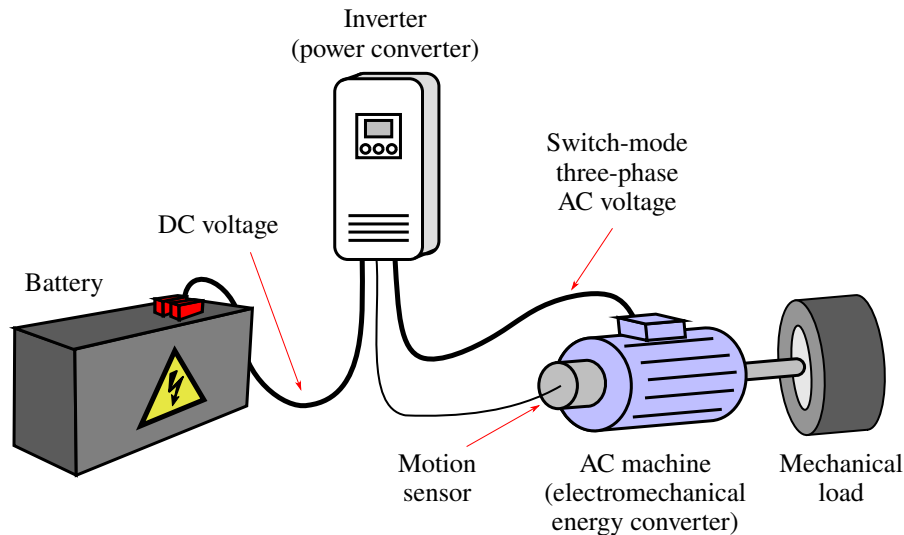
Figure 1.4: Example of an electric motor drive. The power converter enables the speed (or the driving torque) of the electric machine to be controlled. The converter includes an embedded controller. In this example, the drive is equipped with a motion sensor, but many industrial drives can operate without such an external sensor. In many applications, a mechanical transmission (such as a fixed-speed gearbox) is used between the electric machine and the mechanical load.

system having the efficiency of 95%. These example values indicate that saving of 1 kWh in the final energy use result in the saving of 2.6 kWh in primary energy.

1.4 Electric Machine Drives

1.4.1 Definition

An electric machine drive can be defined as a system, which converts electrical energy into mechanical work. Figure 1.4 shows an example of an electric machine drive, equipped with a battery pack, a power converter, a three-phase AC machine, and a mechanical load coupled to the shaft of the machine. Since the battery is a DC source, the power conversion is between the DC and three-phase variable-frequency AC. The direction of the energy flow can also be opposite, i.e., mechanical work can be converted to electrical energy. The electric machine acts as an electromechanical energy converter. If the power flows mainly from the electrical source to the mechanical load, the electric machine is referred to as a motor. If the mechanical work is converted to the electrical energy, the electric machine is called as a generator. The wind turbine is an example of electric machine drive, in which the mechanical work is converted to electrical energy.

In this material, we will focus mainly on converter-fed electric machine drives. Such drives can be designed to operate in both directions of rotation and in both directions of power flow. For example, an electric vehicle can drive forward and backward, and can in both directions regenerate energy when braking. The energy flow and the mechanical motion can be controlled by means of a power converter. Even if electric machines themselves are capable to work both as a motor and a generator, some power converter topologies do not allow bidirectional power flow.

1.4.2 Applications

As already mentioned, electric machine drives are needed in generation of electrical energy, e.g., in thermal power stations, hydro power plants, and wind turbines. In the consumption side, more than 50% of all electrical energy is converted to mechanical work or, in other words, used in electric motor drives. The majority of motor drives are in the low-power (fractional kW) and medium-power (1–100 kW) ranges. In the higher power ranges, there are industrial drives rated up to tens of megawatts. Examples of applications are pumps, fans, compressors, conveyors, elevators and escalators, cranes and hoists, machine tools, and rolling mills. Traction applications include electric vehicles, light-rail vehicles, subway trains, locomotives, off-road machines, and ships.

Regardless of the application, high efficiency is one of the most important factors in electric machine drives. Typical efficiencies are in the range of 75–95% at the rated operating point. Similarly to other energy-conversion devices, the efficiencies typically increase with the increasing rated power. In addition to high efficiency, some applications such as electric vehicles also require high power densities (power per unit volume). Liquid cooling and advanced materials are necessary to reach very high power densities.

Converter-fed motor drives enable fast and accurate motion control, which is necessity in many applications, such as robotics, elevators, and cranes. Furthermore, the energy efficiency can be significantly improved in many processes, such as pumps and fans. Finally, electric machine drives allow conserving braking energy. This feature is important, e.g., in electric vehicles where a part of the kinetic energy can be stored to the battery while braking.

Chapter 2

DC Machines

Although there are some DC machines still commercially available, essentially, AC machines have replaced them in almost all new industrial applications. Nevertheless, DC machines are a pedagogically reasonable starting point, when studying electrical machines. The models of DC machines are simpler than those of AC machines. Furthermore, their models, characteristics, and control methods can be extended to AC machines.

2.1 Structure

Figure 2.1(a) shows Edison's historical DC machine from 1882. This machine was equipped with the stator field winding placed in the long legs. Figure 2.1(b) shows a more modern DC machine, where the stator is magnetized using permanent magnets (PMs). Figure 2.2 illustrates a cross-section of a conceptual DC machine equipped with permanent magnets (PMs). This example machine has two poles, but operating principles and characteristics are the same for the machines having more poles.

In Figure 2.2, the DC stator field is produced by the PMs. Among different

(a)   (b)
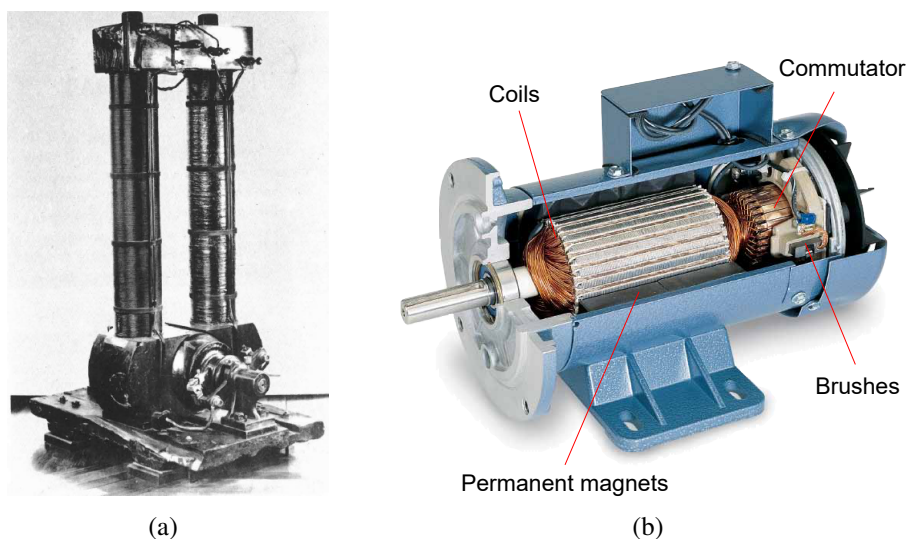
Figure 2.1: DC machines: (a) Edison's DC generator from 1882, where the field winding is placed in the long legs; (b) PM DC motor (Kollmorgen).
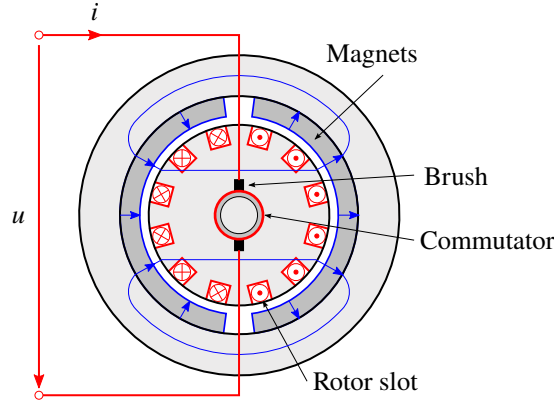
Figure 2.2: Cross-section of a conceptual DC machine equipped with PMs. The PM flux lines are also illustrated. In the electric circuit, the arrows define the positive directions of the voltage and the current. Furthermore, positive directions of the currents in the cross-section are marked with the crosses and dots: the cross indicates that the current flows away from the reader and the dot indicates that the current flows towards the reader.

types of PMs, ferrite magnets are cheap and easy to manufacture, but their energy product is poor. Rare-earth magnets provide much higher energy products, but they are expensive and difficult to manufacture and handle. A neodymium (NdFeB) magnet is the most common rare-earth magnet type, made from an alloy of neodymium (Nd), iron (Fe), and boron (B). A samarium-cobalt (SmCo) is another common rare-earth magnet type. Alternatively, the DC stator field can be produced by a field winding, Figure 2.3(a). Both the PMs and the field winding ideally produce a uniform radial magnetic flux density B_f in the air gap, as illustrated in Figure 2.3(b). However, the flux density B_f can be adjusted only in the case of a field winding (by controlling its DC current i_f). Due to the DC field, there are very small eddy-current losses, allowing the stator core to be made of solid iron.

The rotor has a set of identical coils placed in slots [1, 2]. The coils consist of many conductors connected in series. Each coil is connected to two segments of a commutator, which, via mechanical sliding contacts, converts the DC current i fed to the stator terminals into the AC current in the rotor coils (i.e., DC machines are internally AC machines, as seen subsequently). Brushes, typically made of carbon, slide on the commutator. The current i enters the rotor via one brush, flows through all the rotor coils, and leaves via the other brush. All the power to be converted into mechanical output power is fed into the rotor through the brushes and commutator. Commutation losses and the need for replacing brushes regularly make DC machines less desirable than AC machines.

The rotor core is made of thin laminated steel sheets. The laminated structure in the rotor is needed since the stator field varies as seen from the rotating rotor. If a solid core rotor were used, large eddy currents would be induced in the rotor, causing losses and deteriorating the performance of the machine.

2.2 Elementary Single-Coil Machine

First, an elementary single-coil machine shown in Figure 2.4(a) is considered. The angular position of the rotor is denoted by ϑ_M (rad). Therefore, the angular
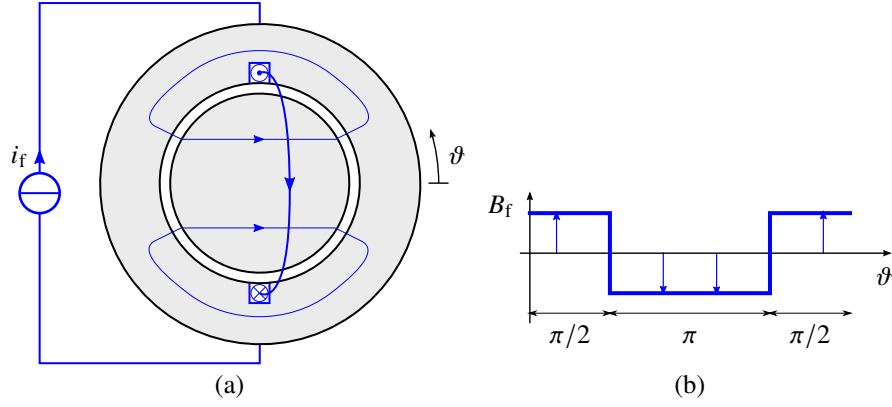
Figure 2.3: Stator field: (a) conceptual field winding; (b) air-gap flux density distribution. The magnitude of B_f is proportional to the field current i_f (or constant in the case of PMs in Figure 2.2).

speed of the rotor (rad/s) is

$$\omega_M = \frac{d\vartheta_M}{dt} \tag{2.1}$$

Consequently, tangential velocity of the conductors is $v = r\omega_M$, where r is the radius of the rotor.

The rotor coil consists of N conductors connected in series. The rotor coil sees a uniform radial flux density B_f, which is orthogonal to the direction of the current and whose polarity depends on the coordinate ϑ, see Figure 2.3(b). The voltage $B_f \ell v$ is induced in each conductor moving in the magnetic field, where ℓ is the effective length of the rotor. Since the conductors are in series, the voltage $e_a = 2Nr\ell B_f\omega_M$ is induced in the coil. This induced voltage is proportional to the angular speed of the rotor, and it is also known as the back electromotive force (back-emf). If the current in the coil is zero, $i_a = 0$, the voltage at the terminals equals the induced voltage, $u_a = e_a$. This induced voltage could be measured, e.g. using an oscilloscope, from the terminals of the open coil while the machine rotates.

In a general case, the coil voltage can be expressed as

$$u_a = R_a i_a + \frac{d\psi_a}{dt} \tag{2.2}$$

where R_a is the resistance of the coil and ψ_a is its flux linkage. The first term $R_a i_a$ is the resistive voltage drop, originating from Ohm's law. Any real coil has a nonzero resistance R_a that causes losses when the current flows through it. The second term $d\psi_a/dt$ originates from Faraday's law of induction: if the flux linking with the coil varies due to any reason, a voltage corresponding to the time rate of change of the flux linkage is induced in the coil. The voltage equation (2.2) is of fundamental nature.

The flux linkage of the coil is

$$\psi_a = L_a i_a + \psi_{af} \tag{2.3}$$

where L_a is the self-inductance of the coil and ψ_{af} is its flux linkage due to the external field (caused by either the PMs or the field winding). Based on the geometry,

$$\psi_{af} = 2Nr\ell B_f \left(\frac{\pi}{2} - \vartheta_M\right) \qquad (0 < \vartheta_M < \pi) \tag{2.4}$$

9
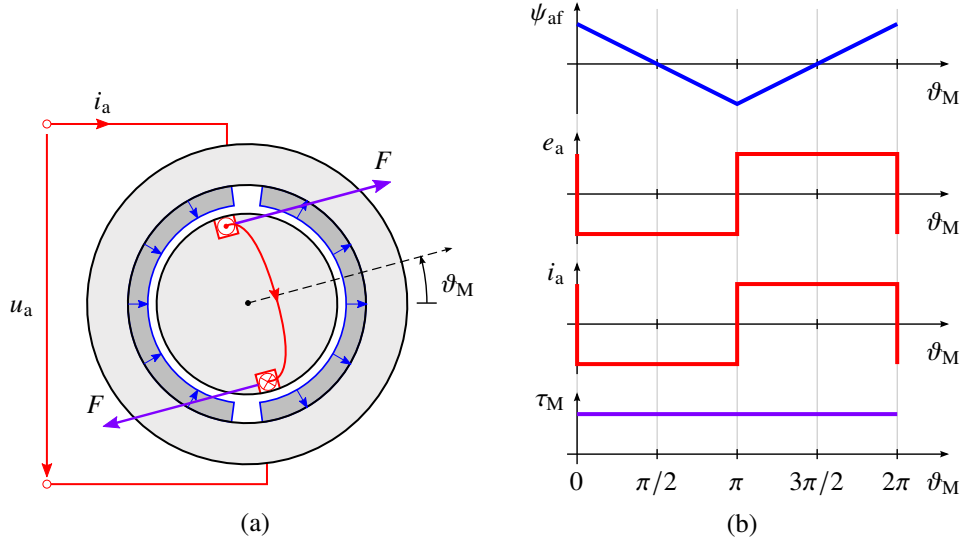
Figure 2.4: Elementary single-coil machine: (a) cross-section; (b) waveforms as functions of the rotor angle ϑ_M.

The form of the flux linkage equation depends on the machine type, its geometry, and in practice, also on the magnetic saturation. In this presentation, the magnetic saturation is omitted.

Inserting (2.3) into (2.2), the coil voltage can be further expressed as

$$u_\mathrm{a} = R_\mathrm{a} i_\mathrm{a} + L_\mathrm{a} \frac{\mathrm{d}i_\mathrm{a}}{\mathrm{d}t} + e_\mathrm{a} \tag{2.5}$$

where the voltage induced by the external field is

$$
\begin{aligned}
e_\mathrm{a} &= \frac{\mathrm{d}\psi_\mathrm{af}}{\mathrm{d}t} = \frac{\partial \psi_\mathrm{af}}{\partial \vartheta_\mathrm{M}} \frac{\mathrm{d}\vartheta_\mathrm{M}}{\mathrm{d}t} \\
&= -2Nr\ell B_\mathrm{f}\omega_\mathrm{M} \qquad (0 < \vartheta_\mathrm{M} < \pi)
\end{aligned}
\tag{2.6}
$$

which is the same result as earlier.

The force $F = B_\mathrm{f}\ell i_\mathrm{a}$ acts on each conductor placed in the magnetic field. Therefore, the electromagnetic torque

$$\tau_\mathrm{M} = -2Nr\ell B_\mathrm{f} i_\mathrm{a} \qquad (0 < \vartheta_\mathrm{M} < \pi) \tag{2.7}$$

is proportional to the current. The mechanical power is

$$p_\mathrm{M} = \tau_\mathrm{M}\omega_\mathrm{M} = e_\mathrm{a} i_\mathrm{a} \tag{2.8}$$

where the last form is obtained by applying (2.6) and (2.7).

Figure 2.4(b) shows waveforms of the elementary single-coil machine as a function of the rotor angular position ϑ_M. If the rotor speed ω_M is constant, the angle $\vartheta_\mathrm{M} = \omega_\mathrm{M}t$, i.e., these waveforms can also be understood as functions of time. The flux linkage ψ_f depends only on the rotor position, see (2.4). The magnitude of the induced voltage e_a is proportional to the rotor speed ω_M, see (2.6). In order to have constant positive torque τ_M, the current i_a should have the same shape as the induced voltage e_a, as illustrated in the figure.

Based on these waveforms in Figure 2.4(b), it can be realized that this elementary machine is an AC machine. Figure 2.5 illustrates the operating principle

10
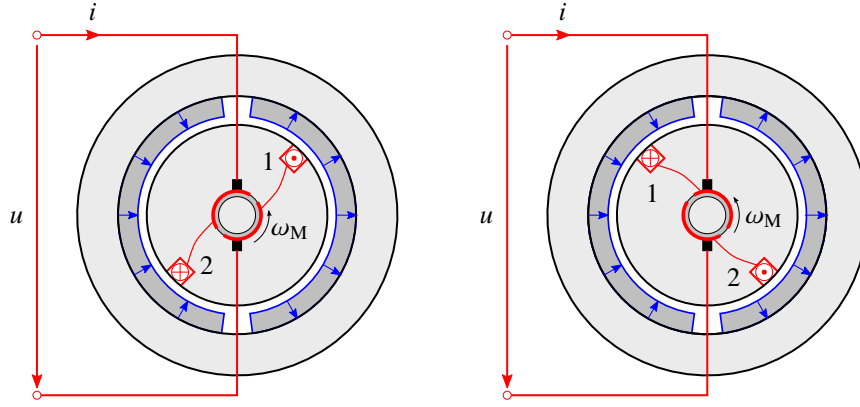
Figure 2.5: Principle of a commutator. The commutator converts the DC current i into the AC current i_a in the rotor coil. The two conductors are labeled with 1 and 2. The rotor is assumed to rotate counterclockwise. The figure on the left shows the situation before the commutation. The figure on the right shows the situation after the commutation, i.e., the polarity of the rotor coil current is reversed as a function of the rotor position.
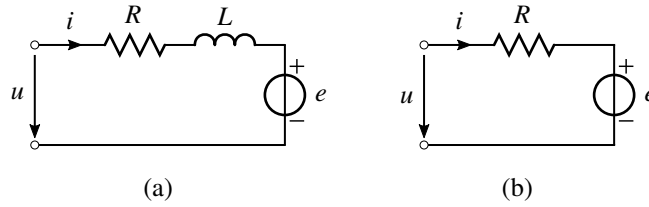
Figure 2.6: Equivalent circuit of a DC machine: (a) dynamic; (b) steady state.

of a commutator for the this single-coil machine. The commutator mechanically reverts the DC current i fed to the terminals into the AC current i_a for the rotor coil.

2.3 Dynamic Model

2.3.1 Equivalent Circuit

Figure 2.6(a) shows an equivalent circuit of a DC machine. The model of a DC machine can be reasoned based on the model of an elementary single-coil machine. The terminal voltage is

$$u = Ri + L\frac{di}{dt} + e \tag{2.9}$$

where u is the DC terminal voltage. The term e originating from the induced voltage is proportional to the speed

$$e = k\omega_M \tag{2.10}$$

where k is the flux factor (known also as the back-emf constant or the torque constant). The electromagnetic torque

$$\tau_M = ki \tag{2.11}$$

11
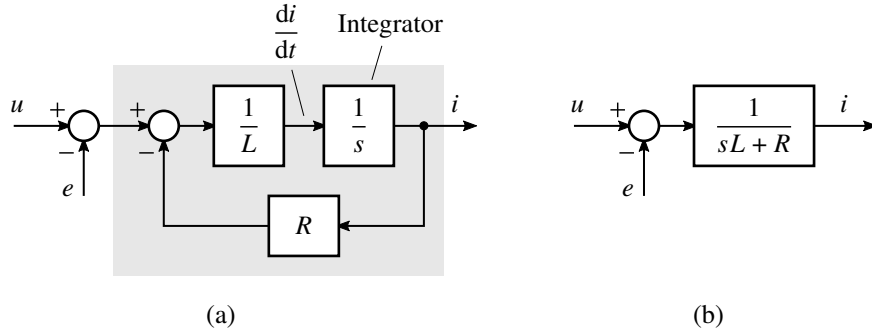
Figure 2.7: Block diagram representation of the electrical subsystem (2.14): (a) form based on the integrator; (b) form based on the first-order transfer function. Notice that these block diagrams can be interpreted either in the time domain ($s = $ d$/$dt is the differential operator) or in the Laplace domain (s is the complex variable).

is proportional to the current. The flux factor is ideally constant in PM machines, while it can be adjusted in machines equipped with field winding. Based on (2.10), the flux factor could be identified by rotating the rotor at known speed and measuring the induced voltage from the terminals in a no-load condition (at zero current).

Using (2.9), the power $p = ui$ fed to the terminals can be expressed as

$$p = Ri^2 + \frac{\mathrm{d}}{\mathrm{d}t}\left(\frac{1}{2}Li^2\right) + ei \tag{2.12}$$

where the first term represents the resistive losses, the second term is the rate of change of the magnetic energy in the inductance L, and the last term equals the mechanical power

$$p_\mathrm{M} = \tau_\mathrm{M}\omega_\mathrm{M} = ei \tag{2.13}$$

2.3.2 Block Diagram

The differential equation (2.9) can be rewritten as

$$L\frac{\mathrm{d}i}{\mathrm{d}t} = u - Ri - e \tag{2.14}$$

This equation can be called a state equation, where the current i is the state variable and the voltages u and e are the inputs. Dividing both sides of (2.14) by the inductance L and integrating over time yields

$$i(t) = i(0) + \frac{1}{L}\int_0^t (u - e - Ri)\,\mathrm{d}t \tag{2.15}$$

where $i(0)$ is the initial current at $t = 0$. Figure 2.7(a) shows the corresponding block diagram, which can be directly drawn based on (2.14). In other words, the state equation defines what is the input signal of the integrator. The block diagram can be interpreted to represent the system in the time domain, where $s = $ d$/$dt is the differential operator and $1/s$ is the integration operator.[1]

---

[1]In some textbooks, the symbol $p = $ d$/$dt is used for the differential operator.
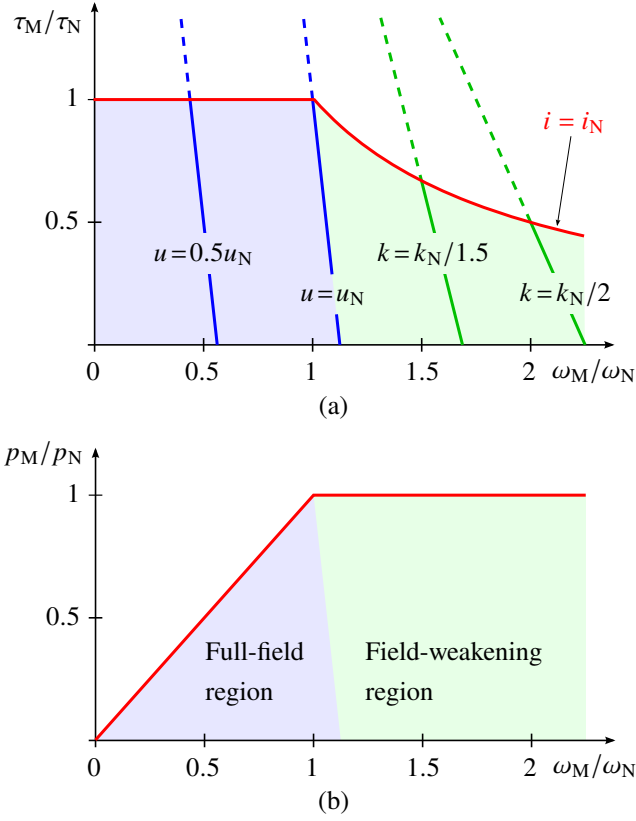
Figure 2.8: Steady-state characteristics as function of the speed: (a) electromagnetic torque; (b) mechanical power. The shaded area shows the feasible operating area, which is limited by the current in the full-field region and by the current and the voltage in the field-weakening region.

Alternatively, the same block diagram in Figure 2.7(a) can also be understood to represent signals and systems in the Laplace domain, in which case $s = \sigma + j\omega$ is a complex variable. The differential equation (2.14) can be transformed to the Laplace domain as

$$
\begin{aligned}
i(s) &= \frac{1}{sL + R}[u(s) - e(s)] \\
&= Y(s)[u(s) - e(s)]
\end{aligned}
\tag{2.16}
$$

In electrical engineering, the transfer function

$$
Y(s) = \frac{1}{sL + R} = \frac{1/R}{1 + Ts}
\tag{2.17}
$$

is also known as an admittance. It corresponds to a first-order low-pass filter, whose DC gain is $1/R$ and time constant is $T = L/R$, see also Appendix A.1. Figure 2.7(b) shows the block diagram representation corresponding to (2.16). It will be seen later that the mechanical and thermal subsystems can be represented by similar state equations and transfer functions. It is also worth noticing that the equivalent circuit in Figure 2.6(a) and the block diagram in Figure 2.7 represent the same system and contain the same information.

13
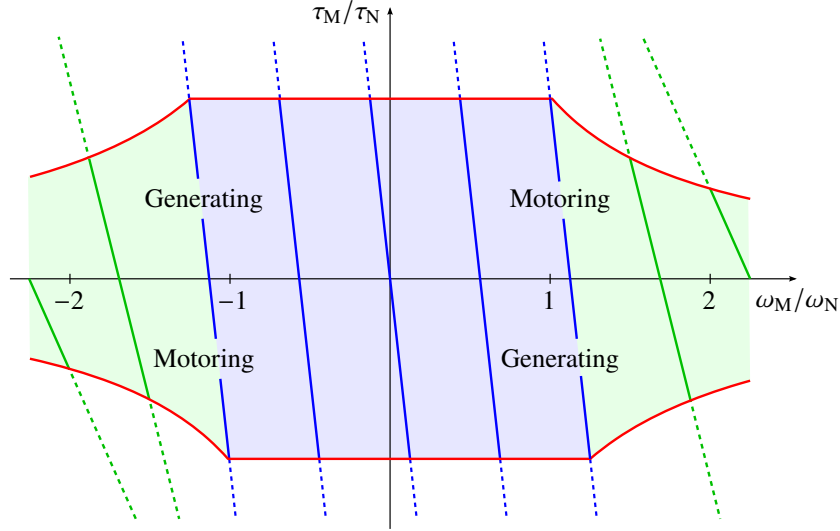
Figure 2.9: Four operating quadrants.

2.4 Steady-State Characteristics

Figure 2.6(b) shows the steady-state equivalent circuit. In the DC steady state, the time derivatives are zero, $\mathrm{d}/\mathrm{d}t = 0$, and the terminal voltage (2.9) reduces to

$$u = Ri + e \tag{2.18}$$

Except at lowest speeds, the resistive voltage drop Ri is small compared to the induced voltage $e = k\omega_\mathrm{M}$. Therefore, $u = k\omega_\mathrm{M}$ can be assumed at higher speeds, i.e., voltage is proportional to the speed.

Electric machines are often characterized by their rated values, given in the nameplate or data sheet, marked here with the subscript N. The rated values refer to the maximum values that the machine can withstand in continuous operation. The rated voltage u_N is limited by insulation (commutator and coils). The rated current i_N corresponds to the maximum acceptable resistive losses Ri_N^2. The rated field (and, therefore, the rated flux factor k_N) is determined by magnetic saturation. The rated speed is obtained using the above-mentioned rated values,

$$\omega_\mathrm{N} = \frac{u_\mathrm{N} - Ri_\mathrm{N}}{k_\mathrm{N}} \tag{2.19}$$

The rated power refers to the output power in the rated operating point, i.e, the mechanical power $p_\mathrm{N} = \tau_\mathrm{N}\omega_\mathrm{N}$ in the case of motors, where τ_N is the rated torque.

Figure 2.8(a) shows the torque as a function of the speed at different voltages. The steady-state torque as a function of the speed is obtained from (2.11) and (2.18) as

$$\tau_\mathrm{M} = k\frac{u - k\omega_\mathrm{M}}{R} \tag{2.20}$$

The continuous current of the machine is limited due to the resistive losses. In continuous operation, $|i| \leq i_\mathrm{N}$ should hold, which consequently limits the torque as well, as can be seen in the figure.

The voltage is limited due to motor insulation and the source voltage, $|u| \leq u_\mathrm{N}$. The rated voltage is approximately reached at the rated speed, which is
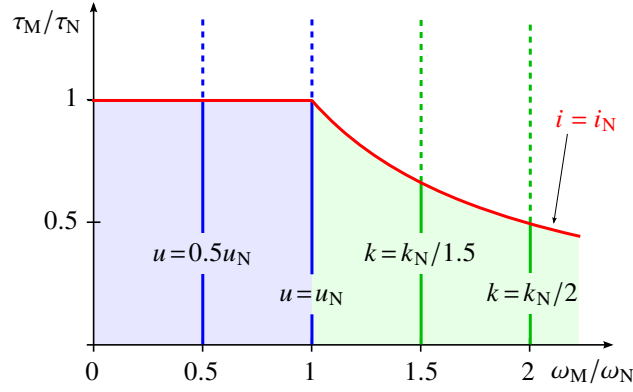
Figure 2.10: Steady-state torque as a function of the speed when the losses are omitted.

also the maximum speed for PM machines. In machines equipped with the field winding, the operating range can be extended to higher speeds by lowering the flux factor k inversely proportional to the speed,

$$k = \frac{\omega_N}{|\omega_M|} k_N \qquad \text{if } |\omega_M| > \omega_N \qquad (2.21)$$

This principle is called field weakening. Even if the current is kept at its rated value, the maximum value of the torque $\tau_M = ki$ reduces in the field-weakening region since k reduces. The field-weakening region is also known as constant-power region.

A DC machine can operate in four quadrants, as shown in Figure 2.9. In the motoring quadrants, the machine produces positive mechanical power $p_M = \tau_M \omega_M$. In the generating quadrants, the mechanical power is negative and the machine operates as a generator.

The resistive voltage drop Ri is much smaller than $e = k\omega_M$, except at the lowest speeds. If the losses are omitted ($R = 0$), the steady-state machine model reduces to

$$u = k\omega_M \qquad \tau_M = ki \qquad p_M = \tau_M \omega_M = ui \qquad (2.22)$$

These expressions describe an ideal electromechanical energy converter. Figure 2.10 shows the corresponding torque characteristics. The characteristics of AC machines are similar to these of the DC machines.

2.5 Rated Torque vs. Rotor Volume

Consider a machine shown in Figure 2.2. Assume that the machine has n rotor slots in total. The maximum acceptable continuous current flowing through each rotor slot is denoted by I. If the coils in the slots have several turns, this total slot current I is divided into several conductors. Based on (2.7), the electromagnetic torque of this machine at this current is $\tau_N = nr\ell B_f I$, where the notation refers to the rated torque due to the above assumptions on the slot current I. This rated torque can be further expressed as

$$\tau_N = 2B_f A V_r \qquad (2.23)$$

15

where $V_r = \pi r^2 \ell$ is the rotor volume and A is the specific current loading. It gives the linear current density around the air gap circumference (A/m), [3]

$$A = \frac{nI}{2\pi r} \tag{2.24}$$

The specific current loading A is limited by the resistive losses. Similarly, the magnetic loading B_f is defined as an average flux density at the air gap, limited by magnetic saturation and core losses. Even if cooling system, selected materials, and details of the machine geometry affect allowable B_f and A, the rotor (and motor) volume is roughly proportional to the rated torque of the machine.

The rated output power p_N depends on the rated speed ω_N,

$$p_N = \tau_N \omega_N \tag{2.25}$$

To produce the required mechanical power, the designer can choose between a large (expensive) low-speed motor or a small (cheaper) high-speed one. For industrial motors, typical rated speeds are from a few hundred r/min up to 10 000 r/min. High-speed motors require a speed reduction gear unless the application also requires high speed.

Figure 2.11 shows an example catalog page of DC machines. It can be noticed that these machines have the same mass and approximately the same rated torque even though other rated values (voltage, current, power) vary in a wide range. The above-mentioned fundamental constraints and sizing equations are independent of the amount of turns of the windings (if the filling factor is omitted). The amount of turns allow the machine to be winded for a desired voltage. These results are approximately valid for AC machines as well.

16

General data / Caractéristiques générales / Generelle Daten			
I_{max}/I_N = 180 %	J = 0.6 kgm²	P_f = 1600 W	p_Δ = 1050 Pa
T_{max}/T_N = 160 %	n_0 = 10 min⁻¹	V_{diss} = 0.25 m³/s	W = 350 kg
			U_{fN} = 110-440 V

U_N (V) $[U_N > 1,1\ x\ U_{fN}\ ^{1)}]$ — n (min⁻¹); n_{max} (min⁻¹)

400	420	440	470	520	550	620	750	815	P (kW)	I_N (A)	T (Nm)	η (%)	n₂ (min⁻¹) 3800	n₃/n₄ (min⁻¹) 4500	Cat. No. / No de catalogue / Bestellnummer
617									28	88	435	75,6	1738	1851	R_a = 803 mΩ, L_a = 10.71 mH, U_{fN}/U_{vN} = D — 3BSM003050-··· ··· = **BPA** ²⁾ ··· = **BPB** ³⁾ ··· = **BPC** ⁴⁾
	655								30	88	435	76,6	1738	1964	
		693							32	88	435	77,5	1739	2078	
			749						34	88	435	78,7	1740	2247	
				844					38	88	434	80,4	1741	2263	
					900				41	88	434	81,3	1742	2264	
						1032			47	88	433	83,0	1744	2267	
							1278		58	88	432	85,4	1747	2271	
								1400	63	88	431	86,2	1749	2273	
810									40	121	471	79,6	2336	2429	R_a = 485 mΩ, L_a = 5,63 mH, U_{fN}/U_{vN} = D — 3BSM003050-··· ··· = **BQA** ²⁾ ··· = **BQB** ³⁾ ··· = **BQC** ⁴⁾
	858								42	120	470	80,5	2341	2573	
		906							44	120	469	81,2	2347	2717	
			978						48	120	467	82,2	2355	2933	
				1098					53	119	464	83,6	2368	3079	
					1170				57	119	463	84,4	2377	3089	
						1337			64	118	458	85,8	2396	3115	
							1649		78	116	451	87,7	2433	3162	
1064									51	147	455	83,9	1955	2541	R_a = 302 mΩ, L_a = 4.04 mH, U_{fN}/U_{vN} = D — 3BSM003050-··· ··· = **BRA** ²⁾ ··· = **BRB** ³⁾ ··· = **BRC** ⁴⁾
	1125								54	147	455	84,5	1955	2541	
		1185							56	147	455	85,0	1955	2541	
			1275						61	147	455	85,8	1955	2541	
				1426					68	147	454	86,8	1955	2541	
					1516				72	147	454	87,4	1955	2541	
1361									62	176	433	85,2	3800	4083	R_a = 210 mΩ, L_a = 2,79 mH, U_{fN}/U_{vN} = B — 3BSM003050-··· ··· = **BSA** ²⁾ ··· = **BSB** ³⁾ ··· = **BSC** ⁴⁾
	1437								65	176	433	85,8	3800	4310	
		1512							68	176	432	86,2	3800	4500	
			1625						74	176	432	86,9	3800	4500	
				1814					82	176	431	87,7	3800	4500	
					1927				87	175	430	88,2	3800	4500	
						2191			98	175	429	89,0	3800	4500	
							2682		120	175	426	90,1	3800	4500	
								2928	130	174	425	90,5	3800	4500	
1758									83	234	454	87,5	3800	4500	R_a = 126 mΩ, L_a = 1,45 mH, U_{fN}/U_{vN} = B — 3BSM003050-··· ··· = **BTA** ²⁾ ··· = **BTB** ³⁾ ··· = **BTC** ⁴⁾
	1853								88	233	453	87,9	3800	4500	
		1949							92	233	452	88,3	3800	4500	
			2092						99	233	451	88,8	3800	4500	
				2331					110	232	450	89,5	3800	4500	
					2474				116	232	449	89,8	3800	4500	
						2808			131	231	446	90,5	3800	4500	
2250									96	264	408	89,4	3800	4500	R_a = 78 mΩ, L_a = 1,04 mH, U_{fN}/U_{vN} = B — 3BSM003050-··· ··· = **BUA** ²⁾ ··· = **BUB** ³⁾ ··· = **BUC** ⁴⁾
	2369								101	264	408	89,7	3800	4500	
		2489							106	264	407	89,9	3800	4500	
			2668						114	263	406	90,2	3800	4500	
				2966					126	263	405	90,7	3800	4500	
					3145				133	262	403	90,9	3800	4500	
2859									113	310	379	90,0	3800	4500	R_a = 51 mΩ, L_a = 0,59 mH, U_{fN}/U_{vN} = C — 3BSM003050-··· ··· = **BVA** ²⁾ ··· = **BVB** ³⁾ ··· = **BVC** ⁴⁾
	3009								119	310	378	90,2	3800	4500	
		3158							125	310	378	90,4	3800	4500	
			3383						134	310	378	90,6	3800	4500	
				3757					148	309	375	90,8	3800	4500	
					3982				156	308	374	91,0	3800	4500	

5

Explanation of motor data cross-references, see page 70/
Explication des références croisées des caractéristiques moteur, voir page 70/
Erklärung der Motorreferenzwerte, siehe Seite 70

ABB Motors and Generators | DC motors type DMI EN, FR, DE 01-2011 75

Figure 2.11: Example catalog page of DC machines (ABB).

Chapter 3

Mechanics

The equation of motion for rotating mechanical systems and typical load torque profiles are considered in this chapter. The equation of motion defines the causal relationships between the torque and the speed. If the electromagnetic torque and the load torque are known, one can simulate (or sketch in simple cases) the resulting speed response. In the simplest case considered here, the equation of motion has only one parameter, the moment of inertia. Understanding the mechanical concepts is important both in the field of electric machine drives as well as in power systems.

The equation of motion is also needed when choosing a suitable machine for a mechanical load. For this purpose, the equivalent moment of inertia and load torque profile (both referred to the motor shaft speed) are typically first calculated. Then, if the speed profile is known, the torque required from the electric machine can be calculated.

3.1   Equation of Motion

Assuming the moment of inertia J (kgm^2) to be constant, the rotational dynamics of a rigid body are governed by the equation of motion

$$J\frac{d\omega_M}{dt} = \tau_M - \tau_L \tag{3.1}$$

where ω_M is the angular speed of the rotor, τ_M is the electromagnetic torque produced by the electric machine, and τ_L is the load torque. The accelerating torque is the difference $\tau_M - \tau_L$. In the steady state, the speed ω_M is constant and $\tau_M = \tau_L$ holds. It can be seen that this equation is analogous with Newton's second law of linear motion: the torque corresponds to the force, the angular speed to the linear speed, and the inertia to the mass. The block diagram in Figure 3.1(a) presents the equation of motion, augmented with an example load torque characteristics.

Multiplying both sides of (3.1) by the rotor speed ω_M, the mechanical power produced by the electric machine is obtained, i.e.,

$$p_M = \tau_M\omega_M = \frac{d}{dt}\left(\frac{1}{2}J\omega_M^2\right) + \tau_L\omega_M \tag{3.2}$$
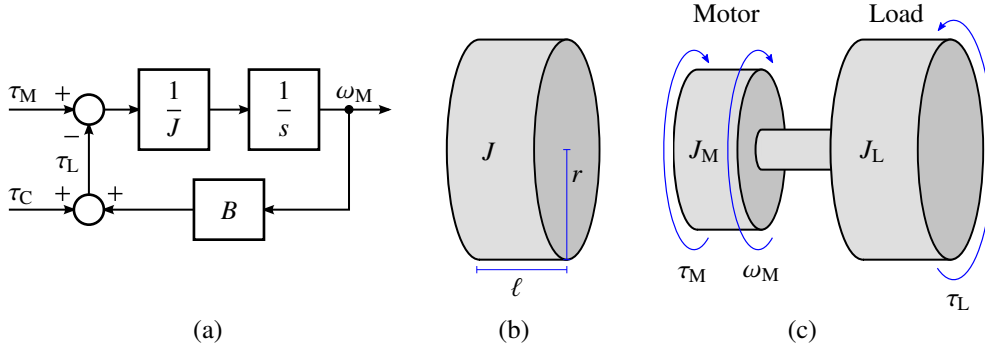
Figure 3.1: Mechanical system: (a) block diagram of the equation of motion, augmented with an example load torque model, $\tau_L = B\omega_M + \tau_C$; (b) solid cylinder; (c) typical two-mass system. In (a), the block $1/s$ is an integrator.

where the first term is the rate of change of the kinetic energy and the second term is the power needed due to the load torque. If the losses in the machine drive are omitted, the power p_M is drawn from the power supply (e.g., from an electric grid or a battery). The work done by the machine is

$$W_M(t) = \int_0^t p_M dt \qquad (3.3)$$

3.2 Moment of Inertia

The moment of inertia of a rotating rigid body is the integral over its mass m,

$$J = \int r^2 dm \qquad (3.4)$$

where r is the radius. The infinitesimal mass element can be expressed as $dm = \rho dV$, where ρ is the density and V is the volume. For a thin-walled cylinder, this integral results in $J = mr^2$. For a solid cylinder, shown in Figure 3.1(b), the inertia becomes

$$J = \frac{1}{2}mr^2 = \frac{\pi}{2}\rho\ell r^4 \qquad (3.5)$$

where ℓ is the length of the cylinder. It can be noticed that the inertia depends strongly on the radius r of the cylinder. For a given volume, the longer cylinder has a smaller inertia as compared to a shorter one.

Figure 3.1(c) illustrates a typical mechanical system in electric machine drives, consisting of two rotating masses connected with a shaft. If torsional resonances are of interest, the shaft could be modeled as a spring. If the shaft is assumed to be rigid and inertialess, the system in Figure 3.1(b) reduces to a single-mass system, whose inertia is $J = J_M + J_L$.

3.3 Load Torque Characteristics

Figure 3.2(a) shows typical load torque characteristics. In hoists, cranes, and elevators, a constant load torque component τ_C occurs due to the effect of gravity.
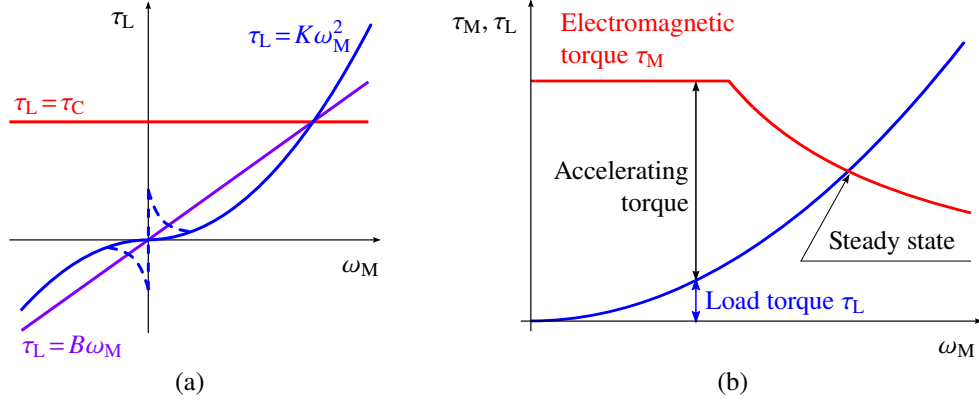
Figure 3.2: (a) Typical load torque characteristics. (b) Examples of electromagnetic torque and load torque characteristics.
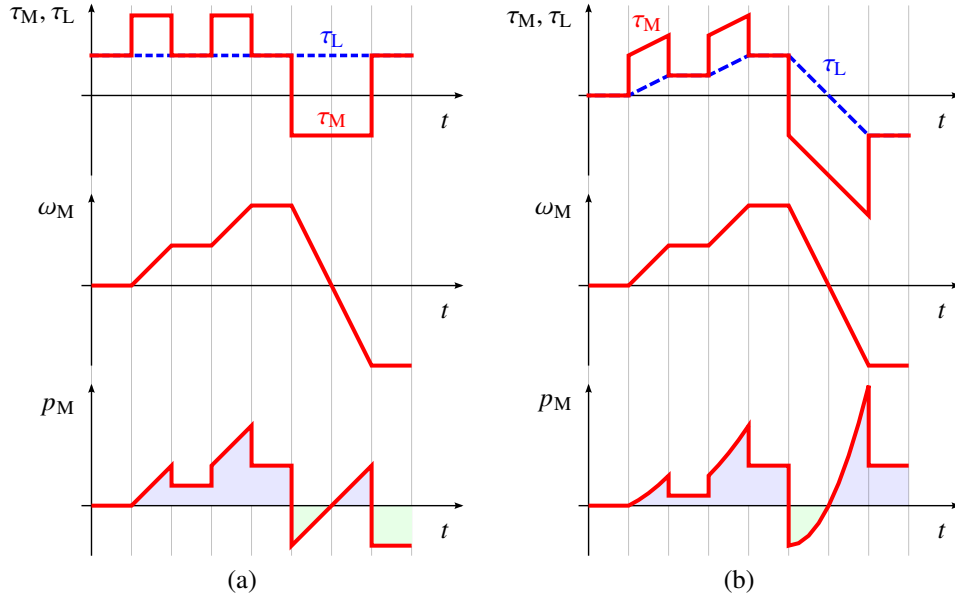

Figure 3.3: Example waveforms for torque, speed, and power $p_M = \tau_M \omega_M$: (a) constant load torque $\tau_L = \tau_C$; (b) viscous friction $\tau_L = B\omega_M$. In the last subplots, the shaded areas shows the energy. The blue and green areas correspond to motoring and generating, respectively.

This component is active: it resists the motion when lifting (positive speeds) but assists when lowering (negative speeds).

Load torque components related to friction are passive: they always oppose the motion independently of its direction. At zero speed, static friction (stiction) may exist, opposing the motion. The Coulomb friction (dry friction) can be modeled using $\tau_L = \tau_C \operatorname{sign}(\omega_M)$, where τ_C is constant. The viscous friction component is proportional to the rotation speed, $\tau_L = B\omega_M$. Such a component is caused, e.g., due to the laminar fluid flow in bearings. In fans and pumps, the turbulent flow of fluid causes a load torque component that is quadratic to the speed, $\tau_L = K\omega_M^2 \operatorname{sign}(\omega_M)$. For the same reasons, the quadratic load component also appears in high-speed transport applications due to air resistance. In practice, several of these components are present, but typically one or two of them are dominant.

20

If both electromagnetic torque and load torque depend on the rotor speed, they can be presented in the same graph, as exemplified in Figure 3.2(b). In this example, the load torque is quadratic, $\tau_L = K\omega_M^2$. As the speed increases, the accelerating torque decreases due to the quadratically increasing load torque but also due to the limited torque capability of the machine drive in the field-weakening region (known also as the constant-power region). In the intersection point $\tau_M = \tau_L$ holds, corresponding to the constant speed (or the steady-state speed). Based on (3.2), the mechanical power in the steady state depends cubically on the speed, $p_M = K\omega_M^3$. It can be realized that adjustable speed enables significant energy savings in such pumps and fans, where the maximum fluid flow is not continuously needed.

Figure 3.3 shows example waveforms in the time domain. Figure 3.3(a) assumes that the load torque is constant, corresponding to hoisting applications. Figure 3.3(b) assumes the viscous friction. According to (3.1), the speed is the integral of the accelerating torque $\tau_M - \tau_L$. The electromagnetic torque is selected so that the speed is identical in both load torque cases. The mechanical power (3.2) is also presented. If the machine drive is assumed to be lossless, the power p_M is fed from the power source. It is worth noting that the power p_M is negative in both cases in the beginning of deceleration, meaning that the machine operates as a generator and the power is fed from the load to the power source. This might be surprising in the case of the passive load in Figure 3.3(b). The reason for momentarily operating as a generator is the release of kinetic energy when braking the rotating inertia. This kind of regeneration may have to be taken into account in the main circuit of the power converter (e.g., by means of using four-quadrant converter, an energy store, or a braking resistor). Alternatively, if the mechanical system allows, the deceleration time could be lengthened, thus reducing the regenerated power spike.

3.4 Mechanical Transmissions

Various mechanical transmissions (such as toothed belt, rack and pinion, and gearbox) can be used between the shaft of an electric machine and the mechanical load. The gear ratio is given by[1]

$$i = \frac{\omega_1}{\omega_2} \tag{3.6}$$

where ω_1 and ω_2 are the angular speeds of the driving shaft and driven shaft, respectively. In electric motor drives, a speed-reduction gear is typical, corresponding to the gear ratio $i > 1$.

Figure 3.4(a) shows a conceptual gear based on two wheels, whose radii are r_1 and r_2. Assuming that there is no slip, the tangential velocity in the contact point is the same for both wheels, i.e., $\omega_1 r_1 = \omega_2 r_2$. Consequently, the gear ratio can be expressed using the radii as $i = r_2/r_1$. In the case of toothed wheels, Figure 3.4(b), the gear ratio is $i = n_2/n_1$, where n_1 and n_2 are the numbers of teeth. In a similar manner, gear ratios could be found for other mechanical transmissions.

---

[1]Notice that the same symbol is used for the gear ratio as for the electrical current. The context should make it clear which one is meant.
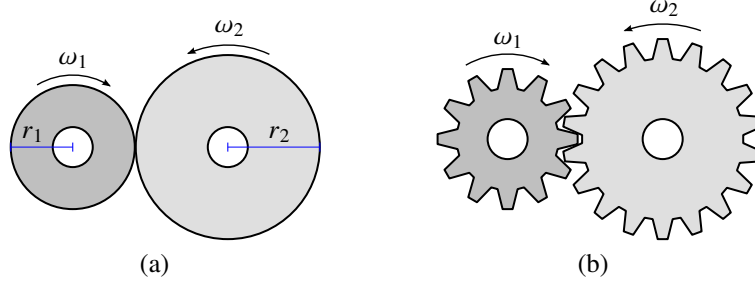
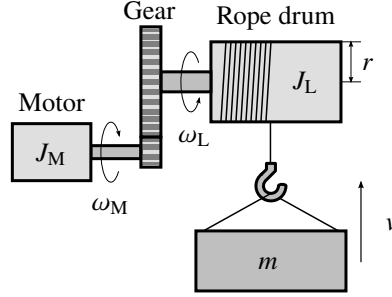Figure 3.4: Gear wheels: (a) conceptual; (b) toothed.

Figure 3.5: Example: crane drive.

It is often convenient to calculate the equivalent total moment of inertia and the equivalent total load torque at the driving shaft speed, which allows the equation of motion (3.1) to be directly applied.[2] Assume that the inertia J_2 is connected to the driven shaft and thus rotating at ω_2. Its equivalent inertia referred to the driving shaft speed ω_1 is denoted by J_1. The mechanical transmission is assumed to be lossless. Therefore, the kinetic energy has to be conserved in the transformation, $J_1\omega_1^2/2 = J_2\omega_2^2/2$, resulting in

$$J_1 = \frac{J_2}{i^2} \tag{3.7}$$

Similarly, the torque referred to the driven speed ω_2 is denoted by τ_2, and the equivalent torque referred to the machine speed is τ_1. The power has to be conserved in the transformation, $\omega_1\tau_1 = \omega_2\tau_2$, giving

$$\tau_1 = \frac{\tau_2}{i} \tag{3.8}$$

The conservation of power and energy naturally holds in linear motion as well, which allows to simplify computations in many cases, where linear motion is involved.

As an example, consider a crane drive shown in Figure 3.5, where J_L is the inertia of the rope drum and m is the mass to be lifted. The angular speeds of the motor and the rope drum are ω_M and ω_L, respectively. In order to apply the equation of motion (3.1), the equivalent total inertia J and the equivalent load torque τ_L, both referred to the motor side, should be known. Based on (3.4), the inertia due to the mass m at the load side is $J_m = mr^2$, where r is the radius of the

---

[2]A lossless mechanical transmission is analogous to an ideal transformer in electrical circuits.

rope drum according to the figure. Therefore, based on (3.7), the total equivalent inertia seen by the motor is

$$J = J_{\mathrm{M}} + \frac{J_{\mathrm{L}} + J_m}{i^2}$$

The mass m also causes the load torque mgr on the rope drum. Based on (3.8), the equivalent load torque seen by the motor is

$$\tau_{\mathrm{L}} = \frac{mgr}{i}$$

It is worth noticing that the mass m affects both the total inertia J and the load torque τ_{L}. Furthermore, as an example, if the gear ratio is $i = 10$, the motor sees only a hundredth of the load inertia and a tenth of the load torque.

Chapter 4

Thermal Analysis

This chapter aims to give an overview of losses and heat transfer in electric machines and power converters. First, the main loss components are introduced. The dependency between the losses and the load is explained. Then, an elementary heat transfer model is introduced. The response of the temperature rise to loss steps is considered in order to understand the concept of thermal time constant. The selection of an electric machine for a periodic duty cycle based on the average temperature rise (corresponding to the rms or effective torque) is discussed. Finally, the differences between the time constants of electric machines and power converters are discussed.

4.1   Losses

The power losses in an electric device turn into heat, which has to be transferred from the device to its surroundings. The power losses serve as an input to the thermal model, which is used to predict the temperature rise of the device.

4.1.1   Electric Machines

Figure 4.1 shows the steady-state model of a conceptual electric machine, which includes both resistive losses and core losses.[1] The thermal time constants of electrical machines are typically much longer than the electrical time constants. Hence, in thermal analysis, losses can typically be modeled assuming a quasi-steady state, where electrical transients are omitted. The core-loss resistance R_{Fe} is typically very large. Hence, the core losses can typically be omitted from dynamic models and control methods, since their effect on the current i and the torque τ_{M} is minor.

   The resistive losses (also known as copper losses or Joule losses) occur in conductors. They are proportional to the square of the current,

$$p_{\mathrm{Cu}} = Ri^2 \approx R\frac{\tau_{\mathrm{M}}^2}{k^2} \tag{4.1}$$

where the latter form shows the dependency on the electromagnetic torque τ_{M} and the flux factor k (i.e., the level of magnetization or the flux density). The flux

---

[1]This model corresponds to the DC machine model. AC machines have the same loss components and similar dependencies.
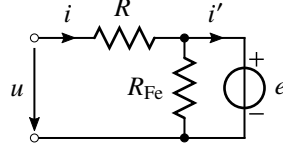
Figure 4.1: Steady-state model of a conceptual electric machine including core losses. Two poles are assumed, thus ω_M represents both electrical and mechanical rotor speed. The back-emf is $e = k\omega_M$ and the electromagnetic torque is $\tau_M = ki'$.
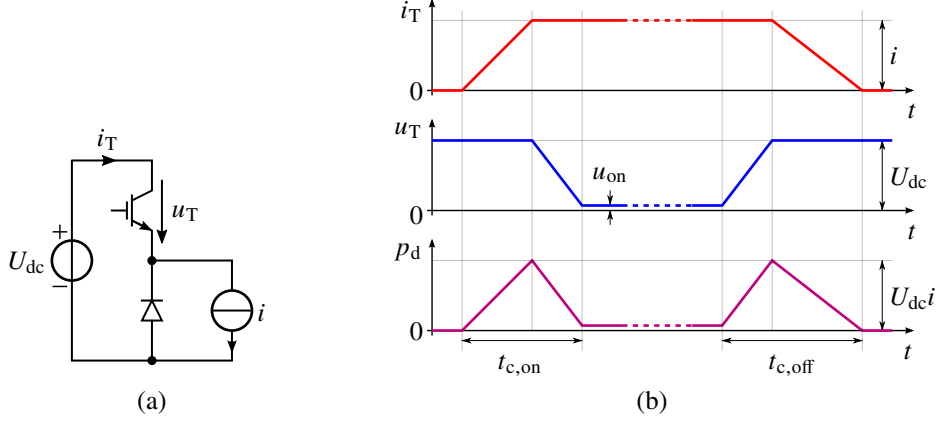

Figure 4.2: Losses in a power semiconductor switch: (a) buck converter; (b) conceptual switching waveforms.

factor is typically kept constant in the base-speed region and reduced inversely proportional to the rotor speed in the field-weakening region. It is to be noted that the winding resistance R depends on the temperature (by about 0.4%/K).

Core losses (also known as iron losses) are caused by eddy currents and hysteresis in the magnetic core. The eddy-current losses are proportional to the square of the frequency, while the hysteresis losses are proportional to the frequency. Both are proportional to the square of the flux density. In accordance with Figure 4.1, the core losses can be expressed as

$$p_{Fe} = \frac{e^2}{R_{Fe}} = \frac{k^2\omega_M^2}{R_{Fe}} \tag{4.2}$$

If the resistance R_{Fe} is constant, the losses predicted by (4.2) correspond to eddy-current losses. To include also hysteresis losses, a nonlinear core-loss resistance is needed,

$$R_{Fe}(\omega_M) = \frac{|\omega_M|}{\Gamma_{Hy} + G_{Ft}|\omega_M|} \tag{4.3}$$

which results in $p_{Fe} = G_{Ft}k^2\omega_M^2 + \Gamma_{Hy}k^2|\omega_M|$. Hence, the parameters G_{Ft} and Γ_{Hy} define the amount of the eddy-current and hysteresis losses, respectively. Typically, the majority of the core losses are hysteresis losses in the full-field region.

Other electromagnetic losses are known as additional losses. Furthermore, mechanical losses occur due to friction and windage. Typically, these loss components are comparatively small.

4.1.2 Power Converters

The main power losses in power semiconductors are switching and conduction losses [4]. The switching losses are caused by the finite switching speed and the conduction losses are caused by nonzero on-state voltage. As an example, consider a buck converter shown in Figure 4.2(a), consisting of a transistor and a diode. The transistor could be an insulated-gate bipolar transistor (IGBT) or a metal-oxide-semiconductor field-effect transistor (MOSFET). The converter is fed from the DC voltage source U_{dc}. The load is modeled as the DC current sink i, representing a generic inductive load in short time intervals. Real diodes also have switching and conduction losses, but, for simplicity, an ideal diode is assumed in the following.

Figure 4.2(b) shows linearized switching waveforms of the voltage u_T and the current i_T for the transistor. The instantaneous power loss $p_d = u_T i_T$ is also shown. Initially, the transistor is in the off-state, and the current i thus flows through the diode. After the transistor is controlled to turn on, its current i_T starts to increase. The diode becomes reverse biased after the transistor current i_T has reached the load current i, after which the voltage u_T across the transistor starts to decrease towards the on-state voltage u_{on}. Consequently, during the turn-on crossover interval $t_{c,on}$, both voltage and current are nonzero, which results in the switching loss. The situation is similar also during the turn-off crossover interval $t_{c,off}$. The turn-on and turn-off crossover intervals are typically in the range of a few hundreds of nanoseconds (or even less for wide-bandgap semiconductors).

The transistor is repetitively switched. During one switching period T_{sw}, the transistor is turned on and off. The switching frequency $f_{sw} = 1/T_{sw}$ describes the number of such on-and-off switching events per second. Consequently, the switching losses averaged over the switching period are

$$p_{sw} = \frac{1}{2} U_{dc} i (t_{c,on} + t_{c,off}) f_{sw} \tag{4.4}$$

The switching losses are proportional to the switching frequency, which varies depending on the application and the type of power semiconductors. In machine drives equipped with silicon IGBTs, a typical range is $f_{sw} = 1\ldots 20$ kHz, corresponding to the switching periods $T_{sw} = 50\ldots 1\,000$ μs. It is worth noticing that the switching period is much longer than the crossover intervals. Furthermore, the shorter the crossover intervals, the lower are the switching losses.

In the on-state, conduction losses occur in the transistor due to its voltage drop, which can be approximated as $u_{on} = U_{th} + R_{on} i$, where U_{th} is the threshold voltage and R_{on} is the on-state resistance. Hence, the conduction losses averaged over the switching period are

$$p_{on} = \frac{t_{on}}{T_{sw}} (U_{th} i + R_{on} i^2) \tag{4.5}$$

where t_{on}/T_{sw} is the duty ratio, i.e., the ratio of the on-state duration over the whole switching period.

The switching and conduction losses in three-phase voltage-source converters behave similarly as presented above. The losses can be evaluated by means of either simulations or analytical models [5].
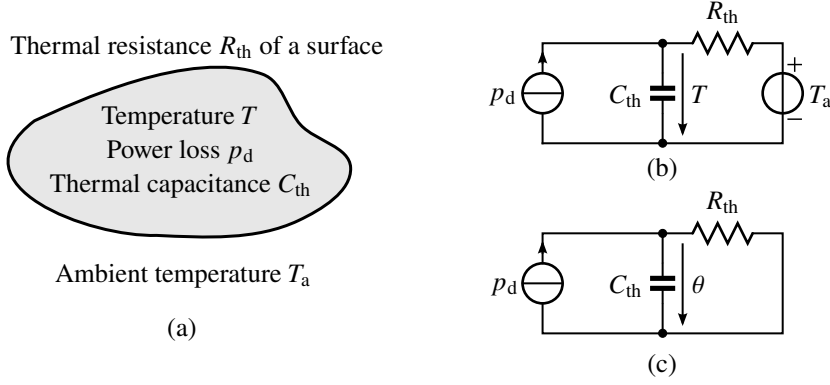
Figure 4.3: Elementary heat transfer model: (a) homogenous solid body with spatially uniform temperature T; (b) thermal equivalent circuit; (c) thermal equivalent circuit expressed using the temperature rise $\theta = T - T_a$.

4.2 Basics of Heat Transfer

4.2.1 Lumped Element Thermal Model

Consider an elementary heat transfer model, shown in Figure 4.3(a). The homogenous body has spatially uniform temperature T. The ambient temperature T_a is assumed to be constant. The body has internal power dissipation p_d. The thermal resistance (K/W) of the surface is [6]

$$R_{th} = \frac{1}{\alpha_{th} S} \tag{4.6}$$

where α_{th} is the heat transfer coefficient (W/K/m^2) and S is the surface area of the body. The thermal resistance is inversely proportional to the surface area. Hence, the larger the surface area, the smaller the thermal resistance.

The thermal capacitance (J/K) of the body is

$$C_{th} = c_p m \tag{4.7}$$

where c_p is the specific heat capacity (J/K/kg) and m is the mass of the body. The specific heat capacity is the amount of heat required to raise the temperature of one kilogram of the body by one kelvin. The thermal capacitance of the body is proportional to the mass, i.e., the larger the mass, the larger the thermal capacitance.

The temperature difference between the body and its ambient causes heat transfer through the surface. The heat transfer rate is proportional to the temperature rise

$$\theta = T - T_a \tag{4.8}$$

which is analogous to the voltage in electrical circuits. Based on the overall power balance, the heat stored in the body has to be equal to the heat generated inside the body minus the heat removed through the surface, i.e.,

$$C_{th} \frac{dT}{dt} = p_d - \frac{1}{R_{th}} (T - T_a) \tag{4.9}$$
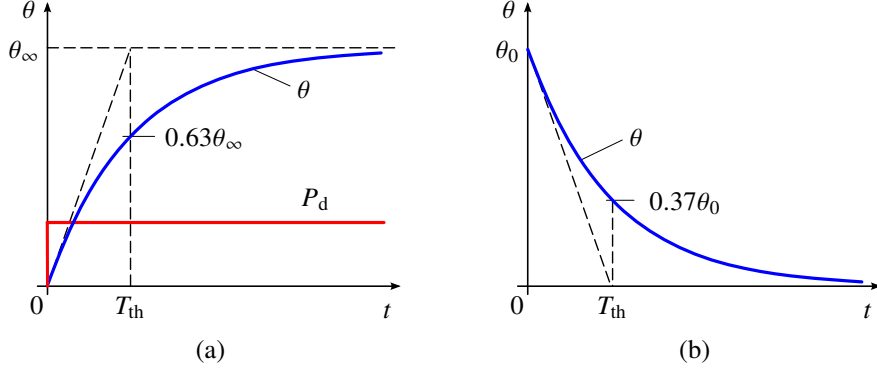
27

Figure 4.4: Temperature rise in response to a loss step: (a) from 0 to P_d; (b) from P_d to 0.

Figure 4.3(b) shows the corresponding thermal equivalent circuit. The model can be expressed in a simpler form by using the temperature rise,

$$C_{th}\frac{d\theta}{dt} = p_d - \frac{1}{R_{th}}\theta \tag{4.10}$$

whose thermal equivalent circuit is depicted in Figure 4.3(c). This model is analogous to that of an electric circuit consisting of a current source, a capacitor, and a resistor connected in parallel.

4.2.2   Response to Loss Steps

The thermal model (4.10) can be expressed in the Laplace domain as

$$\frac{\theta(s)}{p_d(s)} = \frac{R_{th}}{1 + T_{th}s} \tag{4.11}$$

where $T_{th} = R_{th}C_{th}$ is the thermal time constant. This transfer function corresponds to a first-order low-pass filter, whose DC gain is R_{th} and time constant is T_{th}, see Appendix A.1. The response to the loss step can be solved as

$$\theta(t) = \theta_0 + (\theta_\infty - \theta_0)\left(1 - e^{-t/T_{th}}\right) \tag{4.12}$$

where $\theta_0 = \theta(0)$ is the initial temperature rise, $\theta_\infty = R_{th}P_d$ is the temperature rise in the steady state, and P_d is the magnitude of the loss step. Figure 4.4(a) shows the temperature rise in response to a loss step from zero to P_d. Similarly, Figure 4.4(b) shows the temperature rise in response to a loss step from P_d back to zero.

4.2.3   Heat Transfer Mechanisms

The heat transfer may happen by conduction, convection, and radiation, as illustrated in Figure 4.5. The conduction refers to the heat transfer between objects that are in physical contact. The convection refers to the heat transfer due to natural or forced motion of fluid (typically air or liquid). The radiation refers to the heat transfer due to electromagnetic radiation.

The heat transfer coefficient α_{th} in (4.6) depends on the heat transfer mechanism. The *conduction* heat transfer coefficient $\alpha_{th} = \lambda/\ell$ is inversely proportional
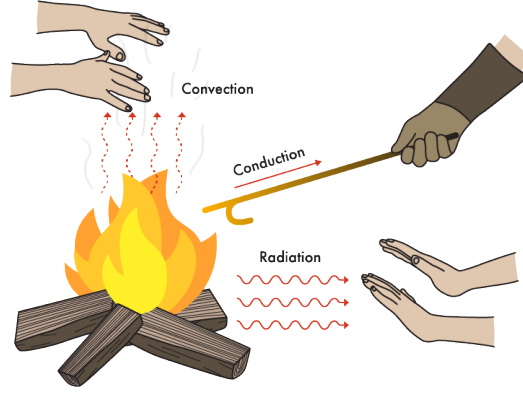
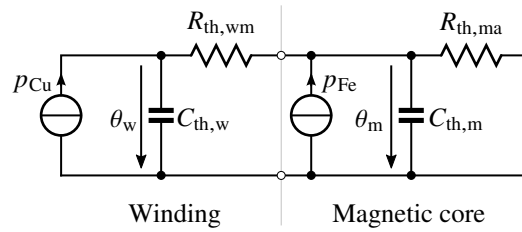Figure 4.5: Heat transfer mechanisms (source: https://en.wikipedia.org/wiki/Heat_transfer, license: https://creativecommons.org/licenses/by-sa/4.0/deed.en).

Figure 4.6: Second-order thermal model of an electric machine.

to the thickness ℓ of the surface. The thermal conductivity λ is analogous to the electrical conductivity. As an example, the power semiconductor losses are transferred mainly in a conductive manner from the switching junction to the heat sink.

In radiation, the transferred heat is proportional to the fourth power of the absolute temperature. Correspondingly, the *radiation* heat transfer coefficient can be expressed as $\alpha_{th} = \varepsilon\sigma(T^4 - T_a^4)/(T - T_a)$, where σ is the Stefan-Boltzmann constant, $0 \leq \varepsilon \leq 1$ is the emissivity, and T_a refers to the temperature of the absorbing surface. In electric machines, the radiation heat transfer coefficient is around $\alpha_{th} = 6$ W/K/m^2 with a typical temperature difference of 40 K between the outer surface and the surroundings [7].

The *convection* can be split into natural and forced convection. As an example of natural convection, warm air rises up from a hot surface and is replaced by cooler ambient air, causing heat transfer along with the outgoing air. In forced convection, the fluid is forced to flow by means of a fan or a pump. The heat transfer coefficient for forced convection is typically much larger than that for free convection. According to [6], a typical heat transfer coefficient range is $\alpha_{th} = 2\dots25$ W/K/m^2 for natural convection, $\alpha_{th} = 25\dots250$ W/K/m^2 for forced-air cooling, and $\alpha_{th} = 100\dots20\,000$ W/K/m^2 for liquid cooling. In electric machines, the convection heat transfer coefficient depends on the operating conditions, e.g., the rotor speed. It is also worth noticing that the cooling fan of a machine may have its own motor or, alternatively, the fan may be connected to the shaft of the machine. In the latter case, cooling of the machine becomes poor at low rotor speeds.
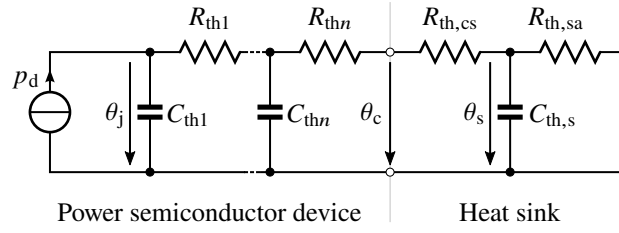
Figure 4.7: Thermal model of a power semiconductor device and its heat sink. The dissipated power consists of switching losses and conduction losses, $p_\mathrm{d} = p_\mathrm{sw} + p_\mathrm{on}$.

4.3 Thermal Models

4.3.1 Electric Machines

The temperature rise of winding insulations in electric machines is the limited. The allowed maximum temperature rise depends on the winding insulation class (e.g., IEC class B allows a temperature rise of 80 K at a maximum ambient temperature of 40°). The increase of 10 K in the operating temperature may approximately halve the lifetime of the insulations.

As an example, Figure 4.6 shows a second-order thermal model for predicting the average temperature rise of the winding [8]. This model can be generalized to different machine types. It has two inputs: resistive losses p_Cu and other losses p_Fe. The thermal resistance between the winding and the magnetic core is $R_\mathrm{th,wm}$. The thermal resistance between the magnetic core and the ambient is $R_\mathrm{th,ma}$. The resistance $R_\mathrm{th,ma}$ is related to conduction from the magnetic core to the external frame and, further, to convection (natural and forced) from the frame to the ambient. Consequently, $R_\mathrm{th,ma}$ depends on the operating conditions, e.g., the rotor speed. The thermal capacitances $C_\mathrm{th,w}$ and $C_\mathrm{th,m}$ are for the winding and the magnetic core, respectively.

The second-order thermal model can be implemented in a control system of an electric machine drive. Furthermore, its parameters can be experimentally identified. The real-time winding temperature estimation allows to improve the overload-capability of a machine. The second-order model can be understood to consist of two first-order thermal models (4.10) connected in series.

The first-order model (4.10) can be used to approximate the second-order model. A dominant thermal time constant increases with the machine size (from a few minutes to hours in typical industrial motors). The time constant may depend on the operating speed due to the convection heat transfer coefficient.

4.3.2 Power Converters

Similar lumped capacity thermal models can be used for power converters. As an example, Figure 4.7 shows a typical thermal model. The thermal impedance of the power semiconductor device is modeled using the nth-order Cauer network, where θ_j and θ_c are the junction and case temperature rises, respectively. The thermal capacitance of the heat sink is denoted by $C_\mathrm{th,s}$ and the thermal resistance between the sink and the ambient by $R_\mathrm{th,sa}$. The switching and conduction losses $p_\mathrm{d} = p_\mathrm{sw} + p_\mathrm{on}$ are obtained from the electrical model of the power device. It is to be noted that heat dissipation depends on the junction temperature.

As in the case of electric machines, the first-order model (4.10) can be used to approximate the higher-order model. It is important to notice that the dominant thermal time constant of power devices is much shorter (typically only seconds or tens of seconds) than that of electric machines.

4.4 Selection of an Electric Machine

In the following, the conceptual model of an electric machine shown in Figure 4.1 is assumed. To simplify the analysis, the total losses p_d are assumed to be solely resistive.[2] Furthermore, the first-order thermal model is assumed.

4.4.1 Continuous Duty

The maximum allowable temperature rise of the windings is limited. The rated values of an electric machine inherently include information of the thermal limits. Standard machines are rated for continuous duty (S1 duty), in which a machine works at constant load τ_N and constant speed ω_N, where the subscript N refers to rated values. In continuous duty, resistive losses are constant, $p_{dN} = Ri_N^2$. A thermal equilibrium is reached with the temperature rise $\theta_N = R_{th}p_{dN}$.

In other words, the rated values define a steady-state operating point, in which the machine can be operated continuously. The rated values are typically given in a catalog (or a data sheet) and on the machine nameplate. For a given continuous-duty application, a suitable machine can be easily selected based on the steady-state operating point and rated values of available machines.

4.4.2 Periodic Duty

The load torque and the rotor speed may vary periodically in many applications. Consequently, resistive losses $p_d = Ri^2$ vary as a function of time. S1-type standard machines are often selected for periodic duty as well. For this purpose, the periodic duty has to be transformed into a thermally equivalent S1 duty. The maximum temperature rise θ_{max} should be roughly the same as the rated temperature rise θ_N. A too low temperature rise may lead to a big and expensive machine. A too high temperature rise shortens the lifetime of the machine.

If the thermal time constant T_{th} of a machine is much longer than the cycle length T, the maximum temperature rise θ_{max} is in the steady state approximately equal to the average temperature rise $\overline{\theta}$ over the cycle. The average temperature rise over the period T is

$$\overline{\theta} = \frac{1}{T} \int_0^T \theta \, dt \tag{4.13}$$

The average losses over the period T are

$$\overline{p}_d = \frac{1}{T} \int_0^T p_d \, dt = \frac{1}{T} \int_0^T Ri^2 \, dt = Ri_{rms}^2 \tag{4.14}$$

---

[2]It can be shown that this assumption results in a more conservative selection criterion as compared to the case where the total losses are separated into the resistive and core losses.
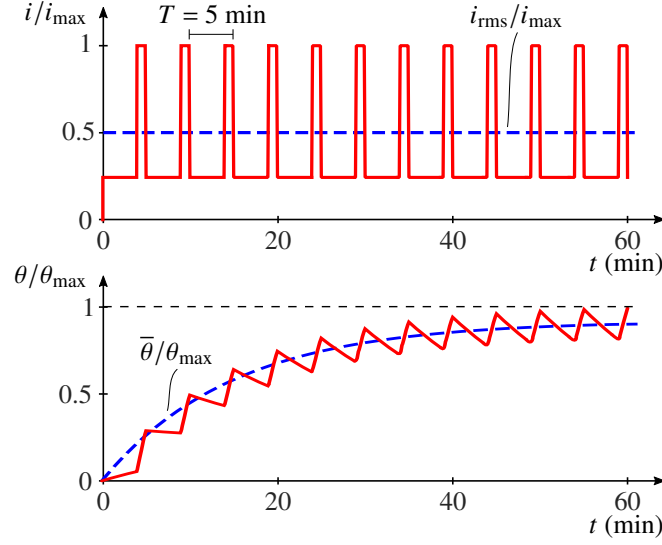
Figure 4.8: Example of periodic duty and temperature rise. The thermal time constant is $T_{\text{th}} = 15$ min. The cycle length $T = 5$ min, where $i = 0.25i_{\text{max}}$ for 4 min and $i = i_{\text{max}}$ for 1 min. The resulting rms current is $i_{\text{rms}} = 0.5i_{\text{max}}$.

i.e., they depend on the rms current

$$i_{\text{rms}} = \sqrt{\frac{1}{T}\int_0^T i^2 \mathrm{d}t} \tag{4.15}$$

The rated temperature rise $\theta_N = R_{\text{th}}p_{\text{dN}} = R_{\text{th}} \cdot (Ri_N^2)$ in the S1 duty is used as a reference case. The average temperature rise in a periodic duty is

$$\overline{\theta} = R_{\text{th}}\overline{p}_{\text{d}} = R_{\text{th}} \cdot (Ri_{\text{rms}}^2) \tag{4.16}$$

Therefore, the condition $\overline{\theta} < \theta_N$ leads to the selection criterion

$$i_N > i_{\text{rms}} \tag{4.17}$$

i.e., the rated current i_N of an S1-type machine should be larger than the rms current of the periodic duty.

Figure 4.8 show an example of a periodic duty. The thermal time constant is $T_{\text{th}} = 15$ min and the cycle length $T = 5$ min. It can be noticed that the maximum temperature rise θ_{max} is approximately equal to the average temperature rise $\overline{\theta}$ in the steady state, even though the thermal time constant T_{th} is only three times longer than the cycle length T in this example.

In the following, the criterion (4.17) is analyzed separately in the full-field and field-weakening regions. The goal is to express the criterion by means of the torque and power profiles of the periodic duty.

Full-Field Region

The machine is assumed to operate only in the full-field region, i.e., the rotor speed is below the rated, $|\omega_M| \leq \omega_N$. The flux factor k is kept constant, $k = k_N$. The current is proportional to the torque, $i = \tau_M/k_N$. Hence, the rms current

(4.15) can be rewritten as

$$i_{\mathrm{rms}} = \frac{1}{k_{\mathrm{N}}} \sqrt{\frac{1}{T} \int_0^T \tau_{\mathrm{M}}^2 \, \mathrm{d}t} = \frac{1}{k_{\mathrm{N}}} \tau_{\mathrm{M,rms}} \tag{4.18}$$

Since the rated current is $i_{\mathrm{N}} = \tau_{\mathrm{N}}/k_{\mathrm{N}}$, the selection criterion (4.17) can be equivalently expressed by means of the electromagnetic torque, $\tau_{\mathrm{N}} > \tau_{\mathrm{M,rms}}$. This form is practical since the rms torque can be computed based on the known electromagnetic torque profile (further obtained using the speed and load torque profiles and the equation of motion). Naturally, the definition of the rms torque corresponds to (4.15).

Field-Weakening Region

The machine is assumed to operate only in the field-weakening region, i.e., the rotor speed is above the rated, $|\omega_{\mathrm{M}}| > \omega_{\mathrm{N}}$. The flux factor k is reduced inversely proportional to the rotor speed, $k = k_{\mathrm{N}}\omega_{\mathrm{N}}/|\omega_{\mathrm{M}}|$. Hence, the current in the field-weakening region is proportional to the mechanical power

$$i = \frac{\tau_{\mathrm{M}}}{k} = \frac{|\omega_{\mathrm{M}}|}{k_{\mathrm{N}}\omega_{\mathrm{N}}} \tau_{\mathrm{M}} = \frac{|p_{\mathrm{M}}|}{k_{\mathrm{N}}\omega_{\mathrm{N}}} \operatorname{sign}(\tau_{\mathrm{M}}) \tag{4.19}$$

In this case, the rms current in (4.15) can be expressed as

$$i_{\mathrm{rms}} = \frac{1}{k_{\mathrm{N}}\omega_{\mathrm{N}}} \sqrt{\frac{1}{T} \int_0^T p_{\mathrm{M}}^2 \, \mathrm{d}t} = \frac{1}{k_{\mathrm{N}}\omega_{\mathrm{N}}} p_{\mathrm{M,rms}} \tag{4.20}$$

Consequently, the selection criterion (4.17) can be expressed equivalently as $\tau_{\mathrm{N}} > p_{\mathrm{M,rms}}/\omega_{\mathrm{N}}$.

If both full-field and field-weakening regions are used, their selection criteria can be combined. The machine is assumed to operate in the full-field region at $t = 0 \ldots T_1$ and in the field-weakening region at $t = T_1 \ldots T$. The effective torque can be defined as

$$\tau_{\mathrm{M,ef}} = \sqrt{\underbrace{\frac{1}{T} \int_0^{T_1} \tau_{\mathrm{M}}^2 \, \mathrm{d}t}_{|\omega_{\mathrm{M}}| \le \omega_{\mathrm{N}}} + \underbrace{\frac{1}{T} \frac{1}{\omega_{\mathrm{N}}^2} \int_{T_1}^T p_{\mathrm{M}}^2 \, \mathrm{d}t}_{|\omega_{\mathrm{M}}| > \omega_{\mathrm{N}}}} \tag{4.21}$$

The selection criterion (4.17) can be equivalently expressed as $\tau_{\mathrm{N}} > \tau_{\mathrm{M,ef}}$. The effective torque can be calculated from the speed and load torque profiles, such as the example profiles in Figure 4.9.

These selection criteria take in the account only the thermal balance based on the average temperature rise. The maximum torque and the maximum speed of an electric machine are also limited. It is important to check that the machine candidate is capable to produce the required torque at all speeds. Furthermore, some margin may be used, e.g., $\tau_{\mathrm{N}} > 1.1\tau_{\mathrm{M,ef}}$. If the length of the duty cycle is not significantly shorter than the thermal time constant, the selection should be based on the maximum temperature rise.
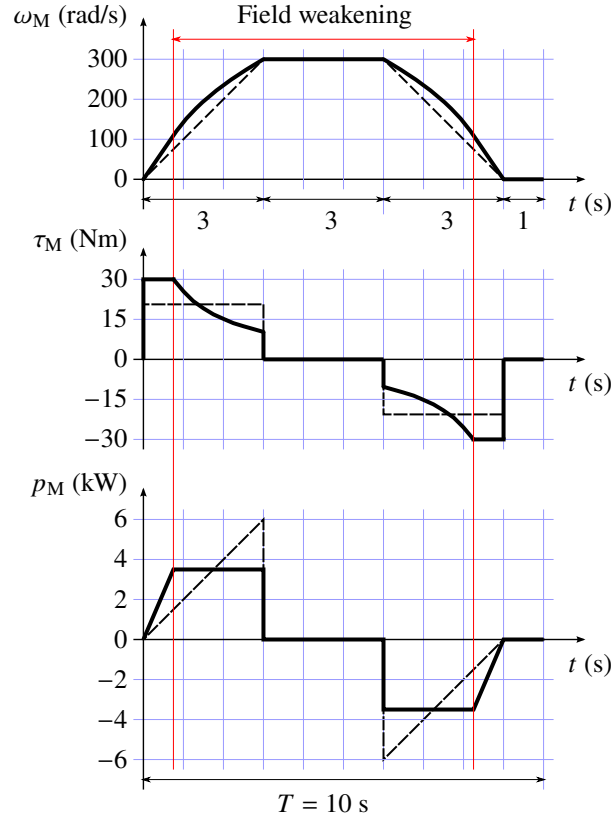
Figure 4.9: Comparison of a full-field drive (dashed) and a field-weakening drive (solid). The acceleration time is the same for both drives. The rated speed of the field-weakening drive is $\omega_N = 120$ rad/s. The load torque $\tau_L = 0$ is assumed.

Comparison of Full-Field and Field-Weakening Drives

Figure 4.9 shows examples of periodic duty cycles, one for a full-field drive and the other for a field-weakening drive. The acceleration and deceleration times are the same for both drives. It can be seen that the maximum power of the field-weakening drive is much smaller than that of the full-field drive. Consequently, a smaller (and cheaper) power converter can be selected for the field-weakening drive, while a larger electric machine is needed. Hence, field weakening allows to optimize the size and the cost of the machine drive system.

In the example sequence shown in Figure 4.9, the field-weakening drive travels a longer distance (which corresponds to the area below the rotor speed curve) than the full-field drive. If the equal distances were required, the needed maximum torque (and the size of the machine) of the field-weakening drive would be smaller than in the case of the equal acceleration times.

4.5 Selection of a Power Converter

Dominant thermal time constants of power semiconductor devices are much shorter than those of electric machines. Consequently, the power converter has to be typically selected based on the maximum current of a periodic duty. The size and the cost of power converters is approximately proportional to the product of the maximum current and the maximum voltage, which do not need to appear
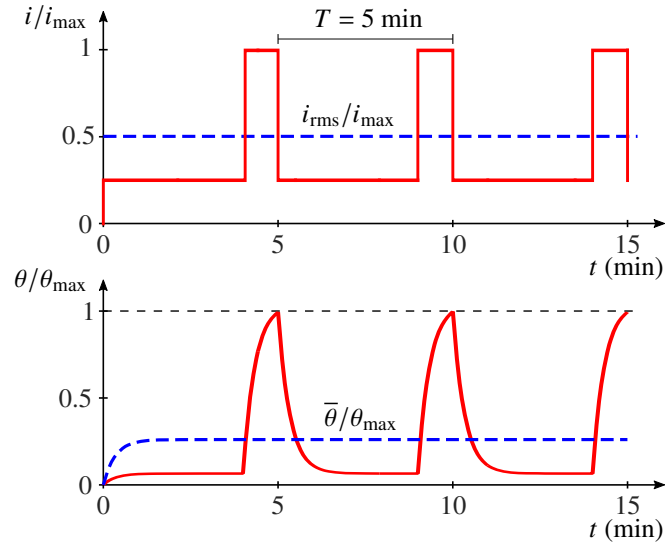
Figure 4.10: Example of a temperature rise inside a power converter. The thermal time constant of the converter is $T_{th} = 20$ s and the cycle length $T = 5$ min.

at the same time.

Figure 4.10 shows an example of a temperature rise inside a power converter. The thermal time constant of the converter is $T_{th} = 20$ s and the cycle length is $T = 5$ min, i.e., the thermal time constant T_{th} is much shorter than the cycle length T. The maximum temperature rise θ_{max} is approximately four times the average temperature rise $\bar{\theta}$. Clearly, the converter selection should be based on the maximum current i_{max} instead of the rms current i_{rms}.

Chapter 5

Open-Loop Dynamics

This chapter examines the open-loop dynamics of an electric machine, which consists of electrical and mechanical subsystems. The responses of the speed and current to the voltage and load torque inputs are analyzed, which helps to understand the dynamic behavior of the machine. This chapter also introduces some system modeling tools, which are commonly used in the field of electric machine drives, e.g., block diagrams, transfer functions, and state-space representations. The links between these tools are highlighted. Time-scale separation between electrical and mechanical subsystems is also presented. A DC machine is used as an example, but the modeling methods are applicable to other systems as well.

5.1 Dynamic Model

5.1.1 State Equations

Figure 5.1(a) illustrates the electrical and mechanical subsystems of a DC machine. These subsystems have been separately studied in Chapters 2 and 3. To highlight the analogy between the electrical and mechanical subsystems, the viscous friction coefficient B is included in the load torque $\tau_L = B\omega_M + \tau_C$, where
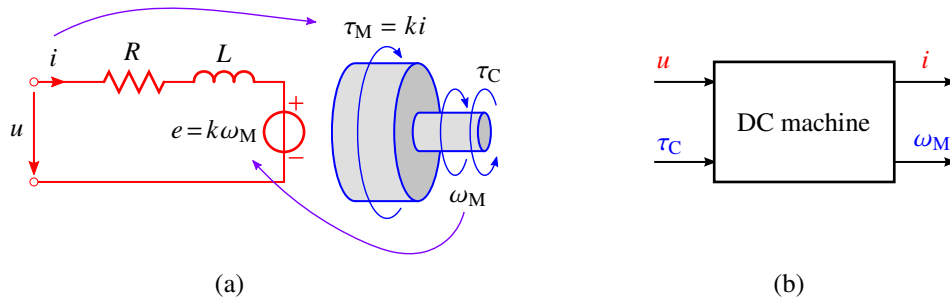

Figure 5.1: Electrical and mechanical dynamics are coupled: (a) electrical and mechanical subsystems; (b) block diagram.
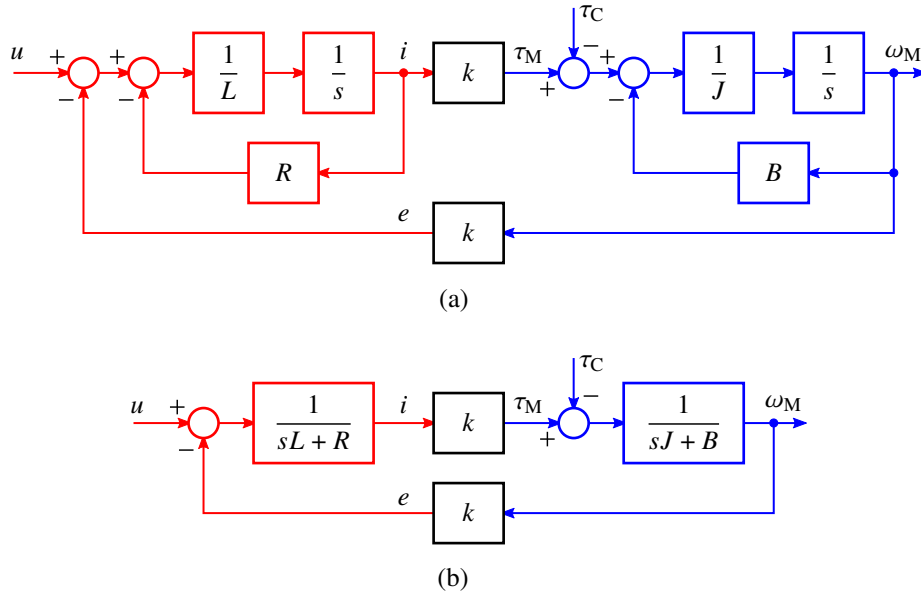
(a)

(b)

Figure 5.2: Block diagrams using: (a) integrators; (b) first-order low-pass filters. The electrical subsystem is shown in red and the mechanical subsystem in blue.

τ_C refers to the external load torque. The corresponding state equations are

$$L\frac{di}{dt} = -Ri - k\omega_M + u \tag{5.1a}$$

$$J\frac{d\omega_M}{dt} = ki - B\omega_M - \tau_C \tag{5.1b}$$

where i and ω_M are the state variables. The flux factor k couples the electrical and mechanical dynamics through the back-emf $e = k\omega_M$ and the electromagnetic torque $\tau_M = ki$. For simplicity, the flux factor k will be assumed to be constant. Under this assumption, the system is linear.

5.1.2 Block Diagrams

Using the state equations (5.1), the block diagram shown in Figure 5.2(a) can be directly drawn, see also Section 2.3.2. Figure 5.2(b) shows an alternative block diagram representation, where first-order low-pass filters are used instead of the integrators. Clearly, the current i and the rotor speed ω_M depend on the voltage u and the external load torque τ_C, i.e.,

$$i(s) = G_{iu}(s)u(s) + G_{i\tau}(s)\tau_C(s) \tag{5.2a}$$

$$\omega_M(s) = G_{\omega u}(s)u(s) + G_{\omega\tau}(s)\tau_C(s) \tag{5.2b}$$

where the four second-order transfer functions could be derived from the state equations (5.1) or from the block diagrams in Figure 5.2, see also Appendix A.4. The voltage u and the external load torque τ_C are the natural inputs of the system, as shown in Figure 5.1(b).

5.1.3 State-Space Representation

State-space representations are commonly used in the analysis and control design, see Appendix A.3. The state equations (5.1) can be collected into a matrix form,

which is known as a state-space representation,

$$\frac{d}{dt}\begin{bmatrix} i \\ \omega_M \end{bmatrix} = \underbrace{\begin{bmatrix} -\frac{R}{L} & -\frac{k}{L} \\ \frac{k}{J} & -\frac{B}{J} \end{bmatrix}}_{A} \begin{bmatrix} i \\ \omega_M \end{bmatrix} + \underbrace{\begin{bmatrix} \frac{1}{L} \\ 0 \end{bmatrix}}_{b_u} u + \underbrace{\begin{bmatrix} 0 \\ -\frac{1}{J} \end{bmatrix}}_{b_\tau} \tau_C \tag{5.3a}$$

where x is under the first bracket.

$$i = \underbrace{\begin{bmatrix} 1 & 0 \end{bmatrix}}_{c_i^T} x \tag{5.3b}$$

$$\omega_M = \underbrace{\begin{bmatrix} 0 & 1 \end{bmatrix}}_{c_\omega^T} x \tag{5.3c}$$

where A, b_u, b_τ, c_i^T, and c_ω^T are system matrices. The stability of a linear system depends on the eigenvalues of its system matrix A.

The transfer functions can be derived from the state-space representation, see Appendix A.3. As an example, the transfer function from $u(s)$ to $\omega_M(s)$ appearing in (5.2) is

$$G_{\omega u}(s) = \frac{\omega_M(s)}{u(s)} = c_\omega^T(sI - A)^{-1}b_u \tag{5.4}$$

Other transfer functions in (5.2) can be obtained in a similar manner. The poles of the transfer function are the eigenvalues of the system matrix A. Consequently, all four transfer functions in (5.2) have the same poles (but different zeros).

5.1.4 Transfer Functions and Their Properties

As examples, the transfer functions from the voltage to the rotor speed and to the current are considered in more detail. The transfer function from the voltage u to the rotor speed ω_M is

$$G_{\omega u}(s) = \frac{\frac{k}{JL}}{s^2 + \left(\frac{R}{L} + \frac{B}{J}\right)s + \frac{k^2 + RB}{LJ}} = \frac{K\omega_0^2}{s^2 + 2\zeta\omega_0 s + \omega_0^2} \tag{5.5}$$

where the denominator in the last form corresponds to a common generic form used for second-order systems. The undamped natural frequency, damping ratio, and DC gain, respectively, are

$$\omega_0 = \sqrt{\frac{k^2 + RB}{LJ}} \quad \zeta = \frac{1}{2\omega_0}\left(\frac{R}{L} + \frac{B}{J}\right) \quad K = \frac{k}{LJ\omega_0^2} = \frac{k}{k^2 + RB} \tag{5.6}$$

This transfer function can be recognized as a second-order low-pass filter. Consequently, general properties (e.g., step and frequency responses) of the second-order low-pass filter hold (see Appendix A.2). For example, if $\zeta < 1$ for given machine parameters, the system is underdamped and the step response has overshoot.

The transfer function from the voltage u to the current i is

$$G_{iu}(s) = \frac{\frac{1}{L}\left(s + \frac{B}{J}\right)}{s^2 + \left(\frac{R}{L} + \frac{B}{J}\right)s + \frac{k^2 + RB}{LJ}} \tag{5.7}$$
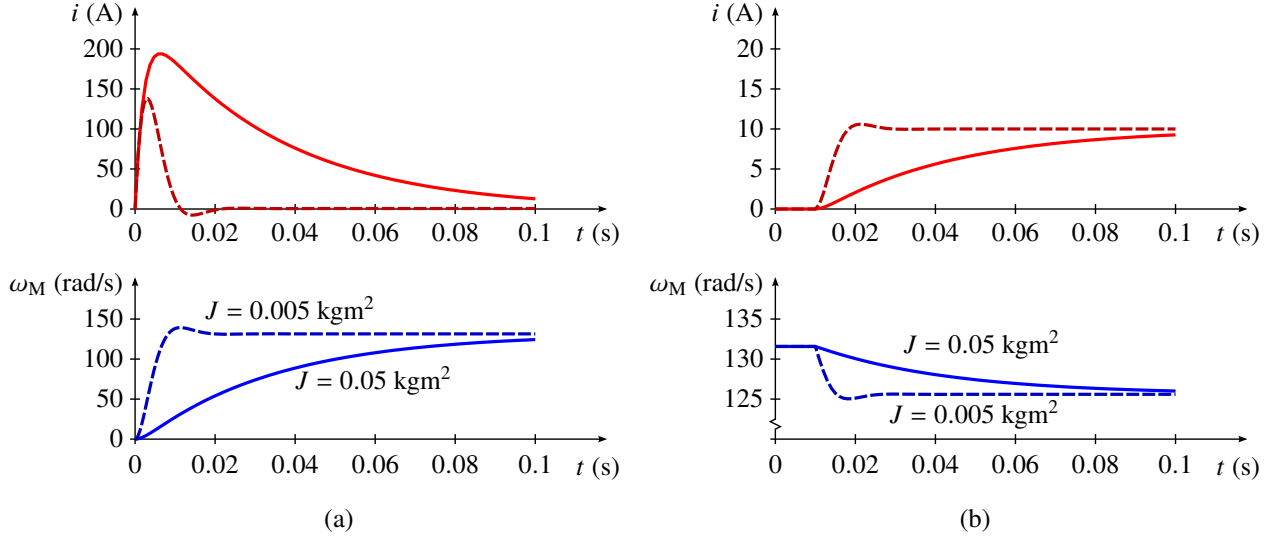
Figure 5.3: Step response of the current and the rotor speed: (a) rated voltage step; (b) load-torque step. Results for two inertia values are shown, $J = 0.005$ kgm^2 (dashed line) and $J = 0.05$ kgm^2 (solid line).

where the characteristic polynomial remains the same as in (5.5). This holds also for other transfer functions of the same system. The numerator, however, is different. The transfer function (5.7) has a zero at $s = -B/J$. Since the viscous damping B is typically small and the inertia J is large, the zero appears at a very low frequency. If $B = 0$, the zero is located at the origin, $s = 0$, which corresponds to derivative action.[1]

It is also worth noticing that if the inertia J approaches infinity, corresponding to constant ω_M, the transfer function (5.7) reduces to

$$G_{iu}(s) = \frac{1}{sL + R} \tag{5.8}$$

which equals the admittance of the electrical subsystem, denoted by $Y(s)$ in Section 2.3.2.

5.2 Simulation Examples

Time-domain responses of a small permanent-magnet DC machine are simulated in open loop, such that the terminal voltage and external load torque are varied. The rated values of the machine are: voltage $u_N = 110$ V; current $i_N = 10$ A; rotation speed $n_N = 1200$ r/min; and angular speed $\omega_N = 2\pi n_N = 125.7$ rad/s. The electrical parameters are $R = 0.5\ \Omega$, $L = 1$ mH, and $k = 0.836$ Vs. The viscous damping is $B = 0$ and two inertia values are used:

- $J = 0.05$ kgm^2 (corresponding to $\zeta = 2.11$ and $\omega_0 = 118$ rad/s)
- $J = 0.005$ kgm^2 (corresponding to $\zeta = 0.67$, $\omega_0 = 374$ rad/s)

Figure 5.3 shows simulation results. Figure 5.3(a) shows the responses of the current i and the rotor speed ω_M to the voltage step from zero to the rated

---

[1]If the viscous damping $B = 0$, the DC gain of (5.7) is zero, $G_{iu}(0) = 0$. According to (5.2a), this means that the steady-state current i depends only on the external load torque $\tau_C = \tau_L$.
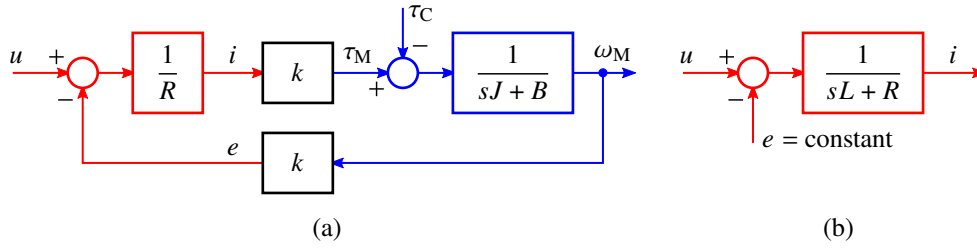
Figure 5.4: Block diagrams showing reduced-order models based on time-scale separation: (a) slow mechanical dynamics; (b) fast electrical dynamics. Notice that the electrical subsystem is modeled by means of its static DC gain in (a).

voltage. In other words, the results show what happens when the rated voltage is connected to the terminals of the machine. The load torque τ_M is zero. It can be seen that the current rises quickly and then decreases towards zero as the back-emf $e = k\omega_M$ increases. From the system theory perspective, this behaviour originates from the zero of (5.7). Furthermore, some overshoot in the speed response in the case of smaller inertia $J = 0.005\ \mathrm{kgm}^2$ can be seen, as expected. The very large current peak (almost 20 times the rated current for $J = 0.05\ \mathrm{kgm}^2$) is undesirable. To prevent this kind of overcurrent condition, the voltage should be ramped up slowly or closed-loop current control should be used, allowing to limit the current.

Figure 5.3(b) shows the load-torque-step response. The voltage u is kept constant at its rated value. The machine operates initially in the no-load condition. It can also be seen that the speed is larger than the rated speed in the no-load condition, as expected based on the steady-state torque-speed characteristic. After the rated load torque is applied, the speed decreases to its rated value.

5.3 Time-Scale Separation

In electric machines, the electrical and mechanical subsystems typically have different time scales. The electrical dynamics are typically much faster than the mechanical dynamics, which is due to the small inductance L and the large inertia J (as considered in per-unit values). This inherent time-scale separation allows to approximate the dynamics of the machine by considering the electrical or mechanical subsystems separately [9]. Furthermore, the time-scale separation is also underlying principle in typical cascaded control methods used in electric machine drives, as will be seen in the latter chapters.

Figure 5.4 shows the block diagrams of the DC machine assuming time-scale separation. When considering the *slow mechanical dynamics*, the quickly converging electrical dynamics may be approximated with the DC gain (or, equally, setting $L = 0$), see Figure 5.4(a). When considering the *fast electrical dynamics*, the slowly varying rotor speed may be assumed to be constant (or, equally, setting $J \to \infty$), see Figure 5.4(b).

Figure 5.5 shows the rated-voltage-step responses of the approximate reduced-order models corresponding to Figure 5.4. Figure 5.5(a) shows the response of the slow mechanical dynamics, while the electrical dynamics are approximated with the DC gain. The speed response of the reduced-order model match very well with that of the full-order model. Figure 5.5(b) shows the re-
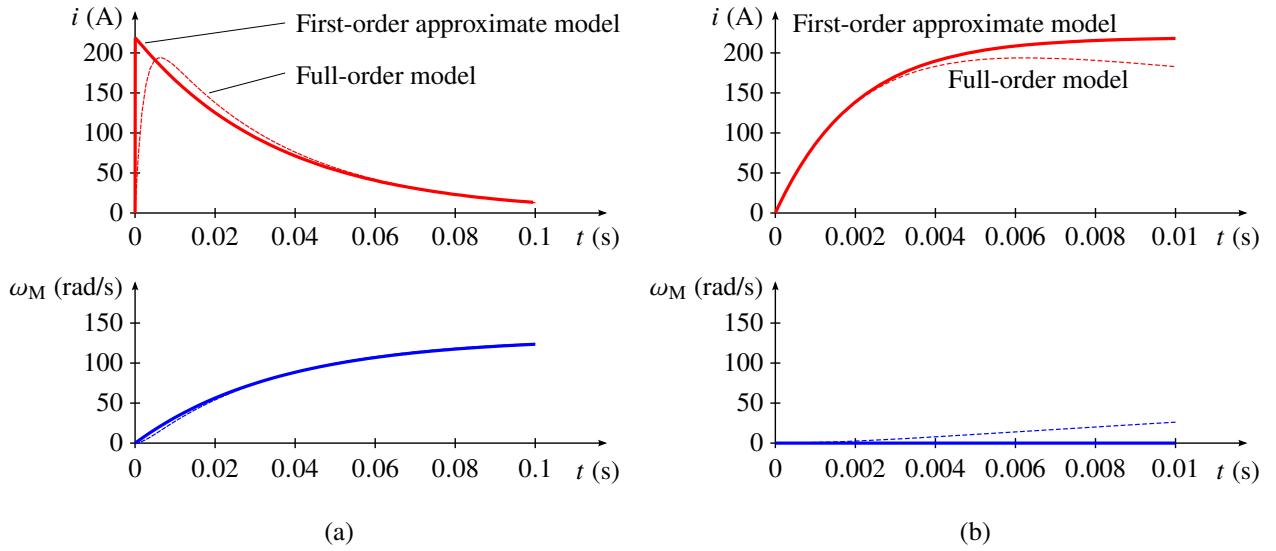
Figure 5.5: Rated-voltage step response of the reduced-order models: (a) slow mechanical dynamics; (b) fast electrical dynamics. Notice the different time scales in (a) and (b).

sponse of the fast electrical dynamics, while the speed is assumed to be constant (zero in this case). Again, the current response of the reduced-order model match very well with the full-order model in the beginning of the transient. As the speed starts to increase, the reduced-order and full-order models start to diverge, but this is not a problem in typical use cases of the reduced-order model (such as the analysis and design of current control).

41

Chapter 6

DC-DC Conversion

The aim of this chapter is to introduce the operating principles of DC-DC converters and pulse-width modulation (PWM) [4]. We start with a buck (step-down) converter and then proceed to a four-quadrant DC-DC converter (also known as a full bridge, an H-bridge, and a single-phase inverter). An equivalent circuit based on bi-positional switches is introduced. Finally, unipolar PWM is considered. These concepts help to understanding the operation of three-phase converters, whose topology and PWM methods are similar.

Figure 6.1 shows two example systems equipped with a DC-DC converter. The DC voltage U_{dc} can be supplied from a battery or a rectifier. The rectifier can be a passive diode bridge or an active front-end rectifier. The main task of the DC-DC converter is to generate the voltage u for the load. The load is modeled as an equivalent circuit shown in Figure 6.2(a), corresponding to the DC machine model studied in Chapter 2. Since the focus is on power-electronics circuits, the more compact symbol shown in Figure 6.2(b) is used to represent the load.

In DC machines, the adjustable voltage enables speed and torque control. The converter output voltage u should be adjustable in the range of $0 \ldots U_{dc}$ or $-U_{dc} \ldots U_{dc}$, depending on the application. Even though the load is assumed to be a DC machine, the same load model could also represent many other DC loads (such as an electrolyzer or a fuel cell behind an inductive filter).

In principle, the voltage u supplied to the load could be adjusted using a rheostat or a transistor in the linear region, as shown in Figure 6.3. However, this is not a good solution because of poor efficiency and high losses. As an example, consider that a linear regulator shown in Figure 6.3(b) feeds a 1-kW DC machine. The source voltage is assumed to be $U_{dc} = 100$ V and the machine is operated at 40% of the rated speed, i.e., the required regulator output voltage is approximately $u = 40$ V. Hence, the voltage across the transistor is $u_T = 60$ V. The efficiency of the linear regulator is only 40% in this operating point. If the
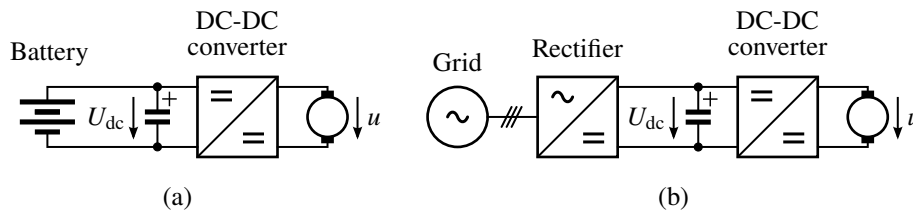

Figure 6.1: DC-DC converter fed from: (a) battery; (b) AC grid through rectifier.
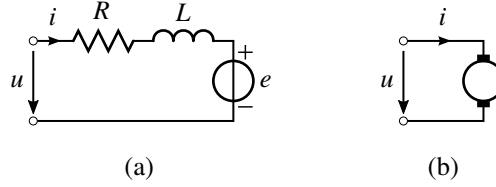
Figure 6.2: DC load model: (a) equivalent circuit; (b) corresponding DC machine symbol. Notice that the symbol in (b) should be understood as the compact representation of the inductive circuit in (a).
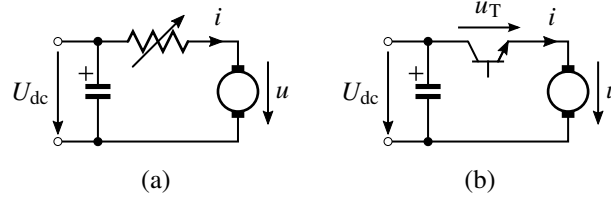

Figure 6.3: Linear voltage regulation: (a) rheostat; (b) transistor in the linear region.

machine produces the rated torque, corresponding to $i = 10$ A, the power loss in the transistor would be 600 W, which is far from tolerable.

6.1 Buck Converter

6.1.1 Operating Principle

Figure 6.4 shows the main circuit and example waveforms of a buck converter, whose transistor is switched on and off periodically so that the desired average voltage in the range $u = 0 \dots U_{dc}$ can be obtained. The current i of an inductive load must flow even when the transistor is switched off. Therefore, the free-wheeling diode is needed in the circuit for this purpose. In the on-state, see Figure 6.4(a), the voltage u_T across the transistor is very low (about 1 V). In the off-state, see Figure 6.4(b), the current i_T through the transistor is zero. Consequently, the power loss $p_d = u_T i_T$ in the transistor is very low (ideally zero). Due to the similar reasons, the losses in the freewheeling diode are also low. This principle of switch-mode conversion is used in power-electronic converters. Typical power semiconductor devices used as active switches in these converters are insulated-gate bipolar transistor (IGBT) and metal-oxide-semiconductor field-effect transistor (MOSFET). In machine drives, typical switching frequencies for IGBTs and MOSFETs are in the range $1 \dots 20$ kHz and $10 \dots 100$ kHz, respectively. Ideal switches will be assumed in the following.

6.1.2 Switching-Period Average and Duty Ratio

Figure 6.4(c) shows example waveforms of the buck converter. The converter output voltage u is a pulse wave, whose instantaneous value is either 0 or U_{dc}. The switching period is $T_{sw} = 1/f_{sw}$, where f_{sw} is the switching frequency. The average of the instantaneous voltage u over the switching period is

$$\overline{u} = \frac{1}{T_{sw}} \int_0^{T_{sw}} u \, \mathrm{d}t \qquad (6.1)$$
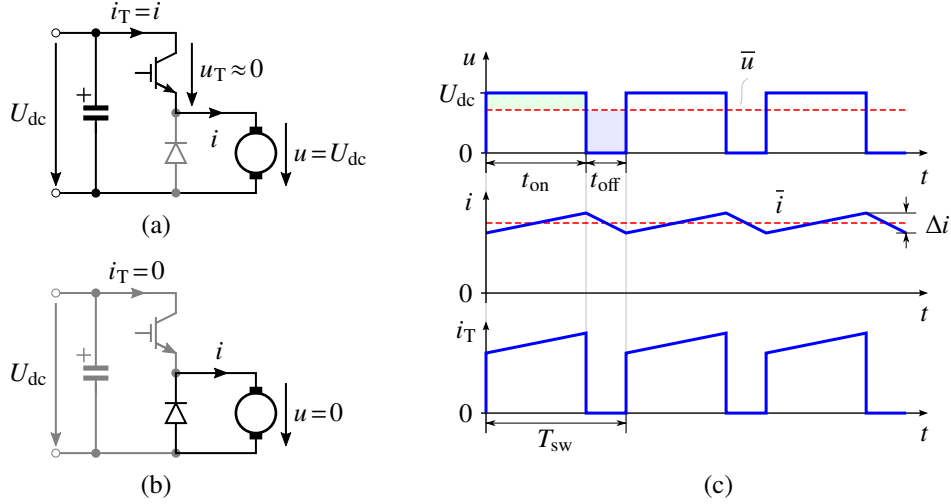
Figure 6.4: Buck converter: (a) on-state; (b) off-state; (c) waveforms. In (a) and (b), the grey lines show the inactive part of the circuit. In the on-state, the load current i goes through the transistor. In the off-state, the load current goes through the freewheeling diode. In (c), the dashed lines show the switching-cycle-averaged voltage $\bar{u}$ and current $\bar{i}$.

where the overline is used to mark the average value. Other averages are defined similarly. Applying (6.1) to the voltage waveform u shown in Figure 6.4(c) gives

$$\bar{u} = \frac{1}{T_{sw}} \int_0^{t_{on}} U_{dc} dt = \frac{t_{on}}{T_{sw}} U_{dc} = dU_{dc} \tag{6.2}$$

where constant U_{dc} is assumed. It can be seen that the average voltage $\bar{u}$ depends linearly on the duty ratio

$$d = \frac{t_{on}}{T_{sw}} \qquad 0 \le d \le 1 \tag{6.3}$$

which is the ratio of the on-time duration t_{on} to the switching period T_{sw}.

The dynamics of the load current i are governed by, see Figure 6.2(a),

$$L\frac{di}{dt} = u - e - Ri \tag{6.4}$$

where e is the back-emf and R is the resistance of the load. Hence, the instantaneous current at time t is

$$i(t) = i(0) + \frac{1}{L} \int_0^t (u - e - Ri)\, dt \tag{6.5}$$

In the periodic steady state, $i(T_{sw}) = i(0)$ holds, see Figure 6.4(c). Using (6.1) and (6.5), the average converter output voltage in the steady state is

$$\bar{u} = \bar{e} + R\bar{i} \tag{6.6}$$

6.1.3   Current Ripple

The pulse-wave voltage u causes a ripple in the current i, which is analyzed next. The maximum current occurs at the end of the on-state, and the minimum current

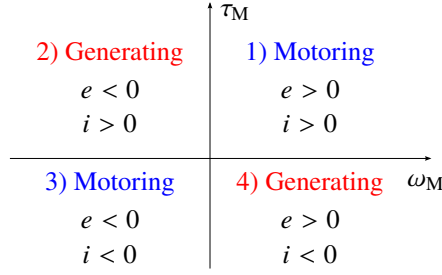|	τ_M	
2) Generating		1) Motoring
$e < 0$		$e > 0$
$i > 0$		$i > 0$
3) Motoring		4) Generating ω_M
$e < 0$		$e > 0$
$i < 0$		$i < 0$

Figure 6.5: Four operating quadrants of of the speed-torque plane.

occurs at the end of the off-state, see Figure 6.4(c). The instantaneous back-emf $e = k\omega_M$ can be assumed to remain constant, because the rotor speed ω_M stays almost constant due to the rotor inertia during short time intervals. Therefore, $e = \bar{e} = \bar{u} - R\bar{i}$ holds for the back-emf, which allows to rewrite (6.5) as

$$i(t) = i(0) + \frac{1}{L}\int_0^t \left[u - \bar{u} - R(i - \bar{i}) \right] dt$$

$$\approx i(0) + \frac{1}{L}\int_0^t (u - \bar{u})\,dt \tag{6.7}$$

where the approximation holds well if the time constant L/R is large as compared to the switching period, which typically is the case. It is worth noticing that the shaded equal areas in Figure 6.4(c) represent the above integral over the first switching period.

The current ripple Δi in the steady state can be obtained by calculating the change in the current during the on-state,

$$\Delta i = \frac{1}{L}\int_0^{t_{on}} (U_{dc} - \bar{u})\,dt = \frac{(U_{dc} - \bar{u})t_{on}}{L} = \frac{d(1-d)U_{dc}}{f_{sw}L} \tag{6.8}$$

where the last form is obtained using (6.2). It can be seen that the current ripple is inversely proportional to the switching frequency f_{sw} and the inductance L. Naturally, the change in the current during the off-state equals (6.8), but with the negative sign, as could be easily shown.

The maximum value of (6.8) appears at $d = 0.5$, i.e., at about 50% of the rated speed in the case of a DC machine,

$$\Delta i_{max} = \frac{U_{dc}}{4 f_{sw} L} \tag{6.9}$$

As an example, consider a 1-kW DC machine with $L = 50$ mH, $U_{dc} = 100$ V, and $f_{sw} = 5$ kHz. These values result in the maximum current ripple $\Delta i_{max} = 0.1$ A. Since the rated current is 10 A, the current ripple is only 1%, while 5 kHz is not a high switching frequency at 1-kW power level. The current ripple Δi and torque ripple $\Delta\tau_M = k\Delta i$ are insignificant in this case.

6.2 Four-Quadrant DC-DC Converter

For a DC machine, the back-emf is $e = k\omega_M$, torque $\tau_M = ki$, and mechanical power $p_M = \tau_M\omega_M = ei$. Figure 6.5 shows the four quadrants of the speed-torque plane. In quadrants 1 and 3, the speed ω_M and torque τ_M have the same

sign, and the machine is motoring. In quadrants 2 and 4, the speed and torque have opposite signs, and the machine is generating (i.e. braking). Notice that the terminal voltage u of the DC machine approximately equals the back-emf e in the steady state. A buck converter can reverse neither its output voltage u nor current i. Consequently, the DC machine fed from a buck converter can operate only in quadrant 1.

6.2.1 Operating Principle

Consider a four-quadrant DC-DC converter shown in Figure 6.6(a). As the name implies, this converter can operate in all four quadrants, i.e., the polarities of the output voltage and current can be reversed. The converter consists of two legs, whose output terminals are marked with a and b. Furthermore, the negative and positive DC-bus potentials are marked with N and P, respectively. The output voltage u is from output terminal a to output terminal b, i.e.,

$$u = u_{aN} - u_{bN} \qquad (6.10)$$

where u_{aN} and u_{bN} are the pole voltages between the output terminals and the negative DC-bus potential. The upper and lower transistors of leg a are labeled as T_{a+} and T_{a-}, respectively, and the similar labeling is used for leg b. To avoid short-circuiting the DC voltage source, the transistors in the same leg should never be in the on-state simultaneously. The transistors have four allowed switching states:

- If T_{a+} and T_{b-} are on, then $u = U_{dc}$.
- If T_{a-} and T_{b+} are on, then $u = -U_{dc}$.
- If T_{a+} and T_{b+} are on, then $u = 0$.
- If T_{a-} and T_{b-} are on, then $u = 0$.

It can be seen that the converter output voltage u can be positive, negative or zero. Figure 6.7 shows the current paths for both positive and negative currents for the allowed switching states. Due to the antiparallel diodes, the converter can operate in all four quadrants.

Assuming ideal transistors and diodes, the converter can be represented with the equivalent circuit shown in Figure 6.6(b), in which the legs are modeled as bi-positional switches. Using leg a as an example, its switching state is $q_a = 0$, if the bi-positional switch is connected to negative potential N. The switching state is $q_a = 1$, if the switch is connected to positive potential P. The switching state q_b is defined accordingly. Consequently, the instantaneous pole voltages

$$u_{aN} = q_a U_{dc} \qquad u_{bN} = q_b U_{dc} \qquad (6.11)$$

as well as the instantaneous output voltage (6.10)

$$u = (q_a - q_b)U_{dc} \qquad (6.12)$$

can be expressed using the switching states.

Figure 6.6(b) shows example waveforms. Similarly to the buck converter, the average quantities over the switching period T_{sw} can be defined using (6.1). The average pole voltages become

$$\overline{u}_{aN} = d_a U_{dc} \qquad \overline{u}_{bN} = d_b U_{dc} \qquad (6.13)$$
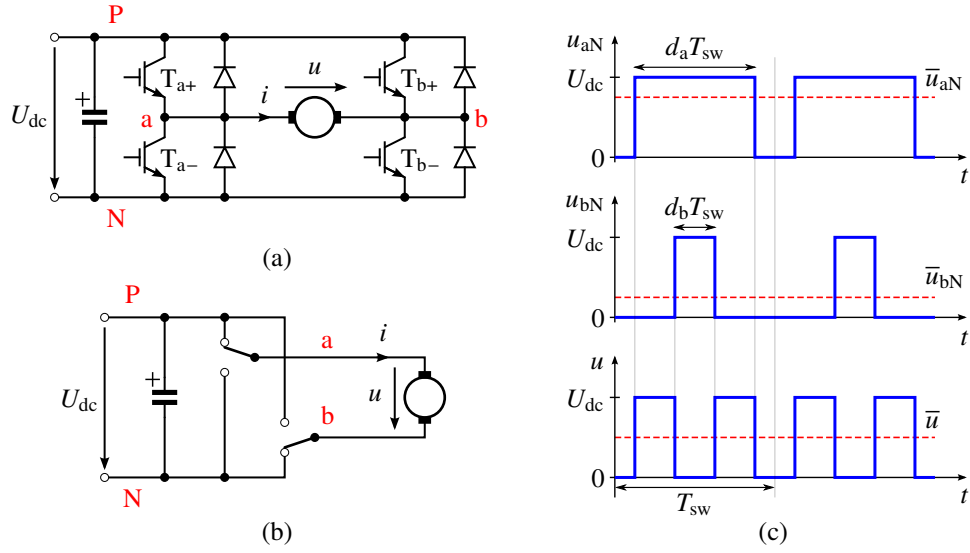
Figure 6.6: Four-quadrant DC-DC converter: (a) main circuit; (b) equivalent circuit; (c) example waveforms. In (c), the solid lines show the instantaneous voltage waveforms, and the dashed lines show their averages over the switching period.
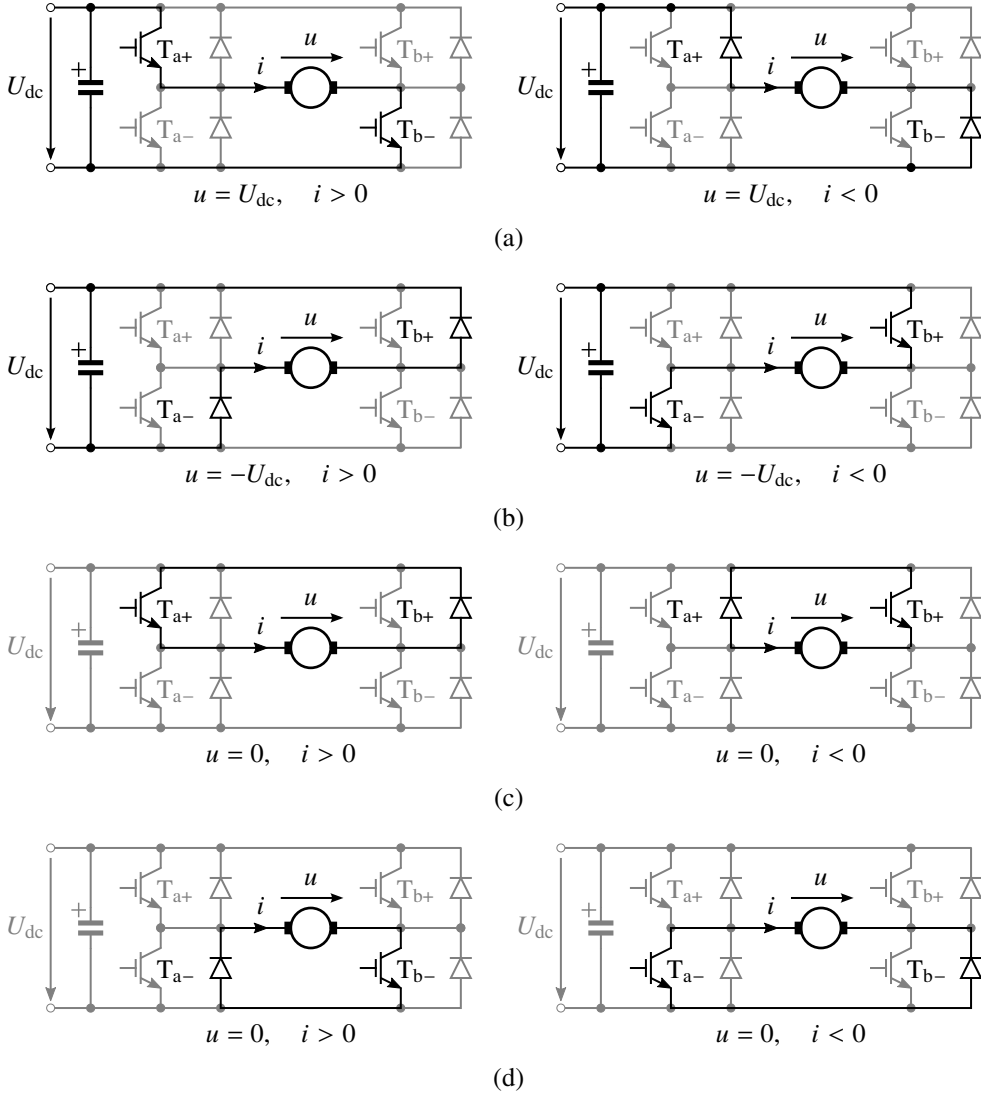

Figure 6.7: Current paths in the four allowed switching states: (a) $u = U_{dc}$; (b) $u = -U_{dc}$; (c, d) $u = 0$. Notice that the arrows define the positive direction of the voltage and the current.
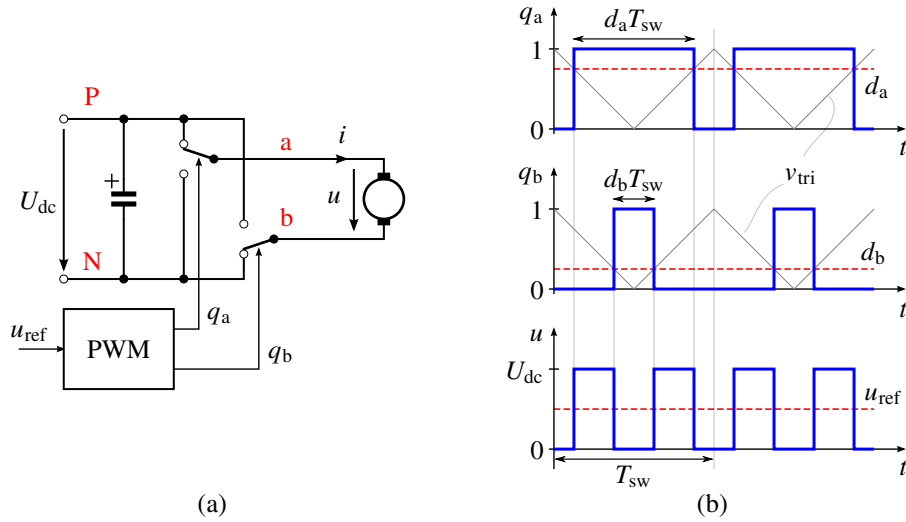
Figure 6.8: Unipolar PWM: (a) switching states q_a and q_b are generated based on the voltage reference u_{ref}; (b) example waveforms. In (b), the dashed lines show the desired duty ratios d_a and d_b and the voltage reference u_{ref}. The duty ratios are compared to the triangular carrier wave, which results in the switching states q_a and q_b. In unipolar PWM, the same carrier is used for both legs. Here, $u_{ref} = 0.5U_{dc}$, resulting in $d_a = 0.75$ and $d_b = 0.25$.

where d_a and d_b are the duty ratios of legs a and b, respectively. The average output voltage can be written as

$$\overline{u} = (d_a - d_b)U_{dc} \tag{6.14}$$

It can be seen that the average output voltage $\overline{u}$ depends linearly on the duty cycles d_a and d_b. Notice also the analogy between the expressions for the instantaneous voltages and the average voltages.

6.2.2 Pulse-Width Modulation

The task of PWM is to generate the control signals q_a and q_b so that converter produces the desired average output voltage $\overline{u}$ over the switching period (or, alternatively, half of the switching period). There are several different PWM methods for the four-quadrant DC-DC converter, all of which produce the desired average voltage, but with different pulse patterns. Bipolar and unipolar PWM are the most common methods [4]. Here, unipolar PWM is considered.

As shown in Figure 6.8(a), the input of the PWM is the voltage reference u_{ref}, and the outputs are the switching states q_a and q_b. The switching states are generated based on carrier comparison. As shown in Figure 6.8(b), the carrier signal v_{tri} is a triangular wave with a period of T_{sw}. The same carrier signal is used for both legs. The scaling of the triangular wave (and, correspondingly, of the voltage reference signals) could be selected in many different ways, which is mainly a matter of implementation. Here, the triangular wave v_{tri} is assumed to vary between 0 and 1. With this choice, the scaled voltage reference signals to be compared to v_{tri} equal the duty ratios d_a and d_b. If the reference signal (in this case the duty ratio) is higher than the carrier signal, the bi-positional switch is connected to the positive DC potential, otherwise to the negative DC potential. Using the switching state, this can be written as follows:
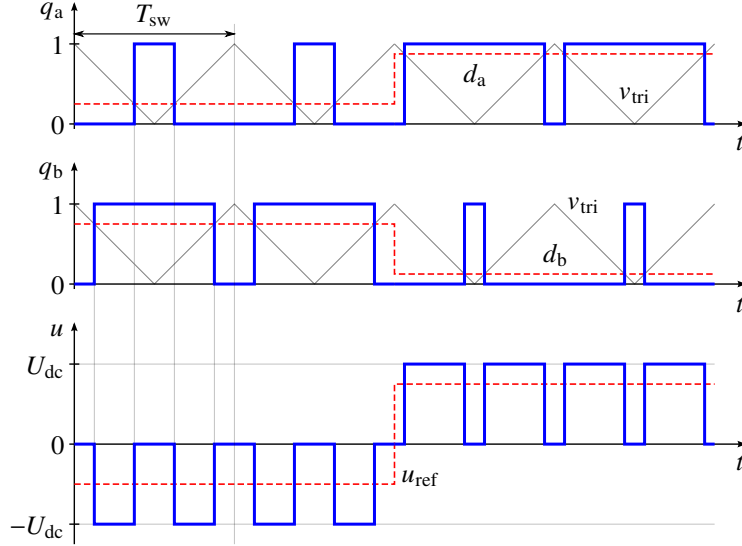
Figure 6.9: Example waveforms showing a step change in the voltage reference u_{ref} from $-0.5U_{\text{dc}}$ to $0.75U_{\text{dc}}$.

- If $d_a < v_{\text{tri}}$, then $q_a = 0$ (i.e. T_{a+} is off and T_{a-} is on).
- If $d_a > v_{\text{tri}}$, then $q_a = 1$ (i.e. T_{a+} is on and T_{a-} is off).

The switching state q_b is obtained similarly.

The duty ratios d_a and d_b are computed from the voltage reference so that $\overline{u} = u_{\text{ref}}$ holds. Since there are arbitrary many duty ratios that satisfy this condition, the second condition is needed. The unipolar PWM is obtained by requiring that $d_a + d_b = 1$ holds.[1] Using these two conditions, the duty ratios can be solved from (6.14) as

$$d_a = \frac{1}{2}\left(1 + \frac{u_{\text{ref}}}{U_{\text{dc}}}\right) \qquad d_b = \frac{1}{2}\left(1 - \frac{u_{\text{ref}}}{U_{\text{dc}}}\right) \qquad (6.15)$$

Figure 6.9 shows example waveforms, where the voltage reference u_{ref} is stepped from $-0.5U_{\text{dc}}$ to $0.75U_{\text{dc}}$. The duty ratios d_a and d_b are computed from the voltage reference using (6.15), and the switching states q_a and q_b are obtained from the carrier comparison. From the example waveforms, it can be noticed that the effective switching frequency (as seen from the output voltage u) is twice the actual switching frequency. Some other PWM methods such as bipolar PWM do not have this feature. Doubling the effective switching frequency is advantageous since it reduces the switching ripple in the output current for a given actual switching frequency (which is limited due to the switching losses of the converter).

6.2.3 Implementation Aspects

In the previous sections, ideal switches were assumed. However, real power semiconductor devices have finite turn-on and turn-off times. To avoid short-circuiting the DC voltage source, a short time interval is needed between the

---

[1]This condition makes the pulse widths of legs a and b symmetric, i.e., $d_a T_{\text{sw}} = (1 - d_b)T_{\text{sw}}$ holds. In other words, switch a is connected to positive potential P the same time as switch b is connected to negative potential N.
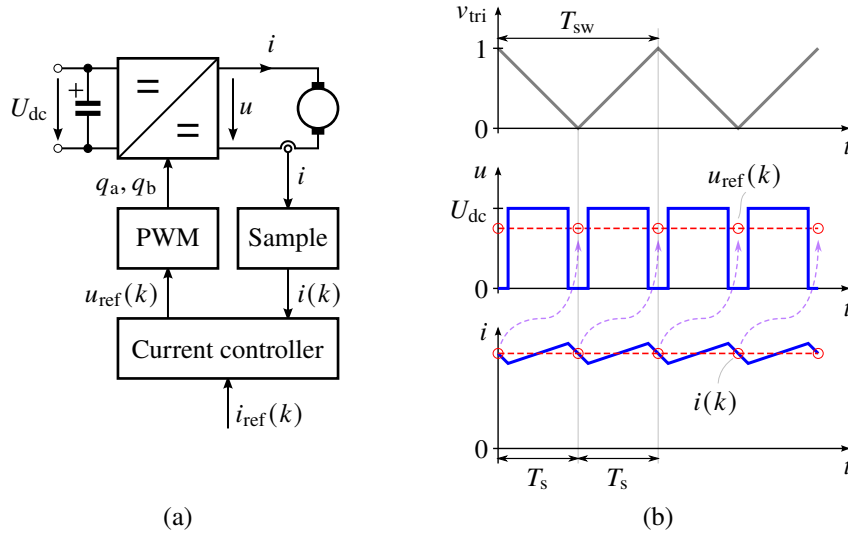
Figure 6.10: Digital control system: (a) carrier comparison and sampling are the interfaces between the discrete-time controller and the continuous-time physical system; (b) sampling synchronized to the PWM carrier. In (b), the voltage reference $u_{\mathrm{ref}}(k)$ can be updated in the beginning and in the middle of the carrier (marked with the circles). The current samples $i(k)$ can be taken at these same time instants. The dashed arrows illustrate the computational delay due to ADC and finite computation time of a digital processor.

turn-off of one switch and the turn-on of the other switch in the same leg. This time interval is called the dead time (or the blanking time). It is typically in the range of one or a few microseconds for IGBTs. During the dead time, the load current flows through the freewheeling diodes. Consequently, the pole voltage is determined by the current direction during the dead time. For example, if the current i is positive, then the pole voltage $u_{\mathrm{aN}} = -U_{\mathrm{dc}}$ in the case of leg a. If the current is negative, then $u_{\mathrm{aN}} = U_{\mathrm{dc}}$. The distortion of the output voltage due to the dead time can be compensated for based on the polarity of the measured current [10].

A control system is almost always implemented digitally, e.g., on a micro-controller, digital signal processor (DSP) or field-programmable gate array (FPGA) or their combination. Figure 6.10(a) shows a block diagram of a current-controlled drive system, where the current i is measured for the feedback. The carrier comparison and sampling of the analog signals are the interfaces between the discrete-time control system and the continuous-time physical system [11].

The voltage reference $u_{\mathrm{ref}}(k)$ is a discrete-time signal, where the argument $k = 0, 1, \ldots$ is the discrete-time index corresponding to $t = kT_{\mathrm{s}}$, where T_{s} is the sampling period. The voltage reference can be updated in the beginning and in the middle of the switching period (double-update PWM). Correspondingly, the sampling period is $T_{\mathrm{s}} = T_{\mathrm{sw}}/2$, see Figure 6.10(b). Alternatively, the voltage reference can be updated only once per switching period, i.e. $T_{\mathrm{s}} = T_{\mathrm{sw}}$ in this case (single-update PWM).

The sampling of the current i is typically synchronized with the carrier signal. In the example scheme shown in Figure 6.10(b), two current samples $i(k)$ per switching period are taken at the beginning and middle of the switching period.[2]

---

[2]It can be noticed that four current samples per switching period could be taken without the current ripple in unipolar PWM.

It can be seen that this sampling scheme effectively (perfectly, in theory, if the load is purely inductive) removes the current ripple from the samples. Furthermore, since the samples are taken in between the switching instants, electromagnetic interference (EMI) due to switching spikes is reduced. An analog anti-aliasing filter in the measurement channel is still preferable, but its cut-off frequency can be set to a comparatively high value, so that the effect of the anti-aliasing filter may be omitted in the control design.

DSPs and other control boards dedicated to power converters have peripherals for PWM outputs, in which the carrier signal is generated by a timer with very high clock frequency (tens or hundreds of megahertz). As an example, the switching frequency could be 5 kHz and the timer clock frequency 25 MHz. With these example values, the carrier signal v_{tri} goes from 0 to 1 in 2 500 small steps in half switching period $T_{sw}/2 = 1/(2f_{sw})$. These quantization effects of carrier comparison can typically be omitted.

The current sampling is implemented using an analog-to-digital converter (ADC), whose sample-and-hold circuit is triggered by the PWM timer. The ADC converts the analog signal to a digital signal, which is then available for the digital controller. The computation of new voltage reference $u_{ref}(k)$ can be started after the ADC has finished the conversion. The computation of the new reference takes also some time. Due to these reasons, typical control systems have a computational delay of one sampling period T_s, see Figure 6.10(b), which may have to be taken into account in the control design.

As can be realized from Figure 6.10(b), the current controller (and other outer controllers) effectively deals with the averaged quantities over the sampling period, i.e., the current and torque ripple due to the PWM is not seen by the digital controller.[3] Hence, in most other chapters of this material, the ripple is omitted from the analysis. It is, however, important to remember that the actual converter output voltage is a pulse wave, which results in some current and torque ripple. When needed, the PWM effects can be included in simulations or studied by means of experiments using an oscilloscope (or other measurement device with high sampling rate).

---

[3]In some other control schemes, such as hysteresis control, ripple has to be included in the measurements, since the switching actions are based on the ripple.

Chapter 7

Control of DC Machine Drives

The aim of this chapter is to introduce cascade control of DC machine drives. The chapter begins with a brief introduction to the cascade control structure. Then, the design of the inner current-control loop is studied in detail, including the controller gain selection based on the model parameters and the desired closed-loop bandwidth. The same design approach and the gain selection principles are applied to the outer speed-control loop.

A proportional-integral (PI) controller is probably the most common controller type. However, this material applies a more general two-degrees-of-freedom (2DOF) PI controller, from which the regular one-degree-of-freedom (1DOF) PI controller is obtained as a special case. The advantage of 2DOF controllers is that disturbance rejection and reference tracking can be designed independently [12].

The presented current controller and its tuning principles can be extended to AC machine drives [13–15]. Furthermore, the speed controller design is independent of the machine type, if ideal torque control can be assumed [16]. Modern AC drives are equipped with self-commissioning algorithms, which automatically identify the machine parameters and then tune the controller gains. Their gain selection is often based on the similar principles as covered in this chapter.

7.1   Cascade Control

The electrical subsystem of an electric machine in open loop is typically much faster than the mechanical subsystem, see Chapter 5. These separate time scales facilitate the use of the cascade control structure, consisting of two nested control loops, see Figure 7.1(a). The current i is measured and fed back to the inner current controller. The rotor speed ω_M is fed back to the outer speed controller. The current and speed references are denoted by i_{ref} and $\omega_{M,ref}$, respectively. The output of the speed controller is the torque reference $\tau_{M,ref}$.

Figure 7.1(b) shows the same cascade control system, but now drawn together with the mathematical machine model. Furthermore, the converter output voltage is assumed to equal its reference, $u = u_{ref}$. The inner current-control loop can be tuned to be much faster than the outer speed-control loop. From the perspective of the current controller, the rotor speed ω_M and the back-emf $e = k\omega_M$ vary slowly. Figure 7.2(a) shows the block diagram, in which the back-emf e is considered
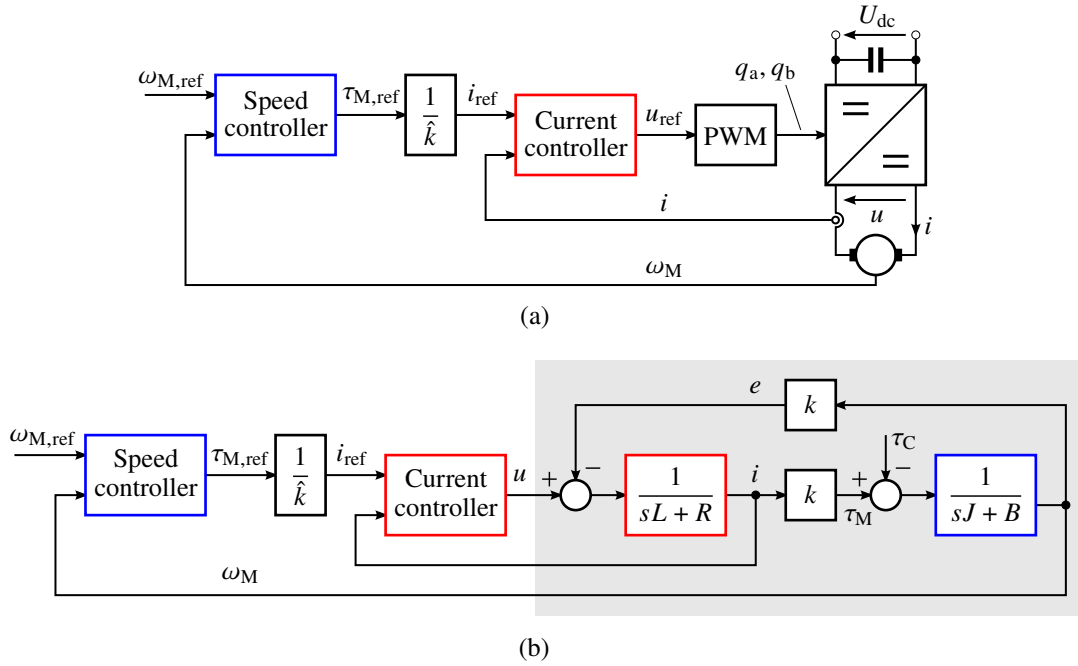
Figure 7.1: Cascade control system shown together with: (a) drive main circuit; (b) system model (shaded). In (b), the pulse-width-modulated converter is assumed to be ideal, $u = u_{ref}$. The flux factor estimate is denoted by $\hat{k}$.
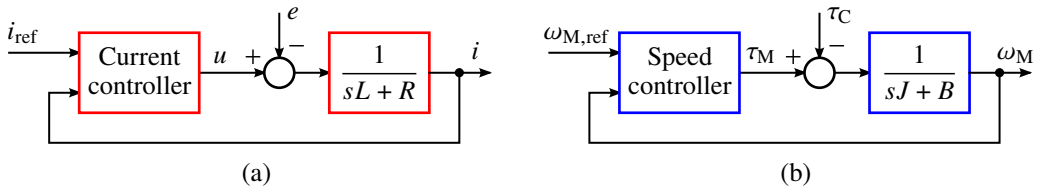
Figure 7.2: Reduced-order closed-loop systems: (a) current control; (b) speed control, assuming $\tau_M = \tau_{M,ref}$.

as an external load disturbance. The closed-loop current control enables precise and fast current control. Since the torque is proportional to the current, $\tau_M = ki$, it can be controlled with good accuracy as well. From the speed controller perspective, the ideal torque control can be assumed, $\tau_M = \tau_{M,ref}$, leading to the block diagram in Figure 7.2(b).

An advantage of the cascade control structure (as compared to speed control without the inner current controller) is that the current i can be limited to a desired maximum value simply by limiting the reference i_{ref}. This is important in order to protect the machine and the converter from overcurrents. Another advantage is that the cascade control structure hides the electrical subsystem from the speed controller, which simplifies the speed controller design. In some applications, the speed controller is not needed, but torque-control mode is used, e.g., in electric vehicles (when the cruise control is disabled) and in various tension-controlled applications. On the other hand, in servo positioning applications, the cascade control system can be extended with a position controller, which can be a simple proportional controller, since the position is the pure integral of the speed.

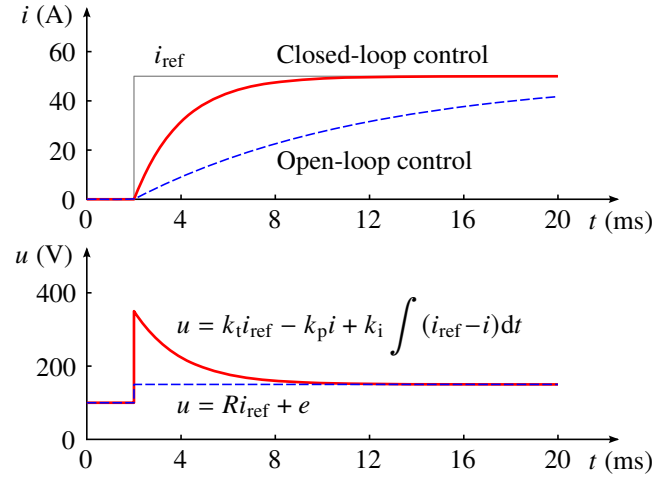Figure 7.3: Simulated current step response. The parameters of the DC machine are $R = 1\ \Omega$ and $L = 10$ mH. The back-emf is constant at $e = 100$ V. The current reference i_{ref} steps from 0 to 50 A at $t = 2$ ms. The dashed and solid lines show the response for the open-loop control and the closed-loop control, respectively. The open-loop and closed-loop time constants are $T = L/R = 10$ ms and $T_{\text{c}} = 1/\alpha_{\text{c}} = 2$ ms. Parameter estimates are accurate.

7.2 Current Control

In this section, the structure and model-based tuning of a 2DOF PI controller is studied in detail. The current controller is used as an example, see Figure 7.2(a). However, the same analysis and control design applies directly to the speed controller as well due to the mathematical analogy.

7.2.1 Open-Loop System

In open loop, the electrical subsystem is

$$L\frac{\text{d}i}{\text{d}t} = u - Ri - e \tag{7.1}$$

where the back-emf e is considered as external load disturbance. Equivalently, the model (7.1) can be represented in the Laplace domain as

$$\begin{aligned} i(s) &= \frac{1}{sL + R}[u(s) - i(s)] \\ &= Y(s)[u(s) - e(s)] \end{aligned} \tag{7.2}$$

where the transfer function $Y(s)$ is known as the admittance.

In principle, the current i could be adjusted by means of open-loop control,

$$u_{\text{ref}} = \hat{R}i_{\text{ref}} + \hat{k}\omega_{\text{M}} \tag{7.3}$$

where the parameter estimates are marked with the hat. This approach, however, has some major drawbacks. Firstly, the parameter estimates $\hat{R}$ and $\hat{k}$ are typically inaccurate, especially in the case of the resistance R, which varies as a function of temperature. The error in parameter estimates is directly translated to the error in the current i. Secondly, the time constant $T = L/R$ (and thus the current rise time) of the open-loop control cannot be affected, but it is determined by the machine parameters. Figure 7.3 shows an example of the open-loop current response in an ideal case without parameter errors.
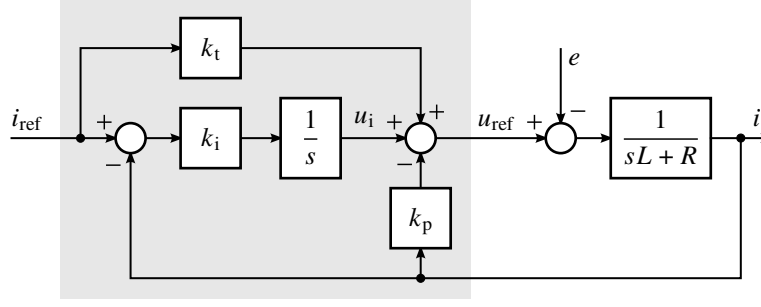
54

Figure 7.4: 2DOF PI controller (shaded) and the system model, with the assumption $u = u_{\text{ref}}$.

7.2.2 Closed-Loop Control

In closed-loop control, the control objective is to minimize the control error $i_{\text{ref}} - i$. Typically, the control error is required to be zero in the DC steady state (when the reference i_{ref} and the disturbance e are constant). Furthermore, the response of the current i to the transient changes in the reference i_{ref} and external disturbance e should be well-damped and sufficiently fast.

Two-Degrees-of-Freedom Proportional-Integral Control

Figure 7.4 shows the block diagram of a 2DOF PI controller and the system model. The measured current i is fed back to the current controller, which generates the voltage reference u_{ref}. In the state-space form, the controller can be expressed as

$$\frac{\mathrm{d}u_{\text{i}}}{\mathrm{d}t} = k_{\text{i}} \left(i_{\text{ref}} - i \right) \tag{7.4a}$$

$$u_{\text{ref}} = k_{\text{t}}i_{\text{ref}} - k_{\text{p}}i + u_{\text{i}} \tag{7.4b}$$

where k_{t} is the reference feedforward gain, k_{p} is the proportional gain, k_{i} is the integral gain, and u_{i} is the integral state. To provide an alternative view, the controller can be equivalently represented in the integral form

$$u_{\text{ref}} = k_{\text{t}}i_{\text{ref}} - k_{\text{p}}i + \int k_{\text{i}}(i_{\text{ref}} - i)\mathrm{d}t \tag{7.5}$$

as well as in the Laplace domain

$$u_{\text{ref}}(s) = k_{\text{t}}i_{\text{ref}}(s) - k_{\text{p}}i(s) + \frac{k_{\text{i}}}{s} \left[i_{\text{ref}}(s) - i(s) \right] \tag{7.6}$$

It can realized that the integral state u_{i} will increase (if $i_{\text{ref}} > i$) or decrease (if $i_{\text{ref}} < i$) until the control error is driven to zero. It is to be noted that the selection $k_{\text{t}} = k_{\text{p}}$ yields the regular 1DOF PI controller. Consequently, the following closed-loop transfer functions apply to this special case as well.

Remark 1. The form (7.6) can be rewritten as

$$u_{\text{ref}}(s) = (k_{\text{t}} - k_{\text{p}})i_{\text{ref}}(s) + \left(k_{\text{p}} + \frac{k_{\text{i}}}{s} \right) \left[i_{\text{ref}}(s) - i(s) \right]$$

$$= (k_{\text{t}} - k_{\text{p}})i_{\text{ref}}(s) + K(s) \left[i_{\text{ref}}(s) - i(s) \right] \tag{7.7}$$

where $K(s)$ is the regular PI controller. The stability of the closed-loop system is often evaluated indirectly via the loop transfer function $L(s) = K(s)Y(s)$. For example, the gain and phase margins are read from the Bode plot or the Nyquist plot of $L(j\omega)$ [12]. Notice that the gain k_t does not affect the stability.

Closed-Loop System

In the following, perfect voltage production is assumed, $u = u_{ref}$. This assumption is feasible in the case of switch-mode DC-DC converters. Inserting (7.6) into (7.2) yields the closed-loop system

$$i(s) = \frac{sk_t + k_i}{Ls^2 + (R + k_p)s + k_i} i_{ref}(s) - \frac{s}{Ls^2 + (R + k_p)s + k_i} e(s)$$
$$= G_{cl}(s)i_{ref}(s) - Y_{cl}(s)e(s) \tag{7.8}$$

where $G_{cl}(s)$ is the reference-tracking transfer function and $Y_{cl}(s)$ is the disturbance-rejection transfer function. The reference-tracking transfer function describes the effect of the reference i_{ref} on the current i. Similarly, the disturbance-rejection transfer function describes the effect of the load disturbance e on the current i. For a positive integral gain k_i, the control error in the steady state is zero ($i = i_{ref}$), i.e., $G_{cl}(0) = 1$ and $Y_{cl}(0) = 0$. It is also worth noticing that increasing the proportional gain k_p affects similarly as increasing the physical resistance R, but without causing power losses.

Remark 2. The proportional controller ($k_i = 0$ and $k_t = k_p$) results in the nonzero steady-state control error, unless both $R = 0$ and $e = 0$. The larger the gain k_p, the smaller the steady-state error. However, the gain k_p cannot be increased arbitrarily, since the noise in the measured current i gets amplified.

Gain Selection

From (7.8), it can be noticed that the characteristic polynomial (i.e. closed-loop poles) depend on the gains k_p and k_i. Furthermore, the zero of the reference-tracking transfer function depends on the gain k_t. Consequently, if the parameter estimates $\hat{L}$ and $\hat{R}$ are available, the poles and the reference-tracking zero can be freely placed. As an example, consider a typical gain selection

$$k_p = 2\alpha_c\hat{L} - \hat{R} \qquad k_i = \alpha_c^2\hat{L} \qquad k_t = \alpha_c\hat{L} \tag{7.9}$$

where α_c is the desired reference-tracking bandwidth.[1] Assume $\hat{L} = L$ and $\hat{R} = R$. Inserting the above gains into (7.8) results in

$$G_{cl}(s) = \frac{\alpha_c}{s + \alpha_c} \qquad Y_{cl}(s) = \frac{s/L}{(s + \alpha_c)^2} \tag{7.10}$$

The gains k_p and k_i place the double pole at $s = -\alpha_c$, i.e., the damping ratio $\zeta = 1$. Furthermore, the gain k_t places the reference-tracking zero at $s = -\alpha_c$, which thus cancels the other pole of the reference-tracking transfer function.

---

[1]In practice, the effect of the resistance is negligible, i.e., $\hat{R} = 0$ can be chosen.
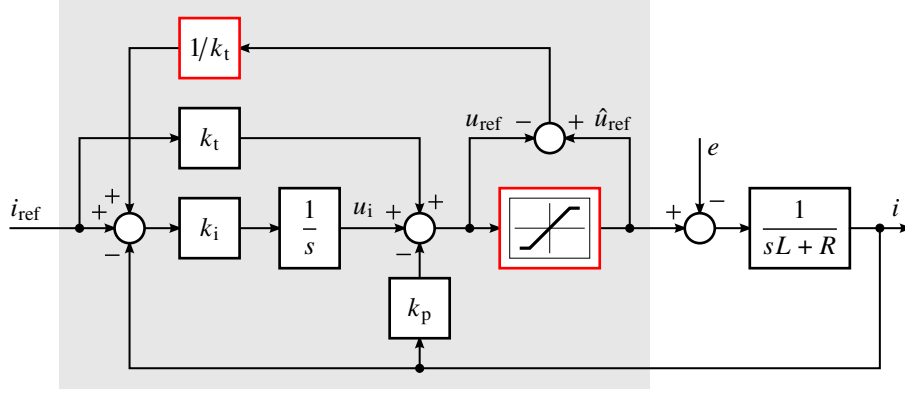
Figure 7.5: 2DOF PI controller equipped with a realizable-reference anti-windup method. Notice that $\hat{u}_{ref} = u_{ref}$ holds in the linear region. The shaded part represents the controller, typically a piece of software.

Figure 7.3 shows the step response of the current i when the gains (7.9) are applied. In this example, the bandwidth has been set five times that of the open-loop bandwidth, $\alpha_c = 5R/L$. As expected, the current response corresponds to the response of the first-order system. The integral action would drive the control error to zero even with inaccurate parameter estimates. However, very large parameter errors may deteriorate the dynamic performance. Furthermore, the closed-loop control can become unstable, if the system has too long delays in the feedback path or if the gains are too large. In discrete-time implementations, the bandwidth α_c should be (at least) one decade smaller than the angular sampling frequency $2\pi/T_s$, where T_s is the sampling period of the control system.

Remark 3. The poles resulting from the regular PI controller can be placed as well, i.e., the same disturbance-rejection transfer function can be achieved as with the 2DOF PI controller. According to (7.8), the integral gain $k_i = \omega_0^2 L$ affects the undamped natural frequency ω_0 and the proportional gain $k_p = 2\zeta\omega_0 L - R$ affects the damping ratio ζ (in addition to ω_0), see Appendix A.2. The reference-tracking zero cannot be independently placed, since the gain $k_t = k_p$ becomes already fixed by the desired poles.

Actuator Saturation and Anti-Windup

All physical actuators have limited operating range. In current control, the actuator is the power converter, which has a limited output voltage. For four-quadrant DC-DC converters, the realizable voltage is $|u| \leq u_{max}$, where the maximum voltage u_{max} is the DC-bus voltage. Consequently, the assumption $u = u_{ref}$ does not hold in the saturated region. The voltage reference $|u_{ref}|$ may exceed u_{max} for large current steps, especially at high rotor speeds due to the large back-emf. During the saturation, the integral state u_i continues accumulating (winding up) unless a suitable anti-windup method is applied.

A realizable-reference anti-windup method can be easily incorporated into the 2DOF PI controller as

$$\frac{du_i}{dt} = k_i \left(i_{ref} - i + \frac{\hat{u}_{ref} - u_{ref}}{k_t} \right) \tag{7.11a}$$

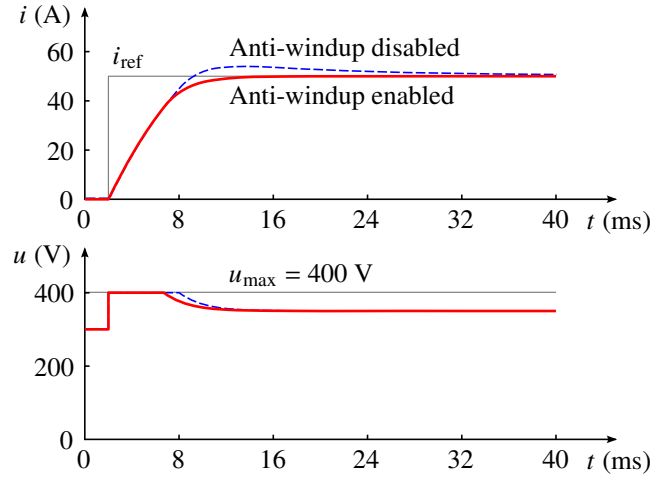$$u_{ref} = k_t i_{ref} - k_p i + u_i \tag{7.11b}$$

Figure 7.6: Simulated current step response, showing the effect of the actuator saturation. The current reference i_ref steps from 0 to 50 A at $t = 2$ ms. The back-emf is constant at $e = 300$ V and the maximum available voltage is $u_\text{max} = 400$ V. The dashed and solid lines show the response when the anti-windup method is disabled and enabled, respectively.

where $\hat{u}_\text{ref}$ is the realized voltage. The realized voltage in the case of a four-quadrant DC-DC converter is

$$\hat{u}_\text{ref} = \begin{cases} u_\text{ref} & \text{if } |u_\text{ref}| \leq u_\text{max} \\ u_\text{max}\, \text{sign}(u_\text{ref}) & \text{if } |u_\text{ref}| > u_\text{max} \end{cases} \tag{7.12}$$

Figure 7.5 shows the corresponding block diagram of the algorithm. In the linear range, $\hat{u}_\text{ref} = u_\text{ref}$ and the anti-windup method does not affect. In the saturated region, the anti-windup method limits the integral state u_i to the value that would result in the realized voltage $\hat{u}_\text{ref}$. The same anti-windup method can be applied to the regular PI controller as well, simply by setting $k_\text{t} = k_\text{p}$.

Figure 7.6 shows step responses with and without anti-windup method. The converter voltage saturates after the current reference step is applied. As compared to Figure 7.3, the reason for reaching the maximum voltage is that now the back-emf (speed) is higher. It can be seen that there is no overshoot when the anti-windup method is enabled. Naturally, the rise time is longer than the specified one.

7.3 Speed Control

7.3.1 Open-Loop System

Consider the first-order mechanical dynamics, see Chapter 3,

$$J\frac{d\omega_\text{M}}{dt} = \tau_\text{M} - B\omega_\text{M} - \tau_\text{C} \tag{7.13}$$

where B is the viscous damping and τ_C is the external load torque disturbance. The viscous-damping term is separated from the total load torque $\tau_\text{L} = B\omega_\text{M} + \tau_\text{C}$ in order to highlight the analogy between the mechanical and electrical subsystems. Equivalently, the model (7.13) can be represented in the Laplace

domain as

$$\omega_M(s) = \frac{1}{sJ + B}[\tau_M(s) - \tau_C(s)]$$
$$= M(s)[\tau_M(s) - \tau_C(s)] \tag{7.14}$$

where the transfer function $M(s)$ is known as the mechanical admittance. Notice the analogy between the mechanical and electrical subsystems:

$$\omega_M \cong i \qquad \tau_M \cong u \qquad \tau_C \cong e \qquad J \cong L \qquad B \cong R \tag{7.15}$$

The external load torque τ_C may change quickly (unlike the back-emf e seen as a load disturbance by the current controller). As an example, the load torque changes almost stepwise in steel-rolling-mill drives at the instant when a rough steel plate hits the rolls.

7.3.2 Closed-Loop Control

Under the assumption of ideal torque control, $\tau_M = \tau_{M,ref}$, the speed control problem is fully analogous to the current control problem considered in the previous section, see Figure 7.2. We can thus directly apply the same 2DOF PI controller and its design principles using the analogy in (7.15).

According to (7.9), the speed controller gains can be selected as

$$k_p = 2\alpha_s \hat{J} - \hat{B} \qquad k_i = \alpha_s^2 \hat{J} \qquad k_t = \alpha_s \hat{J} \tag{7.16}$$

where $\hat{J}$ is the inertia estimate and α_s is the desired bandwidth. In practice, $\hat{B} = 0$ can be selected. For simplicity, the same notation is used above for the gains as in (7.9), although the resulting gains are naturally different. The anti-windup algorithm (7.11) can also be directly applied. The maximum available torque τ_{max} is typically related to the maximum available current i_{max}, i.e., $\tau_{max} = \hat{k} i_{max}$.

Figure 7.7 shows the step response of the speed ω_M, when the 2DOF PI controller (7.11) with the anti-windup method is applied. The gains correspond to (7.16). The speed tracks its reference according to the designed dynamics. Furthermore, the load disturbance is rejected in a well-damped manner and the steady-state error is driven to zero due to the integral action.

Figure 7.7 also shows the results when the regular PI controller is applied, i.e., $k_t = k_p$. The gains k_p and k_i are selected according to (7.16), resulting in the identical poles with the 2DOF PI controller. Consequently, the load-disturbance rejection of the PI controller equals that of the 2DOF PI controller. However, the reference step response has overshoot, since the reference-tracking zero does not match with the pole. The overshoot could be decreased, which, however, worsens the disturbance rejection. Furthermore, the results for the proportional controller are shown, obtained by setting $k_p = k_t = \alpha_s \hat{J}$ and $k_i = 0$. In this case, the reference tracking is identical to that of the 2DOF PI controller, but the disturbance rejection is much worse, having load-dependent steady-state error.

It is worth noticing that the speed controller and its gains are independent of the electric machine type, if the assumption $\tau_M = \tau_{M,ref}$ is valid. Consequently, the same speed controller can be used for AC machine drives as well. It is possible to extend the presented 2DOF PI controller in many ways. For example, in servo
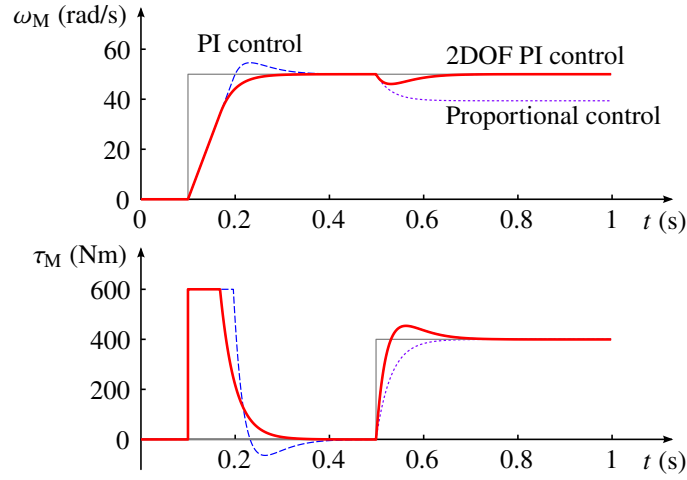
Figure 7.7: Simulated speed step response with $J = 1.2$ kgm^2 and $B = 0$. The speed reference $\omega_{M,ref}$ steps from 0 to 50 rad/s at $t = 0.1$ s, and the load torque τ_L steps from 0 to 400 Nm at $t = 0.5$ s. The solid lines correspond to the 2DOF PI control with $\alpha_s = 2\pi \cdot 5$ rad/s. The dotted lines correspond to the proportional control with the same bandwidth. The PI control is the same as the 2DOF PI control, except that $k_t = k_p$. The maximum available torque is $\tau_{max} = 600$ Nm, and the realizable reference anti-windup method is used in both PI and 2DOF PI control methods. Accurate parameter estimates and $\tau_M = \tau_{M,ref}$ are assumed.

applications, the static reference-feedforward gain k_t can be replaced with a dynamic reference filter, which contains the model of the speed reference profile (e.g. ramp or sinusoid reference). As another example, in a resonant mechanical system, the measured load speed can be fed back to an extended controller in order to damp the resonance.

Chapter 8

Elementary AC Machine Models

In this chapter, an elementary single-phase electric machine is first introduced. The concept of a distributed winding and its sinusoidal idealization is presented. Single-phase machines are uncommon in industrial applications due to their poor power density and inherent torque ripple. They can still be found in some low-power applications, such as in bottle dynamos. Here, the single-phase machine model aims to create a bridge between DC and AC machines. Furthermore, it serves as a building block in a phase-variable model for a three-phase surface-mounted permanent-magnet (PM) synchronous machine, covered at the end of the chapter. The phase-variable model is too complicated for analysis and control purposes, but it enables a solid starting point for presenting simpler and more elegant space-vector models in the next chapter. Appendix B is closely related to this chapter.

8.1 Single-Phase Machines

8.1.1 Elementary Machine

Figure 8.1(a) shows an elementary two-pole single-phase PM machine[1]. The magnet pitch is assumed to be 180°, resulting in the rectangular flux density distribution in the air gap, see Figure 8.1(b) [3]. The stator is equipped with the full-pitch coil. Notice that the machine corresponds to the elementary machine studied in Section 2.2. The only difference is that the structure is reversed: PMs are now placed at the surface of a cylindrical rotor and the winding is placed in the stator.

Figure 8.1(c) shows the resulting waveforms as a function of the rotor angle ϑ_M. The rotor angular speed is $\omega_M = d\vartheta_M/dt$. The waveforms can also be interpreted as functions of time t in the case of constant speed, in which case $\vartheta_M = \omega_M t$ holds. Based on the geometry, the flux linkage due to the PMs is

$$\psi_{af} = k_f \left(\frac{\pi}{2} - \vartheta_M \right) \qquad (0 < \vartheta_M < \pi) \tag{8.1}$$

where $k_f = 2Nr\ell B_f$ is constant, ℓ is the length of the conductor, N is the number of conductors connected in series, and r is the rotor radius. As shown in

---

[1]Later, the phases of three-phase machines will be marked with the subscripts a, b, and c. Based on this convention, the subscript a is already used for single-phase machines.
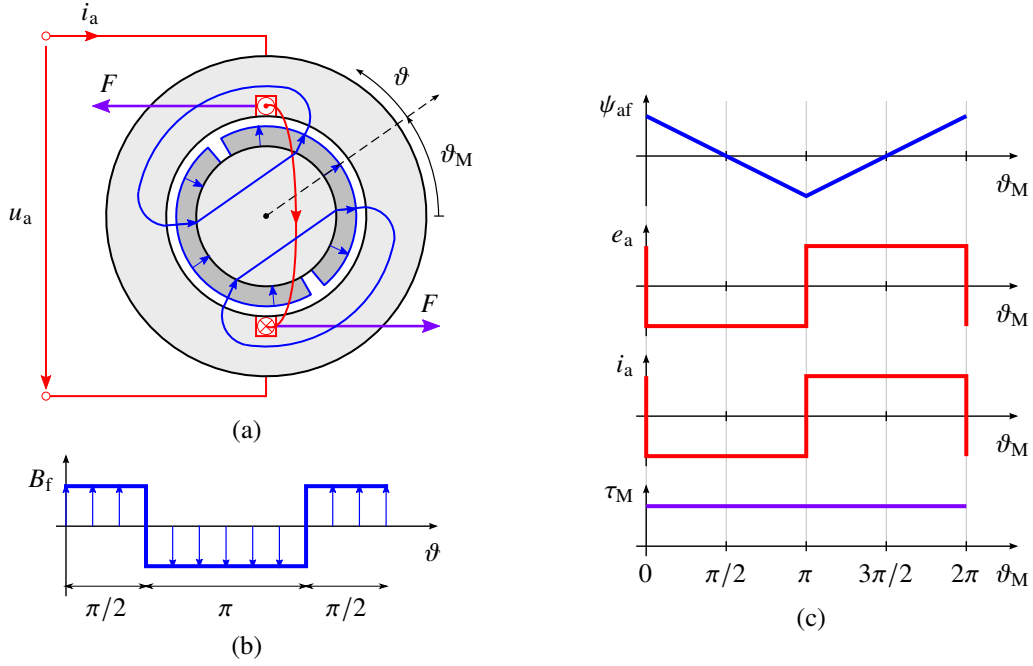
Figure 8.1: Elementary single-phase PM machine: (a) cross-section; (b) air-gap flux density distribution along the air gap; (c) waveforms as functions of the rotor angle ϑ_M. The stator coil is drawn in red. The arrows in the circuit indicate the positive direction of the current and voltage. The blue arrows indicate the magnet polarity. The rotor reference axis is aligned in the positive direction of the magnets. The angle ϑ_M of the rotor is defined as the angle of this reference axis with respect to the stator. The angle ϑ is an angular coordinate used in (b).

Section 2.2, the voltage induced by the magnets is

$$e_a = -k_f \omega_M \qquad (0 < \vartheta_M < \pi) \tag{8.2}$$

The force $F = N B_f \ell i_a$ acts on both coil sides, where i_a is the current. Since opposite counterforces act on the rotor, the electromagnetic torque is

$$\tau_M = -k_f i_a \qquad (0 < \vartheta_M < \pi) \tag{8.3}$$

Assuming perfect current control, arbitrary current i_a can be fed to the machine. Constant positive torque τ_M is obtained if the current i_a has the same shape as the induced voltage e_a, as illustrated in Figure 8.1(c). In practice, the perfectly rectangular current waveform cannot be realized, since the supply voltage and control bandwidth are limited.

8.1.2 Equivalent Circuit

Based on Ohm's and Faraday's laws, the voltage at the winding terminals can be generally expressed as

$$u_a = R_a i_a + \frac{d\psi_a}{dt} \tag{8.4}$$

where R_a is the resistance. The flux linkage is of the form

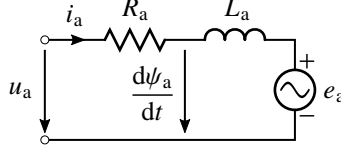$$\psi_a = L_a i_a + \psi_{af}(\vartheta_M) \tag{8.5}$$

62

Figure 8.2: Equivalent circuit of a single-phase machine.

where L_a is the self-inductance. The effective air gap can be assumed to be uniform, since the PMs are mounted at the cylindrical rotor surface. Furthermore, the magnetic saturation is omitted. Consequently, the self-inductance L_a is constant.[2] The flux linkage ψ_{af} due to the PMs depends on the rotor angle ϑ_M.

Inserting (8.5) into (8.4), the voltage can be expressed in an alternative form,

$$u_a = R_a i_a + L_a \frac{di_a}{dt} + e_a \tag{8.6}$$

where the voltage induced by the magnets is

$$e_a = \frac{d\psi_{af}}{dt} = \frac{\partial \psi_{af}}{\partial \vartheta_M} \omega_M \tag{8.7}$$

Figure 8.2 shows the equivalent circuit of the machine. Based on the power balance, it can be shown that the electromagnetic torque is

$$\tau_M = \frac{\partial \psi_{af}}{\partial \vartheta_M} i_a \tag{8.8}$$

The mechanical power is

$$p_M = \tau_M \omega_M = e_a i_a \tag{8.9}$$

where the last form is obtained by applying (8.7) and (8.8). In the special case of the elementary machine, the function $\partial \psi_{af} / \partial \vartheta_M$ is a pulse wave with the magnitude k_f, see Figure 8.1(c).

8.1.3 Distributed Winding

Figure 8.3(a) shows a single-phase machine equipped with am example distributed winding, known as a short-pitched winding [1]. Notice that the stator slots are located such that phases b and c could also be added. Using the previous assumptions, Figure 8.3(b) shows the resulting waveforms for the flux linkage ψ_{af} and the back-emf $e_a = (\partial \psi_{af} / \partial \vartheta_m) \omega_m$. These waveforms can be obtained, e.g., by superposing the waveforms in Figure 8.1(c), taking into account the spatial phase shift of the slots. It can be noticed that distributing the winding into a few slots results in almost sinusoidal flux linkage ψ_{af}, even if the PMs are assumed to produce a rectangular air-gap flux density distribution, shown in Figure 8.1(b). Real machines may have even more sinusoidal waveforms, achieved using advanced winding topologies, PM geometries, and skewing.

---

[2]The permeability of the magnets is almost equals to the permeability of the air. If the PMs are placed inside the rotor, the rotor becomes magnetically anisotropic, further causing the inductance $L_a = L_a(\vartheta_M)$ to depend on the rotor angle. Such interior PM or salient-rotor machines are not considered in this chapter.
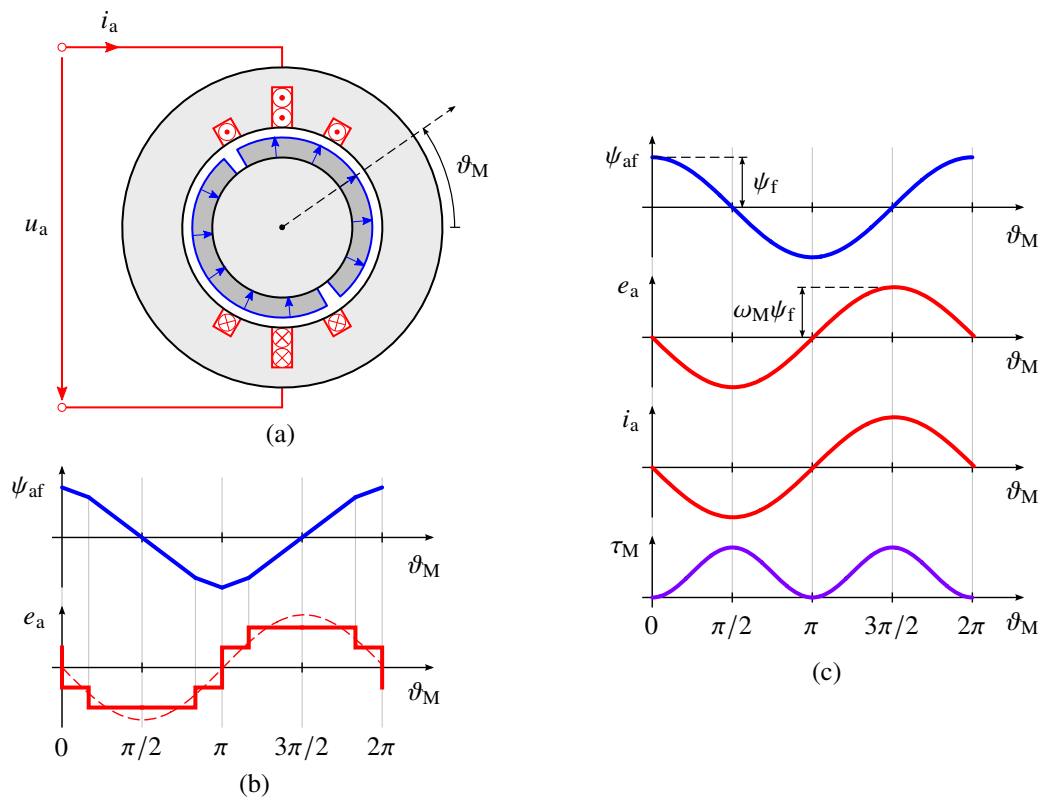
Figure 8.3: Simple distributed winding: (a) cross-section; (b) resulting waveforms of the PM flux linkage ψ_{af} and the back-emf e_a as a function of the rotor position; (c) waveforms as a function of the rotor position, assuming ideal sinusoidally distributed winding. In (c), sinusoidal current i_a in phase with e_a is fed to the machine.

8.1.4 Ideal Distributed Winding

Next, the stator winding is assumed to be sinusoidally distributed along the air gap, which results in the sinusoidal magnetomotive force (mmf) distribution. Since the air gap is assumed to be uniform, the flux density distribution at the air gap due to the stator mmf is also sinusoidal. Notice that the PMs can still be assumed to produce a rectangular air-gap flux density distribution, see Figure 8.1(b).

Figure 8.3(c) shows the waveforms under these assumptions. The PM flux linkage ψ_{af} varies sinusoidally as a function of the rotor position,

$$\psi_{af} = \psi_f \cos(\vartheta_M) \tag{8.10}$$

where ψ_f is the PM-flux constant, proportional to $Nr\ell B_f$. According to (8.7), the back-emf also varies sinusoidally,

$$e_a = -\omega_M \psi_f \sin(\vartheta_M) \tag{8.11}$$

Based on (8.8), the electromagnetic torque is

$$\tau_M = -i_a \psi_f \sin(\vartheta_M) \tag{8.12}$$

where the waveform of the current i_a can be freely controlled. In Figure 8.3(c), the machine is fed with sinusoidal current i_a, which is in phase with the back-emf e_a. The resulting electromagnetic torque (and the produced mechanical power) oscillates at twice the fundamental frequency. The oscillating power is the fundamental property of single-phase sinusoidal AC systems (see Appendix B.1). The single-phase machines are not suitable for high-power applications due to torque oscillations and resulting mechanical vibrations. Furthermore, they can be difficult to get started.

8.2 Three-Phase Machines

Electric power systems and electric machines typically have three phases. The majority of the electric power is generated using three-phase generators. In transmission and distribution, the three-phase systems are more economical than single-phase systems, since less conductor material is needed to transmit the same amount of power. Furthermore, the torque and power of three-phase machines are ideally smooth, unlike those of single-phase machines. The basics of three-phase systems are reviewed in Appendix B.2.

8.2.1 Stator Winding

Three-phase machines have three sets of phase windings in the stator, which typically are distributed in the stator slots. As an example, Figure 8.4(a) shows the short-pitched winding, studied in the case of the single-phase machine. In the following, ideal sinusoidal spatial distribution of the windings will be assumed. For simplicity, only the center of the sinusoidally distributed conductors is shown, see Figure 8.4(b). The figure also shows the magnetic axes of three phases, separated by 120° from each other. The magnetic axis indicates the positive direction of the flux, when the corresponding phase winding is supplied with positive current.
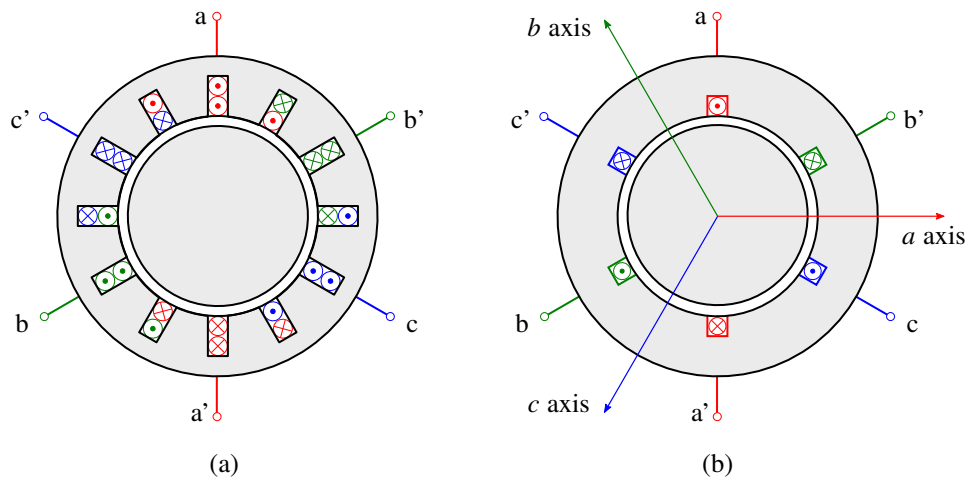
Figure 8.4: Three-phase winding: (a) simple distributed winding; (b) simplified representation and magnetic axes.
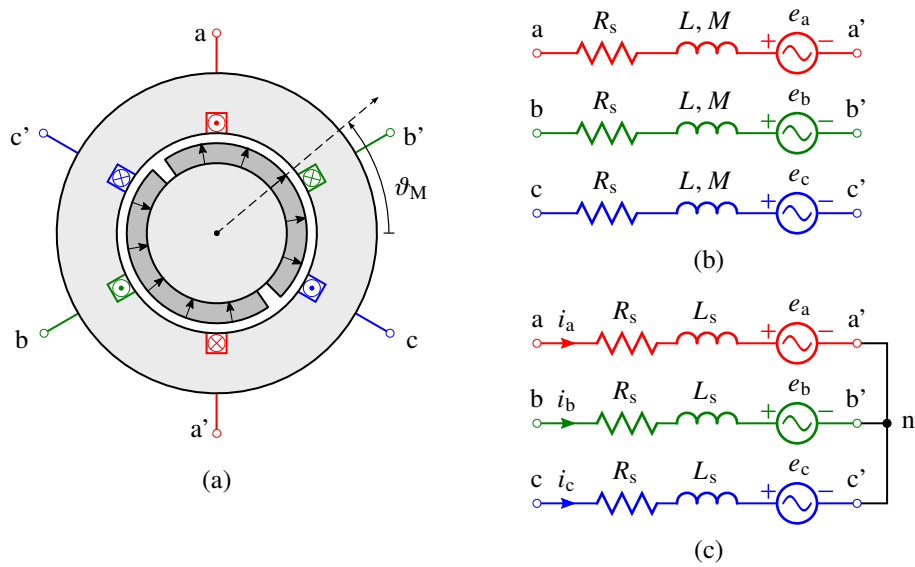

Figure 8.5: PM synchronous machine: (a) cross-section; (b) equivalent circuit with open-ended windings; (c) equivalent circuit with wye-connected windings.

8.2.2 Phase-Variable Model

A surface-mounted PM synchronous machine shown in Figure 8.5(a) is considered. This machine is otherwise equal to the single-phase machine, but phase windings b and c have been added with $\pm 120°$ phase shift with respect to phase a. Consequently, the phase-variable model can be constructed based on the already derived single-phase machine model. The phase voltage equations are

$$u_a = R_s i_a + \frac{d\psi_a}{dt} \tag{8.13a}$$

$$u_b = R_s i_b + \frac{d\psi_b}{dt} \tag{8.13b}$$

$$u_c = R_s i_c + \frac{d\psi_c}{dt} \tag{8.13c}$$

where R_s is the phase resistance, i.e., the same resistance for all the phases is assumed. The phase flux linkages are

$$\psi_a = Li_a + M(i_b + i_c) + \psi_f \cos(\vartheta_M) \tag{8.14a}$$
$$\psi_b = Li_b + M(i_a + i_c) + \psi_f \cos(\vartheta_M - 2\pi/3) \tag{8.14b}$$
$$\psi_c = Li_c + M(i_a + i_b) + \psi_f \cos(\vartheta_M - 4\pi/3) \tag{8.14c}$$

where L is the phase self-inductance and M is the mutual inductance between the phases. Both these inductances are constant in the case of a uniform air gap. The mutual inductance describes the coupling between the phases. As an example, the current i_a flowing in phase a causes the flux linkage Mi_a in phases b and c. Based on the geometry, it can be realized that M is negative.

Except this mutual magnetic coupling, (8.14) remains the same as that of the single-phase machines. The induced voltages are

$$e_a = -\omega_M \psi_f \sin(\vartheta_M) \tag{8.15a}$$
$$e_b = -\omega_M \psi_f \sin(\vartheta_M - 2\pi/3) \tag{8.15b}$$
$$e_c = -\omega_M \psi_f \sin(\vartheta_M - 4\pi/3) \tag{8.15c}$$

The instantaneous electromagnetic torque is

$$\tau_M = -\psi_f \left[i_a \sin(\vartheta_M) + i_b \sin(\vartheta_M - 2\pi/3) + i_c \sin(\vartheta_M - 4\pi/3) \right] \tag{8.16}$$

It is worth noticing that if the machine is supplied with balanced sinusoidal phase currents, the electromagnetic torque is constant.

Figure 8.5(b) shows the corresponding equivalent circuit of the machine with open-ended windings, having six terminals. A regular three-phase configuration is obtained by connecting the terminals either to wye or delta connection. Figure 8.5(c) shows the wye-connected winding. The stator winding has now three terminals, and the sum of the phase currents has to be zero, $i_a + i_b + i_c = 0$. Applying this condition to (8.14) allows to simplify the flux equations,

$$\psi_a = L_s i_a + \psi_f \cos(\vartheta_M) \tag{8.17a}$$
$$\psi_b = L_s i_b + \psi_f \cos(\vartheta_M - 2\pi/3) \tag{8.17b}$$
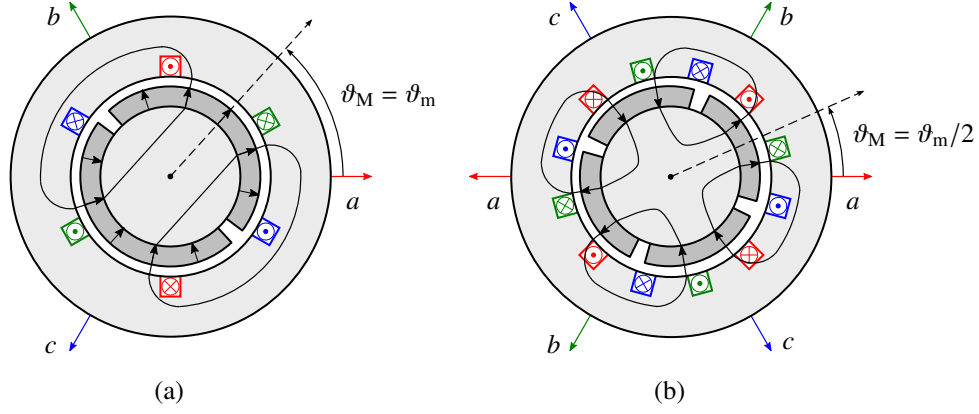$$\psi_c = L_s i_c + \psi_f \cos(\vartheta_M - 4\pi/3) \tag{8.17c}$$

Figure 8.6: Number of poles: (a) two poles ($n_p = 1$); (b) four poles ($n_p = 2$). Magnetic axes of the stator winding are also shown. If the stator frequency is the same for both machines, the rotor of the two-pole machine rotates two times the angle of the four-pole machine in a given time.

Table 8.1: Rotor speeds for $f = 50$ Hz.

Number of pole pairs n_p	Rotation speed n (r/min)
1	3 000
2	1 500
3	1 000
4	750
5	600
6	500

where $L_s = L - M$ is the stator inductance.

This phase-variable model is unnecessarily complicated for analysis and control purposes. In the next chapter, the machine model will be represented in a much simpler manner by means of space-vector transformation.

8.2.3   Number of Poles

Figure 8.6 shows cross-sections of two-pole and four-pole synchronous machines. First, notice that both the stator and the rotor in synchronous machines should have the same number of poles in order to produce the electromagnetic torque. If the stator frequency (supply frequency) is the same for both machines, the rotor of the two-pole machine rotates two times the angle of the four-pole machine in a given time. Consequently, the machine having more poles rotates slower with the same stator frequency. The electrical angular speed and angle of the rotor are defined as

$$\omega_m = n_p \omega_M \qquad \vartheta_m = n_p \vartheta_M \qquad (8.18)$$

respectively, where n_p is the number of pole pairs. A machine with more poles can be modeled using the same model as the two-pole machine. The only differences are that the electrical angular speed ω_m and the electrical angle ϑ_m have to be used in electrical equations (8.14), (8.15), and (8.17). Furthermore, the number n_p of pole pairs appears as a multiplier in the expression for the electromagnetic torque (8.16) since all the pole pairs contribute to the torque.

In the steady state, the electrical angular speed is related to the stator frequency f as $\omega_m = 2\pi f$. The rotor speed is also commonly expressed as rounds per minute (r/min) as

$$n = \frac{f}{n_p} \frac{60 \text{ s}}{\text{min}}$$
(8.19)

Table 8.1 gives the rotor speeds for different pole pair numbers at the stator frequency of 50 Hz. However, notice that the nominal supply frequency of a machine does not need to match with the grid frequency in converter-fed machines.

69

Chapter 9

Space-Vector Models

The aim of this chapter is to introduce the concept of space vectors. The space-vector transformation allows to convert a set of three-phase quantities to a complex quantity, which simplifies models and enables physically insightful interpretations. Unlike complex phasors (Appendix B.2), space vectors are not limited to steady-state conditions. They are commonly used in the analysis, modeling, and control of electric machine drives and power electronics.

Space-vector models can be transformed to different coordinates, which may allow further simplifications of models. A surface-mounted permanent-magnet (PM) synchronous machine considered in Section 8.2.2 will be used as an example. It will be seen that the space-vector model of this machine in rotor coordinates resembles the DC machine model. Under steady-state conditions, space-vector models reduce to the phasor models. The reader is assumed to be familiar with complex numbers, but some of their basic properties are also briefly reviewed.

9.1 Space Vectors

9.1.1 Definition

Figure 9.1 shows the magnetic axes of a three-phase stator winding. In the complex plane, the magnetic axes can be defined by unit vectors e^{j0}, $e^{j2\pi/3}$, and $e^{j4\pi/3}$, corresponding to phases a, b, and c. The phase windings are assumed to be distributed sinusoidally in angular space around the stator, which results in sinusoidally distributed phase currents i_a, i_b, and i_c. The net current distribution can be represented by the vectorial sum, known as the space vector [1]

$$i_s^s = \frac{2K}{3} \left(i_a + i_b e^{j2\pi/3} + i_c e^{j4\pi/3} \right) \tag{9.1}$$

where the superscript s marks the stator reference frame and K is the scaling factor. It is common to use peak-value scaling ($K = 1$), rms-value scaling ($K = 1/\sqrt{2}$) or power-invariant scaling ($K = \sqrt{3/2}$). Figure 9.2(a) illustrates the space-vector transformation. The same transformation applies to other three-phase quantities, such as voltages and flux linkages.

The space vector does not include the zero-sequence component

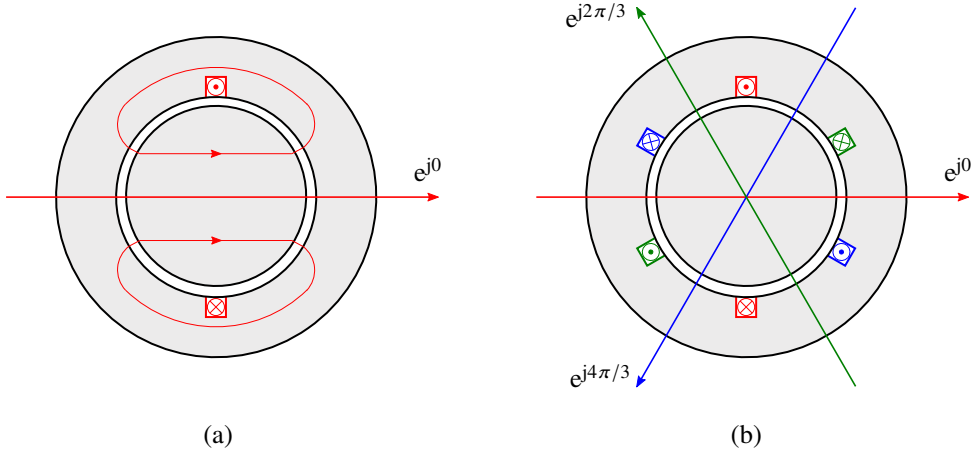$$i_0 = \frac{1}{3} \left(i_a + i_b + i_c \right) \tag{9.2}$$

Figure 9.1: Magnetic axes in the complex plane: (a) phase a; (b) three phases. The windings are assumed to be sinusoidally distributed in the air gap, but only the center of conductors is shown.
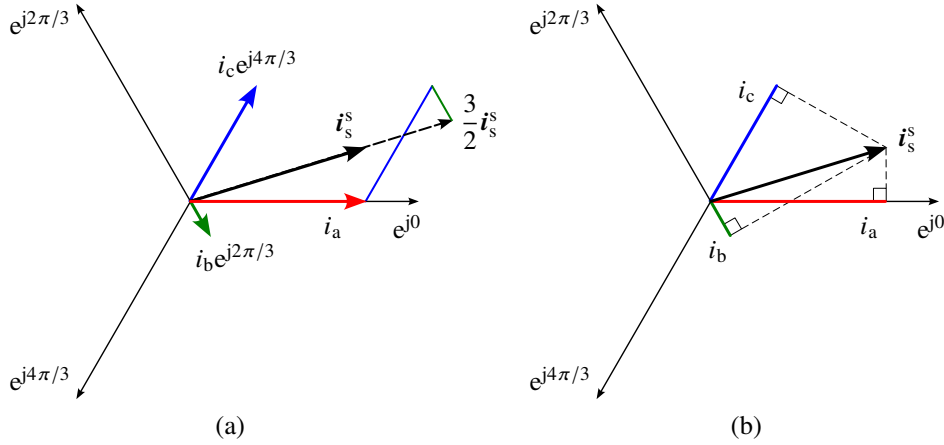
Figure 9.2: Space vector: (a) transformation; (b) inverse transformation. In this example, the scaling factor is $K = 1$.

but otherwise no information is lost in the space-vector transformation. Typically, the zero-sequence component is not of interest in electric machines, since the stator winding is either delta-connected or the star point of the wye-connected winding is not connected. Consequently, the zero-sequence current is zero, $i_0 = 0$. The zero-sequence voltage u_0 typically exists at the output voltage of power converters, but it cannot affect the power or the torque since $p_0 = u_0 i_0 = 0$ holds. In four-wire systems, the zero-sequence component is taken into account separately using (9.2), while the space-vector transformation (9.1) is directly applicable.

The inverse transformation to the phase quantities is obtained by projecting the space vector onto the magnetic axes, as illustrated in Figure 9.2(b). Correspondingly, the inverse transformation is

$$i_a = \frac{1}{K} \operatorname{Re}\left\{i_s^s\right\} + i_0 \tag{9.3a}$$

$$i_b = \frac{1}{K} \operatorname{Re}\left\{i_s^s e^{-j2\pi/3}\right\} + i_0 \tag{9.3b}$$

$$i_c = \frac{1}{K} \operatorname{Re}\left\{i_s^s e^{-j4\pi/3}\right\} + i_0 \tag{9.3c}$$

Figure 9.3: Current space vector: (a) components; (b) relation to the sinusoidal current distribution. The space vector can be understood to represent a sinusoidal distribution in space.

where the zero-sequence component i_0 is included for generality, even though it is typically not needed, as explained above. In the inverse transf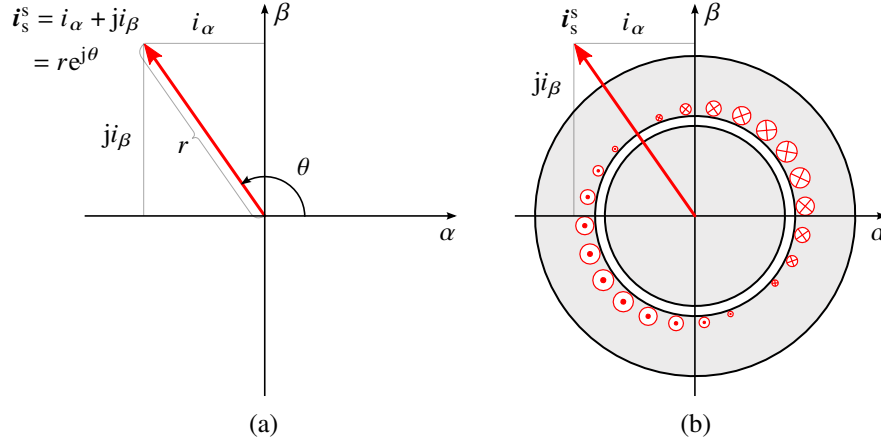ormation, the space vector is first rotated to the opposite direction as compared to (9.1) and then projected onto the real axis.

Figure 9.3(a) shows a space vector and its components. As any other complex numbers, the space vector can be presented in the Cartesian and polar forms,

$$\boldsymbol{i}_\mathrm{s}^\mathrm{s} = i_\alpha + \mathrm{j}i_\beta = r\mathrm{e}^{\mathrm{j}\theta}$$

where i_α and i_β are the real and imaginary components, respectively, and the magnitude is

$$r = |\boldsymbol{i}_\mathrm{s}^\mathrm{s}| = \sqrt{i_\alpha^2 + i_\beta^2} \tag{9.4}$$

The angle (argument) θ can be related to the Cartesian form via Euler's formula

$$\mathrm{e}^{\mathrm{j}\theta} = \cos\theta + \mathrm{j}\sin\theta \tag{9.5}$$

It is a common convention to mark the real and imaginary components of a space vector in stator coordinates with α and β, as done above.

Figure 9.3(b) illustrates the relation of the current space vector and the sinusoidal current distribution that is created by sinusoidally distributed phase windings. The magnetomotive force is also sinusoidally distributed in the air gap. Furthermore, if the magnetic saturation is omitted, the flux density is sinusoidally distributed. Space vectors can be understood to represent this kind of sinusoidal spatial distributions, which can vary arbitrarily in time.

Remark 4. Consider steady-state positive-sequence sinusoidal currents

$$i_\mathrm{a} = \hat{i}\cos(\omega_\mathrm{m}t + \phi) \tag{9.6a}$$
$$i_\mathrm{b} = \hat{i}\cos(\omega_\mathrm{m}t - 2\pi/3 + \phi) \tag{9.6b}$$
$$i_\mathrm{c} = \hat{i}\cos(\omega_\mathrm{m}t - 4\pi/3 + \phi) \tag{9.6c}$$

Applying the space-vector transformation (9.1) with $K = 1$ yields

$$\boldsymbol{i}_\mathrm{s}^\mathrm{s} = \hat{i}\mathrm{e}^{\mathrm{j}(\omega_\mathrm{m}t+\phi)} \tag{9.7}$$
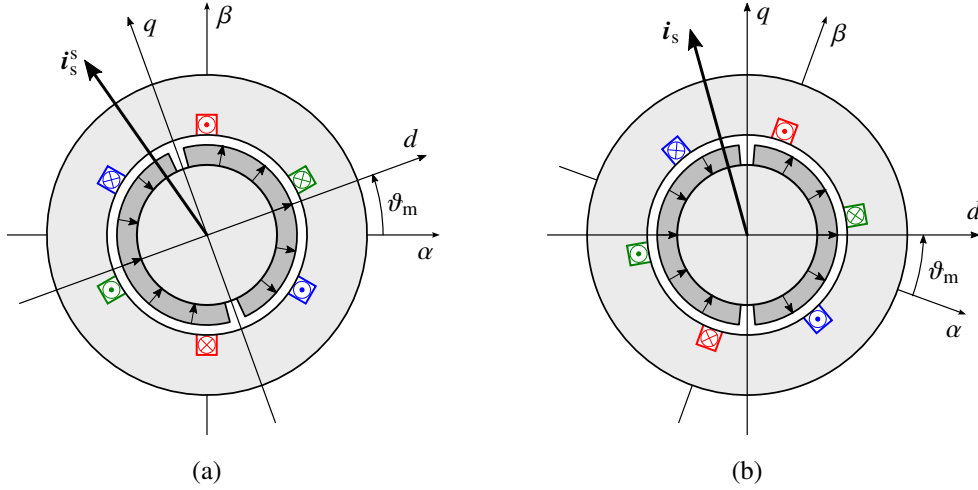
Figure 9.4: Stator current vector: (a) stator ($\alpha\beta$) coordinates; (b) rotor (dq) coordinates.

As expected, the space vector has constant magnitude corresponding to the peak value of the phase currents. Furthermore, the vector rotates to the positive direction with the angular frequency ω_{m}. Let us switch the order of two phase currents, for example, b and c, resulting in negative-sequence currents

$$i_{\mathrm{a}} = \hat{i}\cos(\omega_{\mathrm{m}}t + \phi) \tag{9.8a}$$

$$i_{\mathrm{b}} = \hat{i}\cos(\omega_{\mathrm{m}}t - 4\pi/3 + \phi) \tag{9.8b}$$

$$i_{\mathrm{c}} = \hat{i}\cos(\omega_{\mathrm{m}}t - 2\pi/3 + \phi) \tag{9.8c}$$

Now the resulting space vector is

$$\boldsymbol{i}_{\mathrm{s}}^{\mathrm{s}} = \hat{i}\mathrm{e}^{-\mathrm{j}(\omega_{\mathrm{m}}t + \phi)} \tag{9.9}$$

which rotates to the negative direction. Consequently, the space vector allows an intuitive interpretation of positive-sequence and negative-sequence components. This can be particularly beneficial in the analysis of non-sinusoidal periodic waveforms, which consist of positive and negative sequence components, such as

$$\boldsymbol{i}_{\mathrm{s}}^{\mathrm{s}} = \hat{i}_1\mathrm{e}^{\mathrm{j}(\omega_{\mathrm{m}}t + \phi_1)} + \hat{i}_5\mathrm{e}^{-\mathrm{j}(5\omega_{\mathrm{m}}t + \phi_5)} + \hat{i}_7\mathrm{e}^{\mathrm{j}(7\omega_{\mathrm{m}}t + \phi_7)}\ldots \tag{9.10}$$

9.1.2 Coordinate Transformations

As will be seen subsequently, space-vector models can be transformed to different coordinates, such as rotor coordinates, to simplify them. As a preliminary example, consider a positive-sequence vector $\boldsymbol{i}_{\mathrm{s}}^{\mathrm{s}} = \hat{i}\mathrm{e}^{\mathrm{j}(\omega_{\mathrm{m}}t + \phi)}$ expressed in stator coordinates. This vector rotates to the positive direction with the constant angular frequency ω_{m}. The rotation of the vector can be stopped by the transformation $\boldsymbol{i}_{\mathrm{s}} = \boldsymbol{i}_{\mathrm{s}}^{\mathrm{s}}\,\mathrm{e}^{-\mathrm{j}\omega_{\mathrm{m}}t} = \hat{i}\mathrm{e}^{\mathrm{j}\phi}$. In other words, the transformed vector $\boldsymbol{i}_{\mathrm{s}}$ is now observed in a coordinate system rotating at ω_{m}, in which the vector appears stationary.

The previous example assumed the rotor speed ω_{m} to be constant. In a more general case, the transformation from stator ($\alpha\beta$) coordinates to rotor (dq) coordinates is

$$\boldsymbol{i}_{\mathrm{s}} = \boldsymbol{i}_{\mathrm{s}}^{\mathrm{s}}\mathrm{e}^{-\mathrm{j}\vartheta_{\mathrm{m}}} \tag{9.11}$$

where the rotor angle is $\vartheta_{\mathrm{m}} = \int \omega_{\mathrm{m}} \mathrm{d}t$. In rotor coordinates, space vectors are denoted with no superscripts. Furthermore, the components are commonly marked with d and q subscripts, $\boldsymbol{i}_{\mathrm{s}} = i_{\mathrm{d}} + j i_{\mathrm{q}}$, originating from the terms *direct* and *quadrature* axes, respectively. The d axis is aligned with the PMs. The inverse transformation, obtained from (9.11), is

$$\boldsymbol{i}_{\mathrm{s}}^{\mathrm{s}} = \boldsymbol{i}_{\mathrm{s}} \mathrm{e}^{\mathrm{j}\vartheta_{\mathrm{m}}} \tag{9.12}$$

Figure 9.4 illustrates the current vector in stator and rotor coordinates. Vectors in rotor coordinates are constant in steady state. The above explanations and equations assumed transformation to rotor coordinates, but the same transformations apply for any other coordinates, if only the angle ϑ_{m} is replaced with the corresponding angle.

9.2 Synchronous Machine Model

9.2.1 Stator Coordinates

The space-vector model of a surface-mounted PM synchronous machine is derived starting from the phase-variable model presented in Section 8.2.2. Applying the voltage equations (8.13) and the space-vector transformation (9.1) yields the voltage vector

$$\boldsymbol{u}_{\mathrm{s}}^{\mathrm{s}} = R_{\mathrm{s}} \boldsymbol{i}_{\mathrm{s}}^{\mathrm{s}} + \frac{\mathrm{d}\boldsymbol{\psi}_{\mathrm{s}}^{\mathrm{s}}}{\mathrm{d}t} \tag{9.13}$$

where R_{s} is the stator resistance. Similarly, the flux linkage equations (8.17) result in the stator flux linkage vector[1]

$$\boldsymbol{\psi}_{\mathrm{s}}^{\mathrm{s}} = L_{\mathrm{s}} \boldsymbol{i}_{\mathrm{s}}^{\mathrm{s}} + \boldsymbol{\psi}_{\mathrm{f}}^{\mathrm{s}} \tag{9.14}$$

where the PM flux linkage vector is

$$\boldsymbol{\psi}_{\mathrm{f}}^{\mathrm{s}} = \psi_{\mathrm{f}} \mathrm{e}^{\mathrm{j}\vartheta_{\mathrm{m}}} \tag{9.15}$$

Using space vectors, the electromagnetic torque in (8.16) can be expressed as

$$\tau_{\mathrm{M}} = \frac{3 n_{\mathrm{p}}}{2 K^2} \operatorname{Im}\left\{\boldsymbol{i}_{\mathrm{s}}^{\mathrm{s}} \boldsymbol{\psi}_{\mathrm{s}}^{\mathrm{s}*}\right\} \tag{9.16}$$

where the superscript $*$ marks complex conjugate. The torque expression could be presented in various forms, but the above expression was selected here, since it holds for other AC machines as well. For illustrating torque production, the current and flux linkage vectors can be expressed in the polar form, i.e., $\boldsymbol{i}_{\mathrm{s}}^{\mathrm{s}} = |\boldsymbol{i}_{\mathrm{s}}^{\mathrm{s}}| \, \mathrm{e}^{\mathrm{j}\theta_i}$ and $\boldsymbol{\psi}_{\mathrm{s}}^{\mathrm{s}} = |\boldsymbol{\psi}_{\mathrm{s}}^{\mathrm{s}}| \, \mathrm{e}^{\mathrm{j}\theta_\psi}$, respectively. Substituting these into (9.16) yields

$$\tau_{\mathrm{M}} = \frac{3 n_{\mathrm{p}}}{2 K^2} |\boldsymbol{i}_{\mathrm{s}}^{\mathrm{s}}| \, |\boldsymbol{\psi}_{\mathrm{s}}^{\mathrm{s}}| \sin \gamma \tag{9.17}$$

where $\gamma = \theta_i - \theta_\psi$ is the angle between the two vectors, see Figure 9.5. Nonzero angle γ is needed for torque production. For the machine type under consideration, nonzero angle γ and thus the torque production is possible due to the PMs.

---

[1]The torque equation (8.16) and the flux linkage equations (8.17) assume that the machine has two poles, but this assumption has been lifted here, see Section 8.2.3.
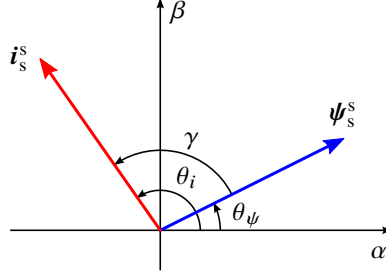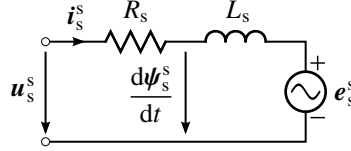
Figure 9.5: Vectors related to torque production.

Figure 9.6: Space-vector equivalent circuit.

Using space vectors, the instantaneous active power fed to the stator can be written as[2]

$$p_{\mathrm{s}} = \frac{3}{2K^2} \operatorname{Re} \left\{ \boldsymbol{u}_{\mathrm{s}}^{\mathrm{s}} \boldsymbol{i}_{\mathrm{s}}^{\mathrm{s*}} \right\} \tag{9.18}$$

The voltage and current vectors can be expressed in the polar form, i.e., $\boldsymbol{u}_{\mathrm{s}}^{\mathrm{s}} = |\boldsymbol{u}_{\mathrm{s}}^{\mathrm{s}}| \mathrm{e}^{\mathrm{j}\theta_u}$ and $\boldsymbol{i}_{\mathrm{s}}^{\mathrm{s}} = |\boldsymbol{i}_{\mathrm{s}}^{\mathrm{s}}| \mathrm{e}^{\mathrm{j}\theta_i}$, respectively. Substituting these into (9.18) yields

$$p_{\mathrm{s}} = \frac{3}{2K^2} |\boldsymbol{u}_{\mathrm{s}}^{\mathrm{s}}| \, |\boldsymbol{i}_{\mathrm{s}}^{\mathrm{s}}| \cos \varphi \tag{9.19}$$

where $\varphi = \theta_u - \theta_i$. The factor $\cos \varphi$ corresponds to the displacement power factor under the steady-state condition. Notice, however, that the above expressions are valid also under transient conditions.

If desired, the flux linkage equation (9.14) can be inserted into the voltage equation (9.13), resulting in

$$\boldsymbol{u}_{\mathrm{s}}^{\mathrm{s}} = R_{\mathrm{s}} \boldsymbol{i}_{\mathrm{s}}^{\mathrm{s}} + L_{\mathrm{s}} \frac{\mathrm{d}\boldsymbol{i}_{\mathrm{s}}^{\mathrm{s}}}{\mathrm{d}t} + \boldsymbol{e}_{\mathrm{s}}^{\mathrm{s}} \tag{9.20}$$

As expected, the back-emf $\boldsymbol{e}_{\mathrm{s}}^{\mathrm{s}} = \mathrm{j}\omega_{\mathrm{m}} \boldsymbol{\psi}_{\mathrm{f}}^{\mathrm{s}}$ is proportional to the rotor speed. Figure 9.6 shows the corresponding space-vector equivalent circuit.

9.2.2 Rotor Coordinates

The space-vector model presented in stator coordinates is still unnecessary complicated since the vectors rotate in the steady state and the stator flux linkage (9.14) depends on the rotor angle. For further simplifications, the model can be transformed to rotor coordinates. Based on (9.12), $\boldsymbol{\psi}_{\mathrm{s}}^{\mathrm{s}} = \boldsymbol{\psi}_{\mathrm{s}} \mathrm{e}^{\mathrm{j}\vartheta_{\mathrm{m}}}$, $\boldsymbol{u}_{\mathrm{s}}^{\mathrm{s}} = \boldsymbol{u}_{\mathrm{s}} \mathrm{e}^{\mathrm{j}\vartheta_{\mathrm{m}}}$, and $\boldsymbol{i}_{\mathrm{s}}^{\mathrm{s}} = \boldsymbol{i}_{\mathrm{s}} \mathrm{e}^{\mathrm{j}\vartheta_{\mathrm{m}}}$ can be inserted into the voltage equation (9.13), resulting in

$$\boldsymbol{u}_{\mathrm{s}} = R_{\mathrm{s}} \boldsymbol{i}_{\mathrm{s}} + \frac{\mathrm{d}\boldsymbol{\psi}_{\mathrm{s}}}{\mathrm{d}t} + \mathrm{j}\omega_{\mathrm{m}} \boldsymbol{\psi}_{\mathrm{s}} \tag{9.21}$$

---

[2]It can be easily shown that this power expression equals the phase-variable expression for the instantaneous power $p_{\mathrm{s}} = u_a i_a + u_b i_b + u_c i_c$. Furthermore, if the power-invariant scaling ($K = \sqrt{3/2}$) is used, the power expression reduces to $p_{\mathrm{s}} = \operatorname{Re}\{\boldsymbol{u}_{\mathrm{s}}^{\mathrm{s}} \boldsymbol{i}_{\mathrm{s}}^{\mathrm{s*}}\}$.
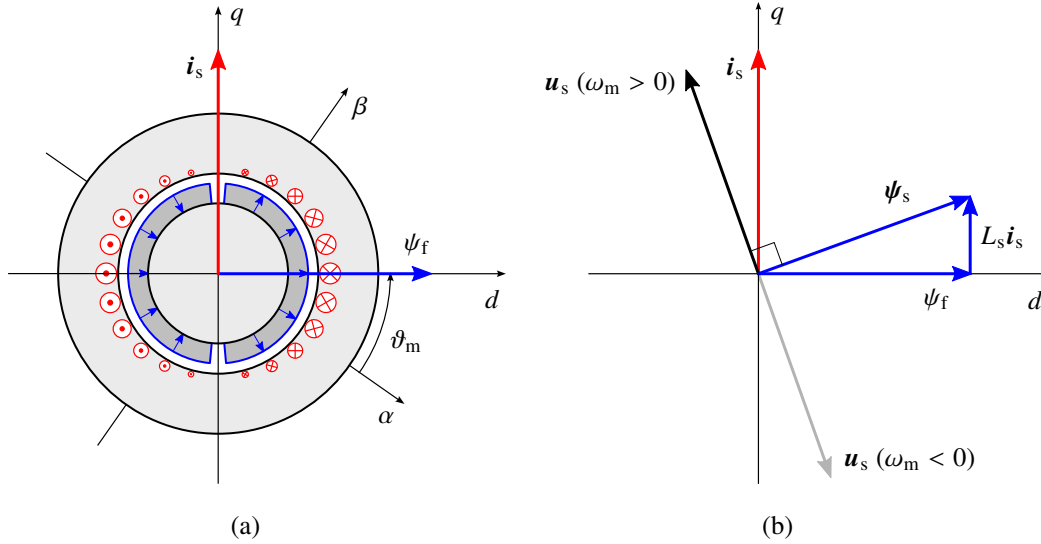
Figure 9.7: (a) Cross-section of a PM synchronous machine in rotor coordinates. The current distribution produced by a three-phase winding is illustrated. In this example, the current vector i_s is along the q axis. (b) Vector diagram. For simplicity, zero stator resistance is assumed, $R_s = 0$, giving $u_s = j\omega_m\psi_s$, which is feasible approximation at medium and high speeds. The gray voltage vector corresponds to the negative rotor speed.

The flux linkage equation (9.14) can be transformed similarly, giving

$$\psi_s = L_s i_s + \psi_f \tag{9.22}$$

The electromagnetic torque expression (8.16) is valid in any coordinates. Applying (9.22), it can be expressed as

$$\tau_M = \frac{3n_p}{2K^2} \, \text{Im}\{i_s\psi_s^*\} = \frac{3n_p}{2K^2}\psi_f i_q \tag{9.23}$$

The torque is proportional to the q-component i_q of the stator current, while the d-component i_d does not contribute to the torque. It can also be noticed that the latter form of the torque expression in (9.23) resembles that of PM DC machines.

Using (9.22), the stator voltage (9.21) can be rewritten as

$$u_s = R_s i_s + L_s \frac{di_s}{dt} + j\omega_m L_s i_s + e_s \tag{9.24}$$

where $e_s = j\omega_m\psi_f$ is the back-emf. Notice that the PMs induce the voltage e_s in the stator winding, if the rotor speed ω_m is nonzero. This aspect is important also from the electrical safety perspective.

Using (9.18) and (9.24), the power fed to the stator can be written as

$$p_s = \frac{3}{2K^2} \, \text{Re}\{u_s i_s^*\} = \frac{3}{2K^2}R_s|i_s|^2 + \frac{3}{2K^2}\frac{L_s}{2}\frac{d|i_s|^2}{dt} + \tau_M\frac{\omega_m}{n_p} \tag{9.25}$$

On the right-hand side, the first term corresponds to the resistive losses, the second term to the rate of change of the field energy related to the inductance L_s, and the last term to the mechanical power. Notice that the second term on the right-hand side is zero in the steady state.

76

Figure 9.7 illustrates a sinusoidal current distribution and a vector diagram in rotor coordinates. In this example, the current vector $\boldsymbol{i}_\mathrm{s}$ is aligned along the positive q axis, corresponding to the positive electromagnetic torque. The stator flux vector is obtained from (9.22). In the steady state, $\mathrm{d}/\mathrm{d}t = 0$ holds in rotor coordinates, giving the stator voltage

$$\boldsymbol{u}_\mathrm{s} = R_\mathrm{s}\boldsymbol{i}_\mathrm{s} + \mathrm{j}\omega_\mathrm{m}\boldsymbol{\psi}_\mathrm{s} = R_\mathrm{s}\boldsymbol{i}_\mathrm{s} + \mathrm{j}\omega_\mathrm{m}(L_\mathrm{s}\boldsymbol{i}_\mathrm{s} + \psi_\mathrm{f}) \tag{9.26}$$

where typically $R_\mathrm{s} = 0$ can be assumed at medium and high speeds. Under this assumption, the voltage magnitude is proportional to the speed. It is also worth noticing that the space-vector model under the steady-state condition reduces to the phasor model.

Chapter 10

Three-Phase Pulse-Width Modulation

The aim of this chapter is to introduce pulse-width modulation (PWM) of a three-phase voltage-source converter [17]. First, the space-vector representation of the converter output voltages is considered. Then, carrier-based implementation for the sinusoidal and space-vector PWM methods is presented [18].

10.1   Voltage-Source Converter

10.1.1   Topology

Figure 10.1(a) shows the main circuit of a three-phase two-level voltage-source converter [4]. This converter resembles the four-quadrant DC-DC converter (Section 6.2). The only difference is that the number of legs is now three instead of two. The basic operating principles and definitions remain the same and are thus not repeated here.

Assuming ideal transistors and diodes, the converter can be represented with the equivalent circuit shown in Figure 10.1(b), in which the legs are modeled as bi-positional switches. Furthermore, a three-phase AC load is also shown in the figure. The same converter can operate as an inverter when the power flows from the DC bus to the AC side and as a rectifier when the power flows from the AC side to the DC bus.
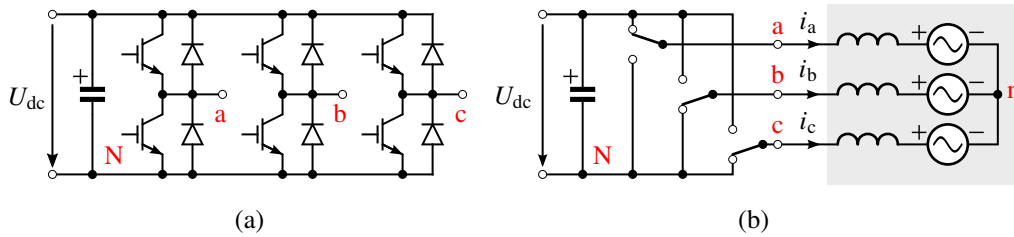

(a)   (b)

Figure 10.1: Three-phase converter: (a) main circuit; (b) equivalent circuit, including a three-phase load. The DC-bus voltage is denoted by U_{dc}. The negative potential of the DC bus is marked with N and the output terminals with a, b, and c. The neutral point of the load is marked with n.
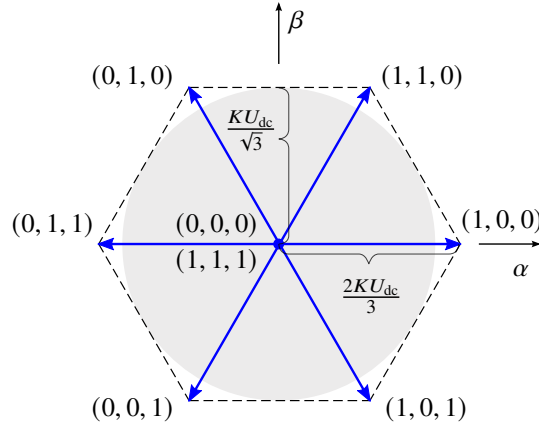
Figure 10.2: Voltage hexagon, showing the instantaneous voltage vectors of a three-phase converter. The circle with radius $KU_{\mathrm{dc}}/\sqrt{3}$ is the limit of the linear modulation region.

10.1.2 Voltage Vectors

A set of three-phase quantities can be transformed to a space vector by means of the space-vector transformation (9.1). If the focus is on an electric machine, its neutral point n is commonly considered as the reference potential for the phase voltages, see Figure 10.1(b). As discussed in Chapter 9.1, the zero-sequence voltage does not affect the space vector. Consequently, the reference potential can be selected arbitrarily, for example,

$$
\begin{aligned}
\boldsymbol{u}_{\mathrm{s}}^{\mathrm{s}} &= \frac{2K}{3}\left(u_{\mathrm{an}} + u_{\mathrm{bn}}e^{\mathrm{j}2\pi/3} + u_{\mathrm{cn}}e^{\mathrm{j}4\pi/3}\right) \\
&= \frac{2K}{3}\left(u_{\mathrm{aN}} + u_{\mathrm{bN}}e^{\mathrm{j}2\pi/3} + u_{\mathrm{cN}}e^{\mathrm{j}4\pi/3}\right)
\end{aligned}
\tag{10.1}
$$

where the reference potential in the latter form is negative DC bus N. This latter form is more convenient when the converter output voltage and PWM methods are considered.[1]

Remark 5. Since the choice of the reference potential is arbitrary, one of the phases can also be selected. As an example, choosing phase b as the reference potential results in

$$
\boldsymbol{u}_{\mathrm{s}}^{\mathrm{s}} = \frac{2K}{3}\left(u_{\mathrm{ab}} - u_{\mathrm{bc}}e^{\mathrm{j}4\pi/3}\right)
\tag{10.2}
$$

where u_{ab} and u_{bc} are the line-to-line voltages. The space vector can be calculated if the instantaneous values of two line-to-line voltages are available. Typically, it is simpler to arrange the measurement of the line-to-line voltages as compared to the line-to-neutral voltages.

Consider the equivalent circuit in Figure 10.1(b). In normal operation, each of three bi-positional switches should be connected to either positive or negative potential in order to provide path for the load current to flow. The state of each switch can be defined using the switching state, which, using phase a as an example, is $q_{\mathrm{a}} = 0$ when the switch is connected to the negative potential and $q_{\mathrm{a}} = 1$ when the switch is connected to the positive potential. Consequently, the

---

[1]Other common convention is to use the middle point of the DC bus as the reference potential. The choice between these two conventions is a matter of taste.

space vector (10.1) of the instantaneous converter output voltage (or the stator voltage) can be expressed using the switching states as

$$\boldsymbol{u}_s^s = \frac{2K}{3}\left(q_a + q_b e^{j2\pi/3} + q_c e^{j4\pi/3}\right) U_{dc} \tag{10.3}$$

Since the converter has three bi-positional switches, there are eight possible switching state combinations in total. For example, choosing $q_a = 1$, $q_b = 0$, and $q_c = 0$ or briefly $(1, 0, 0)$ results in the space vector $\boldsymbol{u}_s^s = 2KU_{dc}/3$.

Figure 10.2 shows all possible switching state combinations in the complex plane. There are two zero vectors, i.e., $(0, 0, 0)$ and $(1, 1, 1)$, and six active vectors. The tips of the active voltage vectors form a hexagon. The circle with radius $KU_{dc}/\sqrt{3}$ is the limit of the linear modulation region. The area between the circle and the hexagon is called the overmodulation region. The largest possible fundamental voltage $2KU_{dc}/\pi$ is obtained using so called six-step modulation, in which only active vectors are used [17, 19].

10.2   Pulse-Width Modulation

10.2.1   Switching-Period Average Voltage

The average voltage over the switching period can be expressed as

$$\overline{\boldsymbol{u}}_s^s = \frac{2K}{3}\left(d_a + d_b e^{j2\pi/3} + d_c e^{j4\pi/3}\right) U_{dc} \tag{10.4}$$

where d_a, d_b, and d_c are the duty ratios, whose value is between 0 and 1. In PWM methods, the duty ratios are selected so that $\overline{\boldsymbol{u}}_s^s = \boldsymbol{u}_{s,ref}$ holds, where $\boldsymbol{u}_{s,ref}$ is the voltage reference. Any voltage vector inside the voltage hexagon can be produced in average. Notice that the mapping from the average voltage to the duty ratios is not unique, i.e., any zero-sequence component can be added to the duty ratios without affecting the average voltage (as long as the duty ratios remain between 0 and 1). Various different PWM methods are available, all of which produce the desired average voltage, but with different zero-sequence voltages and pulse patterns [5, 17, 18, 20].

For a given voltage reference, the duty ratios of two active vectors and the total duty ratio of zero vectors can be solved using the simple geometry in the complex plane. Then, the application sequence of these vectors has to be selected. This approach with a symmetrical switching sequence is commonly referred to as space-vector modulation [11, 20]. This same method can be alternatively obtained by means of a carrier comparison with a proper zero-sequence voltage [18]. The carrier-based approach is considered in the following, since it can be more straightforward to implement.

10.2.2   Carrier Comparison

Assume that the input signal of the PWM method is the voltage reference $\boldsymbol{u}_{s,ref}^s$, which is typically obtained from the current controller after the coordinate transformation. Using the inverse space-vector transformation (9.3), the phase voltage
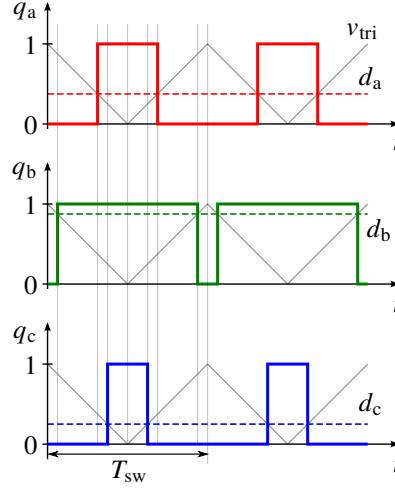
Figure 10.3: Generation of switching signals by means of a carrier comparison. In this example, $u_{0,\text{ref}} = 0$. The instantaneous voltage vectors during the first half of the switching period T_{sw} are: $(0, 0, 0) \rightarrow (0, 1, 0) \rightarrow (1, 1, 0) \rightarrow (1, 1, 1)$. In the second half, the same vectors are applied in the reverse order: $(1, 1, 1) \rightarrow (1, 1, 0) \rightarrow (0, 1, 0) \rightarrow (0, 0, 0)$.

references are obtained as

$$u_{\text{a,ref}} = \frac{1}{K} \, \text{Re}\left\{ \boldsymbol{u}_{\text{s,ref}}^{\text{s}} \right\} \tag{10.5a}$$

$$u_{\text{b,ref}} = \frac{1}{K} \, \text{Re}\left\{ \boldsymbol{u}_{\text{s,ref}}^{\text{s}} e^{-\text{j}2\pi/3} \right\} \tag{10.5b}$$

$$u_{\text{c,ref}} = \frac{1}{K} \, \text{Re}\left\{ \boldsymbol{u}_{\text{s,ref}}^{\text{s}} e^{-\text{j}4\pi/3} \right\} \tag{10.5c}$$

As discussed above, the zero-sequence voltage reference $u_{0,\text{ref}}$ can be added to the phase voltage references without affecting the average voltage space vector.

To generate the switching signals, the phase voltage references are compared with a triangular wave v_{tri}, whose period is denoted by T_{sw}. The same carrier signal is used for all phases. Here, the triangular wave is assumed to vary between 0 and 1, which allows its direct comparison with the duty ratios, as shown in Figure 10.3. The duty ratios are obtained by scaling the phase voltage references by the DC-bus voltage, i.e.,

$$d_{\text{a}} = \frac{1}{2} + \frac{u_{\text{a,ref}} + u_{0,\text{ref}}}{U_{\text{dc}}} \quad d_{\text{b}} = \frac{1}{2} + \frac{u_{\text{b,ref}} + u_{0,\text{ref}}}{U_{\text{dc}}} \quad d_{\text{c}} = \frac{1}{2} + \frac{u_{\text{c,ref}} + u_{0,\text{ref}}}{U_{\text{dc}}} \tag{10.6}$$

Notice that the phase voltage in average is zero if the duty ratio is 50%, which explains the offset terms. In the digital implementation, the voltage references can be updated at the beginning and middle of the carrier. It is also to be noted that the DC-bus voltage U_{dc} used in (10.6) is typically measured.[2] Therefore, the reference voltage is realized despite the variations in the DC-bus voltage (but, of course, the maximum available voltage is limited).

Sinusoidal PWM

In classical sinusoidal PWM, the zero-sequence voltage reference $u_{0,\text{ref}} = 0$ is selected. Figure 10.4(a) illustrates the resulting duty ratios over one fundamental

---

[2]For simplicity, this feedback signal is omitted in the block diagrams of Chapter 11.
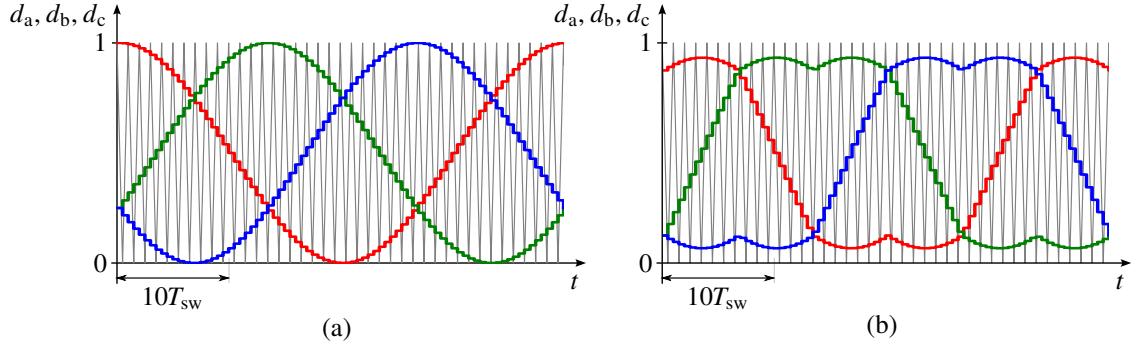
Figure 10.4: Duty ratios over one fundamental period: (a) sinusoidal PWM; (b) space-vector PWM. In both methods, the magnitude of the voltage reference is $|\boldsymbol{u}^{\mathrm{s}}_{\mathrm{s,ref}}| = U_{\mathrm{dc}}/2$. Furthermore, the carrier wave is also shown, assuming that the switching frequency $f_{\mathrm{sw}} = 1/T_{\mathrm{sw}}$ is 40 times the fundamental frequency. The duty references are discretely updated at the beginning and middle of the carrier.
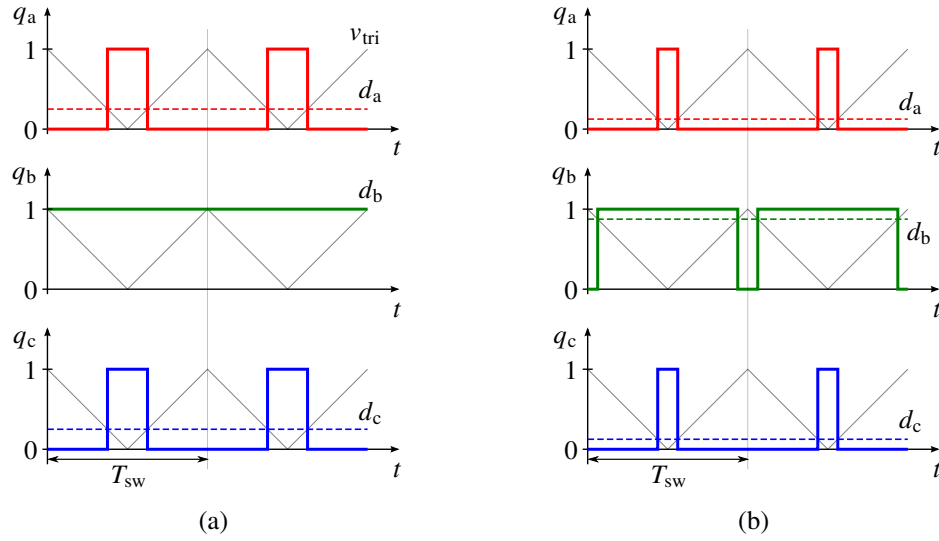

Figure 10.5: Duty ratios and switching states at the switching period level: (a) sinusoidal PWM; (b) space-vector PWM. In this example, the voltage reference is $\boldsymbol{u}^{\mathrm{s}}_{\mathrm{s,ref}} = (KU_{\mathrm{dc}}/2)\mathrm{e}^{\mathrm{j}2\pi/3}$, which yields $u_{\mathrm{a,ref}} = u_{\mathrm{c,ref}} = -U_{\mathrm{dc}}/4$ and $u_{\mathrm{b,ref}} = U_{\mathrm{dc}}/2$. Notice that all duty ratios in (b) have been lowered by the same amount as compared to the duty ratios in (a).

period in a sinusoidal steady state. It can be realized that modulation saturates when $|\boldsymbol{u}^{\mathrm{s}}_{\mathrm{s,ref}}| > KU_{\mathrm{dc}}/2$. Figure 10.5(a) shows details of this saturation phenomenon at the switching period level. It can be seen that one of the duty ratios has reached its maximum value, i.e., $d_{\mathrm{b}} = 1$. Consequently, increasing $u_{\mathrm{b,ref}}$ does not affect the phase voltage, since phase b is already connected to the positive potential during the whole switching period. Thus, only $\sqrt{3}/2$ or 87% of the maximum available linear modulation region can be used [17].

Space-Vector PWM

All available voltage can be utilized by means of a proper zero-sequence component $u_{\mathrm{0,ref}}$. Let us consider the carrier-based implementation of the space-vector PWM method, achieved by selecting

$$u_{\mathrm{0,ref}} = -\frac{\min(u_{\mathrm{a,ref}}, u_{\mathrm{b,ref}}, u_{\mathrm{c,ref}}) + \max(u_{\mathrm{a,ref}}, u_{\mathrm{b,ref}}, u_{\mathrm{c,ref}})}{2} \qquad (10.7)$$

Figure 10.4(b) illustrates the resulting duty ratios over one fundamental period. Furthermore, Figure 10.5(b) shows the details at the switching period level. It can be seen that the selected zero-sequence component places the minimum and maximum of the duty ratios symmetrically between 0 and 1, and the whole voltage hexagon can now be used. This method is identical to the space-vector PWM method [18].

If the voltage reference $\boldsymbol{u}^{\mathrm{s}}_{\mathrm{s,ref}}$ goes outside the voltage hexagon, the duty ratios computed using (10.6) become negative or larger than 1. The duty ratios can be simply clipped between 0 and 1, which results in the minimum-magnitude-error overmodulation method [21]. It is worth noticing that the carrier-based approach can be applied to implement other modern PWM methods as well, including discontinuous PWM methods [18] and methods for multilevel converters [22].

Chapter 11

Field-Oriented Control

The aim of this chapter is to describe field-oriented control principles of AC electric machines. The surface-mounted permanent-magnet (PM) synchronous machine is used as an example, but the presented principles can be extended to other AC machines as well. First, three-phase current control is considered. Then, the field-oriented control is introduced. The chapter ends with a discussion on the current and voltage limits.

11.1 Block Diagram

Figure 11.1 shows an overall block diagram of field-oriented control, which closely resembles cascade control of DC machines (Chapter 7). In the case of synchronous machines, the current vector has to be properly placed in relation to the rotor. Therefore, the rotor angle has to be measured or estimated [23].

The phase currents are measured and transformed to the current vector i_s^s using the space-vector transformation (9.1). The control system contains an inner current-control loop, which typically operates in rotor coordinates. Hence, the current vector $i_s = i_s^s e^{-j\vartheta_m}$ is further transformed to rotor coordinates, where the electrical rotor angle $\vartheta_m = n_p \vartheta_M$ is obtained from the measured mechanical angle. In the steady state, the current vector i_s is stationary, which simplifies the design of the current controller. Another reason for choosing rotor coordinates is that the current reference $i_{s,ref}$ can be easily related to the torque reference $\tau_{M,ref}$.
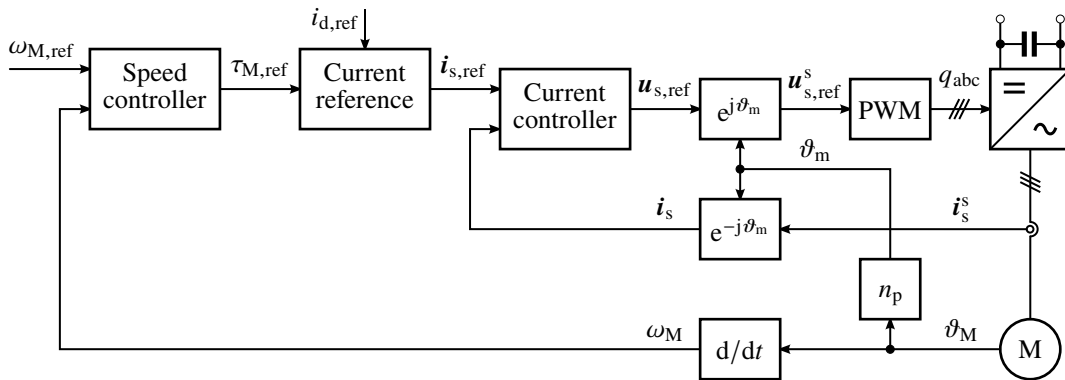

Figure 11.1: Field-oriented control system. The current vector i_s^s is obtained from the phase currents using the space-vector transformation (9.1).
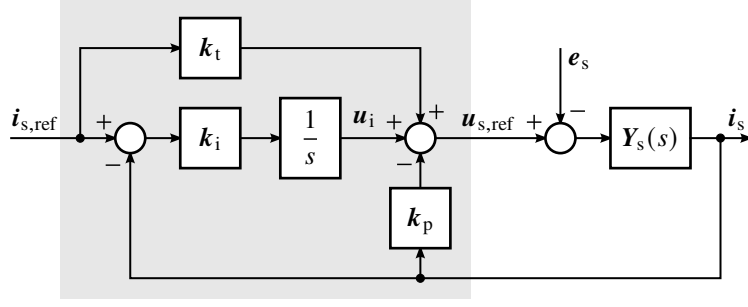
Figure 11.2: 2DOF PI controller (shaded) and the system model, with the assumption $\boldsymbol{u}_s = \boldsymbol{u}_{s,ref}$.

The speed controller is independent of the machine type. For example, a two-degrees-of-freedom (2DOF) proportional-integral (PI) controller can be used, see Chapter 7. In some applications, the speed controller is not used, but the machine is driven in the torque-control mode instead. In the following, the design of current control is first considered. Then, the calculation of the current reference is discussed.

11.2 Current Control

11.2.1 Open-Loop System

The design of 2DOF PI current control presented in Chapter 7 is extended for space vectors. Based on the voltage equation (9.24), the open-loop system seen by the current controller is

$$L_s \frac{\mathrm{d}\boldsymbol{i}_s}{\mathrm{d}t} = \boldsymbol{u}_s - R_s \boldsymbol{i}_s - \mathrm{j}\omega_m L_s \boldsymbol{i}_s - \boldsymbol{e}_s \tag{11.1}$$

where $\boldsymbol{e}_s = \mathrm{j}\omega_m \psi_f$ is the back-emf. The rotor speed ω_m is assumed to be quasi-constant due to the time-scale separation between the fast electrical subsystem and the slow mechanical subsystem. The back-emf $\boldsymbol{e}_s$ is considered as external load disturbance. In the Laplace domain, (11.1) can be expressed as

$$\begin{aligned} \boldsymbol{i}_s(s) &= \frac{1}{(s + \mathrm{j}\omega_m)L_s + R_s} \left[\boldsymbol{u}_s(s) - \boldsymbol{e}_s(s) \right] \\ &= \boldsymbol{Y}_s(s) \left[\boldsymbol{u}_s(s) - \boldsymbol{e}_s(s) \right] \end{aligned} \tag{11.2}$$

where the transfer function $\boldsymbol{Y}_s(s)$ is known as the stator admittance. Unlike the transfer functions in earlier chapters, this transfer function is complex [24]. The imaginary part of the transfer function causes coupling between the d and q channels.

11.2.2 Closed-Loop Control

Two-Degrees-of-Freedom Proportional-Integral Control

Figure 11.2 shows the block diagram of the 2DOF PI current controller and the system model, both in rotor coordinates. The measured current $\boldsymbol{i}_s$ is fed back

to the current controller, which generates the voltage reference $u_{s,ref}$. In the state-space form, the controller can be expressed as

$$\frac{d u_i}{dt} = k_i \left(i_{s,ref} - i_s \right) \tag{11.3a}$$

$$u_{s,ref} = k_t i_{s,ref} - k_p i_s + u_i \tag{11.3b}$$

where k_t is the reference feedforward gain, k_p is the proportional gain, k_i is the integral gain, and u_i is the integral state. The gains are marked in boldface since some of them will be complex. To provide an alternative view, the controller can be represented in the Laplace domain

$$u_{s,ref}(s) = k_t i_{s,ref}(s) - k_p i_s(s) + \frac{k_i}{s} \left[i_{s,ref}(s) - i_s(s) \right] \tag{11.4}$$

The selection $k_t = k_p$ yields the regular PI controller, i.e., the following closed-loop transfer function applies to this special case as well.

Closed-Loop System

In the following, perfect voltage production is assumed, $u_s = u_{s,ref}$. Inserting (11.4) into (11.2) yields the closed-loop system

$$\begin{aligned} i_s(s) &= \frac{(s k_t + k_i) i_{s,ref}(s) - s e_s(s)}{L_s s^2 + (R_s + j\omega_m L_s + k_p)s + k_i} \\ &= G_{cl}(s) i_{s,ref}(s) - Y_{cl}(s) e_s(s) \end{aligned} \tag{11.5}$$

where $G_{cl}(s)$ is the reference-tracking transfer function and $Y_{cl}(s)$ is the disturbance-rejection transfer function. The reference-tracking transfer function describes the effect of the reference $i_{s,ref}$ on the current i_s. Similarly, the disturbance-rejection transfer function describes the effect of the load disturbance e_s on the current i_s.

Gain Selection

From (11.5), it can be noticed that the characteristic polynomial (i.e. closed-loop poles) depend on the gains k_p and k_i. Furthermore, the zero of the reference-tracking transfer function depends on the gain k_t. Consequently, if the parameter estimates $\hat{L}_s$ and $\hat{R}_s$ are available, the poles and the reference-tracking zero can be freely placed. As an example, consider a typical gain selection [13, 15]

$$k_p = (2\alpha_c - j\omega_m)\hat{L}_s - \hat{R}_s \qquad k_i = \alpha_c^2 \hat{L}_s \qquad k_t = \alpha_c \hat{L}_s \tag{11.6}$$

where α_c is the desired reference-tracking bandwidth.[1] Assume $\hat{L}_s = L_s$ and $\hat{R}_s = R_s$. Inserting the above gains into (11.5) results in

$$G_{cl}(s) = \frac{\alpha_c}{s + \alpha_c} \qquad Y_{cl}(s) = \frac{s/L_s}{(s + \alpha_c)^2} \tag{11.7}$$

The gains k_p and k_i place the double pole at $s = -\alpha_c$. Furthermore, the gain k_t places the reference-tracking zero at $s = -\alpha_c$, which thus cancels the other pole of the reference-tracking transfer function. The closed-loop transfer functions are real, i.e., the d and q channels are decoupled.

---

[1]In practice, the effect of the resistance on current control is negligible, i.e., $\hat{R}_s = 0$ can be chosen in (11.6).
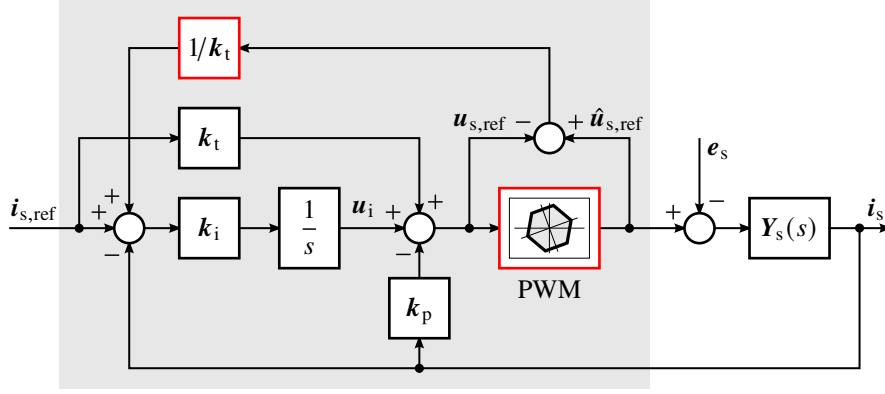
Figure 11.3: Controller equipped with a realizable-reference anti-windup method. The shaded part represents the controller, typically a piece of software. The realized voltage $\hat{u}_{s,ref}$ can be obtained as a side product of the PWM algorithm. Notice that $\hat{u}_{s,ref} = u_{s,ref}$ holds in the linear modulation region. As seen by the current controller operating in rotor coordinates, the converter voltage hexagon rotates.

Actuator Saturation and Anti-Windup

In two-level voltage-source converters, the maximum voltage is limited by the voltage hexagon, see Chapter 10. Consequently, the assumption $u_s = u_{s,ref}$ does not hold in the saturated region. The reference $|u_{s,ref}|$ may exceed the hexagon for large current steps, especially at high rotor speeds due to the large back-emf $|e_s|$. During the saturation, the integral state u_i continues accumulating unless a suitable anti-windup method is applied.

A realizable-reference anti-windup method can be easily incorporated into the 2DOF PI controller as

$$\frac{du_i}{dt} = k_i \left(i_{s,ref} - i_s + \frac{\hat{u}_{s,ref} - u_{s,ref}}{k_t} \right) \tag{11.8a}$$

$$u_{s,ref} = k_t i_{s,ref} - k_p i_s + u_i \tag{11.8b}$$

where $\hat{u}_{s,ref} = \text{sat}(u_{s,ref})$ is the realized voltage limited by the hexagon. The realized voltage is simplest to calculate as a part of the PWM algorithm. Figure 11.3 shows the corresponding block diagram of the algorithm. In the linear range, $\hat{u}_{s,ref} = u_{s,ref}$ and the anti-windup method does not affect. In the saturated region, the anti-windup method limits the integral state u_i to the value that would result in the realized voltage $\hat{u}_{s,ref}$.

11.3 Current Reference

Based on the torque equation (9.23), the current reference can be calculated as

$$i_{s,ref} = i_{d,ref} + jk_\tau \tau_{M,ref} \tag{11.9}$$

where $k_\tau = 2K^2/(3n_p\hat{\psi}_f)$ is constant and $\hat{\psi}_f$ is the estimate of the PM-flux linkage. Below the rated speed, the d-axis current reference $i_{d,ref} = 0$ is chosen, since it minimizes the current magnitude and resistive losses. This locus is also known as the maximum torque per ampere (MTPA).
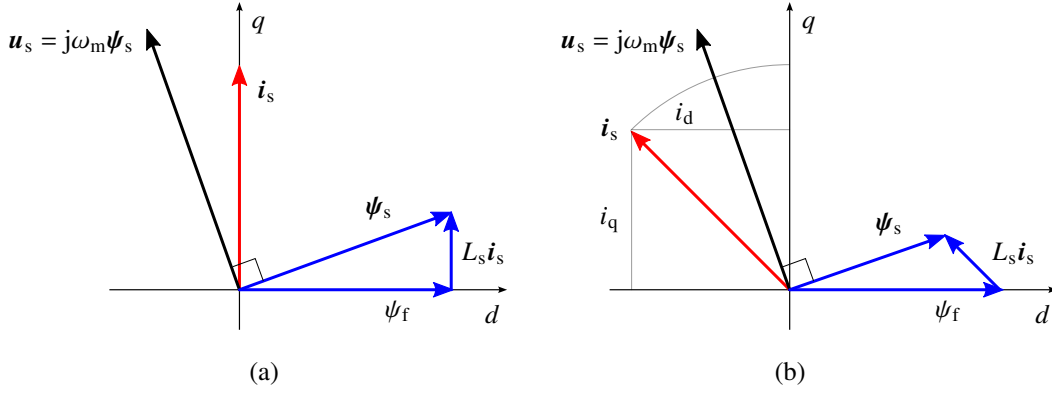
Figure 11.4: Vector diagram: (a) $i_d = 0$; (b) field-weakening region, where $i_d < 0$ to reduce $|\boldsymbol{\psi}_s|$.

The maximum available current i_{max} is limited. Hence, the condition

$$|\boldsymbol{i}_{s,ref}| = \sqrt{i_{d,ref}^2 + i_{q,ref}^2} \leq i_{max} \qquad (11.10)$$

has to be implemented in the current reference computation. Notice that the dominant thermal time constant of an electric machine is typically much longer than that of a power converter, which allows overloading of the machine for short periods. In dynamic applications, the short-term maximum current i_{max} can be significantly larger (for example 150. . . 200%) than the rated current of the machine.

The stator voltage magnitude increases with the rotor speed, as can be realized from the steady-state voltage equation

$$\boldsymbol{u}_s = j\omega_m\boldsymbol{\psi}_s = j\omega_m(L_s i_d + \psi_f + jL_s i_q) \qquad (11.11)$$

where $R_s = 0$ is assumed since higher speeds are considered. The converter sets the limit for the maximum available voltage, $|\boldsymbol{u}_s| \leq u_{max}$. In typical drive systems, the maximum available voltage u_{max} is reached around the rated speed. The operating range can be extended above the rated speed by reducing the magnitude of the stator flux linkage by means of negative d-axis current. The vector diagrams in Figure 11.4 illustrate this principle, which is known as field weakening.[2]

In practice, field weakening can be realized by controlling the unlimited voltage reference $\boldsymbol{u}_{s,ref}$ to the desired maximum value u_{max} by means of an integral controller [25,26]. Several variants of this approach exist. As an example, consider the field-weakening algorithm

$$i_{d,ref} = \int k_\psi (u_{max} - |\boldsymbol{u}_{s,ref}|)dt \qquad (-i_{max} \leq i_{d,ref} \leq 0) \qquad (11.12)$$

where k_ψ is positive gain. If the magnitude of the voltage reference exceeds the maximum value, the d-axis current reference reduces until the maximum value is reached. Furthermore, the upper limit on the integral is set to $i_{d,ref} = 0$, resulting in the MTPA operation if there is enough voltage available. The maximum voltage can be set as $u_{max} = KU_{dc}/\sqrt{3}$, which corresponds to the limit of the

---

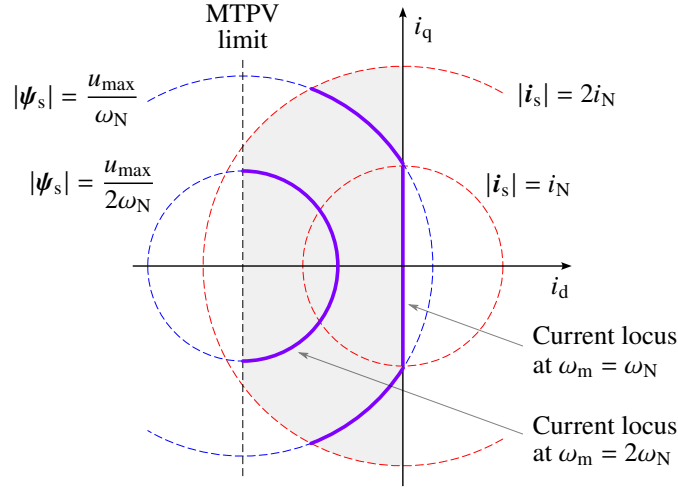[2]If a synchronous machine had a field winding instead of the PMs, ψ_f could also be varied.

Figure 11.5: Maximum current limit circles (dashed red), maximum voltage limit circles (dashed blue), and MTPV limit (dashed black). The shaded area shows the feasible operating region for $i_{max} = 2i_N$. The current loci corresponding to the rated speed and twice the rated speed are also shown. The rated angular speed is denoted by ω_N and the rated current by i_N.

linear modulation region (Figure 10.2). With this choice, the sixth harmonics of the fundamental frequency unavoidably present in the overmodulation region are avoided in the steady state. The overmodulation region can still be utilized during transients.

Figure 11.5 illustrates the above-mentioned current and voltage limits in the complex i_d–i_q plane. The current limit (11.10) corresponds to a circle, whose center is at the origin. Based on (11.11), the maximum voltage limit can be represented as a speed-dependent flux-linkage limit

$$|\boldsymbol{\psi}_s| = \sqrt{(L_s i_d + \psi_f)^2 + (L_s i_q)^2} \leq \frac{u_{max}}{|\omega_m|} \qquad (11.13)$$

which also is a circle with the center point at $\boldsymbol{i}_s = -\psi_f/L_s$. The radius of the voltage-limit circle decreases inversely proportionally to the rotor speed. From (11.13), it can be realized that $i_d = -\psi_f/L_s$ is the smallest feasible d-axis current, known as the maximum-torque-per-volt (MTPV) limit. As illustrated in Figure 11.5, the feasible operating region is the area limited by the MTPA locus (i.e. $i_d = 0$), the maximum current limit, and the MTPV limit. The figure also shows current loci at two different speeds.

It is worth pointing out that the surface-mounted PM synchronous machine considered in this chapter is not well suited for applications requiring a wide field-weakening range. One drawback is that comparatively larger $|i_d|$ is needed at high speeds to reduce the stator flux magnitude (even in the no-load condition, see Figure 11.5), which increases the resistive losses and decreases the available torque and power. Furthermore, high voltages are induced at the stator terminals, if the control system fails at high rotor speeds. The risk of demagnetizing the PMs also exists in some machines [1]. If a wide field-weakening range is needed, an interior PM synchronous machine or PM-assisted synchronous reluctance machine is a better choice in the class of synchronous machines [27].

Finally, Figure 11.6 shows a simulation example of field-oriented control. The machine drive operates below rated speed, and thus the d-axis current is
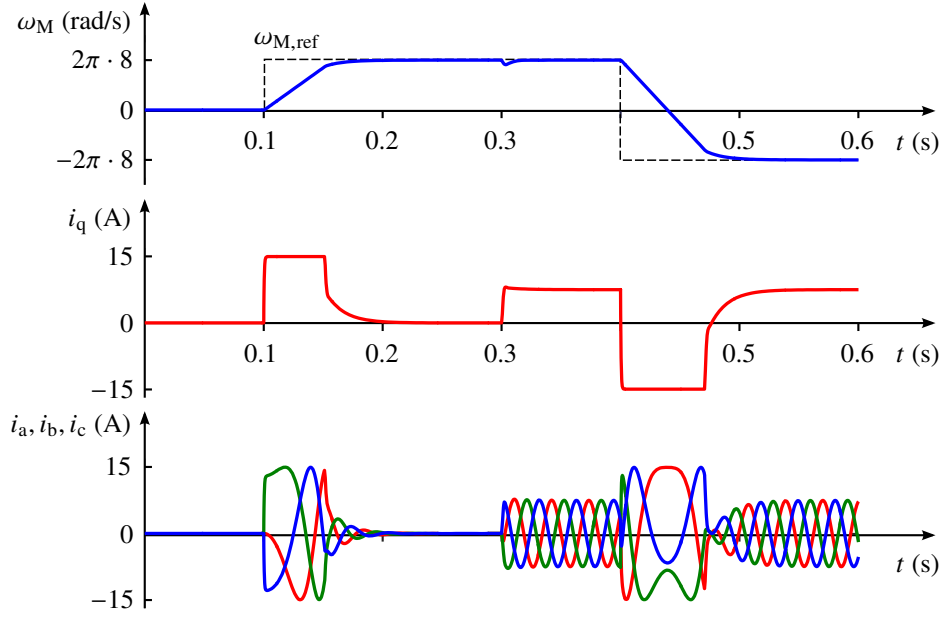
Figure 11.6: Simulation example. The speed reference $\omega_{M,ref}$ is changed stepwise from 0 to $2\pi \cdot 8$ rad/s at $t = 0.1$ s and reversed at $t = 0.4$ s. The load torque τ_L is zero until it increases stepwise at $t = 0.3$ s. Based on the waveforms, it can be reasoned the machine has eight poles, $n_p = 4$.

controlled to zero. The speed reference $\omega_{M,ref}$ is first changed stepwise and then reversed. The load torque is first zero and then increased stepwise. Notice that the machine operates as a generator after the speed reversal. Based on the phase current waveforms, it can be reasoned that the machine has eight poles. It can also be realized that controlling the machine directly based on the phase quantities would be difficult, while the presented transformations reduce the control problem to that of a DC machine. The control method presented here can be extended to other AC machines as well.

Appendix A

Dynamic Models

This appendix summarizes some basic concepts of modeling and control. For further details, the reader is referred to, e.g., [28].

A.1 First-Order Systems

Consider a first-order system

$$G(s) = \frac{y(s)}{u(s)} = \frac{K}{1 + sT} \tag{A.1}$$

where u is the input signal, y is the output signal, K is the DC steady-state gain, and T is the time constant. Substituting $s = 0$ results in the steady-state gain, $G(s) = K$.

To derive the step response, the transfer function $G(s)$ can be multiplied with the unit-step input $u(s) = 1/s$, i.e.,

$$y(s) = G(s)u(s) = \frac{K}{1 + Ts}\frac{1}{s} \tag{A.2}$$

By using the inverse Laplace transform, the unit-step response of the system in the time domain becomes

$$y(t) = K\left(1 - \mathrm{e}^{-t/T}\right) \tag{A.3}$$

Figure A.1(a) shows the step response. The time constant is the time it takes for the output to rise to 63% of the steady-state value, i.e., $y(T) = K(1 - e^{-1}) \approx 0.63K$. The rise time from 10% to 90% is $t_\mathrm{r} = T \ln 9 \approx 2.2T$.

Substituting $s = \mathrm{j}\omega$ in the transfer function (A.1) results in the frequency response

$$G(\mathrm{j}\omega) = \frac{K}{1 + \mathrm{j}\omega T} \tag{A.4}$$

whose magnitude is

$$|G(\mathrm{j}\omega)| = \frac{K}{\sqrt{1 + \omega^2 T^2}} \tag{A.5}$$

A 3-dB bandwidth α refers to the angular frequency at which the magnitude has dropped to $1/\sqrt{2} \approx 0.71$ of the steady-state gain, $|G(\mathrm{j}\alpha)| = K/\sqrt{2}$, resulting in
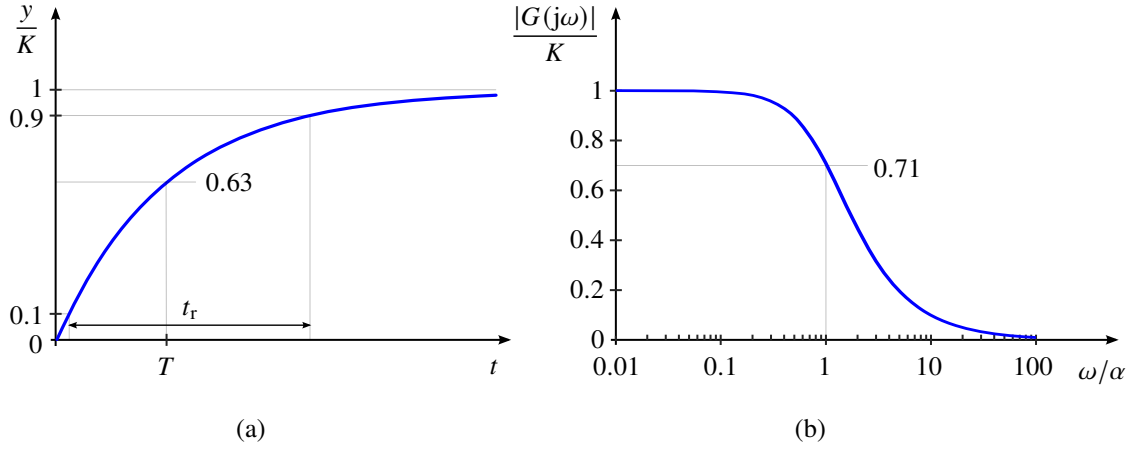
Figure A.1: First-order system: (a) step response; (b) magnitude of the frequency response.

$\alpha = 1/T$. Figure A.1(b) shows the magnitude of the frequency response. Notice that the frequency scale is logarithmic and scaled by α.

The frequency response can be used to analyze the response of the system to a sinusoidal input,

$$u(t) = U \sin(\omega t) \tag{A.6}$$

For $T \geq 0$, the output in the steady state is

$$y(t) = AU \sin(\omega t + \phi) \tag{A.7}$$

where the amplification and phase

$$A = |G(\mathrm{j}\omega)| \qquad \phi = \underline{/G(\mathrm{j}\omega)} \tag{A.8}$$

are obtained from the frequency response. If the angular frequency of signal is above the bandwidth α, the output is significantly attenuated. It is common to represent first-order systems (A.1) in an alternative form

$$G(s) = \frac{K\alpha}{s + \alpha} \tag{A.9}$$

where the bandwidth is readily visible.

A.2   Second-Order Systems

Consider a second-order low-pass filter

$$G(s) = \frac{y(s)}{u(s)} = \frac{K\omega_0^2}{s^2 + 2\zeta\omega_0 s + \omega_0^2} \tag{A.10}$$

where u is the input signal, y is the output signal, ω_0 is the undamped natural frequency, ζ is the damping ratio, and K is the DC gain. The poles of the system are located at $s = \sigma \pm \mathrm{j}\omega_\mathrm{d}$, where $\sigma = -\zeta\omega_0$ and $\omega_\mathrm{d} = \sqrt{1 - \zeta^2}\omega_0$ is the damped natural frequency. The system (A.10) is unstable if $\zeta < 0$, marginally stable if $\zeta = 0$, and stable if $\zeta > 0$. The system is critically damped if $\zeta = 1$ and overdamped if $\zeta > 1$.
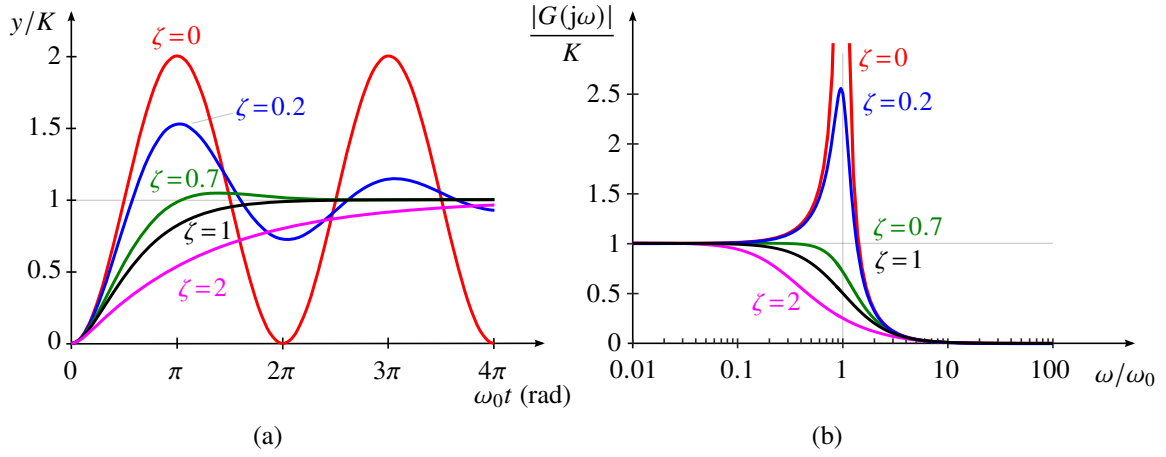
92

Figure A.2: Second-order low-pass filter: (a) step response; (b) magnitude of the frequency response. Notice that the axes are scaled.

Figure A.2(a) shows step responses of (A.10). The step responses can be easily computed using numerical simulation tools. If needed, an analytical solution could be obtained using the inverse Laplace transformation. It can be seen that there is no overshoot if $\zeta \geq 1$. Furthermore, the rise time of the response depends on the undamped natural frequency ω_0, as can be seen from the scaling of the time axis. It is also worth noticing that a second-order system may have zeros, which affect the step response. However, the stability is determined solely by the poles of the system.

Figure A.2(b) shows the magnitudes of frequency responses of (A.10). If $0 \leq \zeta < 1$, the system has a resonance peak at the damped natural frequency ω_d. If the damping ratio is low, the resonance peak is high. It can be seen that the amplification resulting from $\zeta = 0.7$ is negligible, while $\zeta = 0.2$ already results in the amplification by a factor of about 2.5 at the resonance frequency.

A.3   State-Space Representation

A state-space representation is a commonly used form to describe the dynamics of a system. The state-space model is a set of coupled first-order differential equations that describe the dynamics of the system. Vectors and matrices are marked in boldface in the following. For a linear single-input single-output system, the state-space form is

$$\frac{\mathrm{d}\boldsymbol{x}}{\mathrm{d}t} = \boldsymbol{A}\boldsymbol{x} + \boldsymbol{b}u \tag{A.11a}$$

$$y = \boldsymbol{c}^{\mathrm{T}}\boldsymbol{x} + du \tag{A.11b}$$

where $\boldsymbol{x} = [x_1, x_2, \ldots, x_n]^{\mathrm{T}}$ is the state vector, n is the order of the system, u is the input, y is the output. Furthermore, $\boldsymbol{A}$ $(n \times n)$, $\boldsymbol{b}$ $(n \times 1)$, $\boldsymbol{c}^{\mathrm{T}}$ $(1 \times n)$, and d (1×1) are the system matrices, whose dimensions are given in parentheses. It can be seen that the state derivative $\mathrm{d}\boldsymbol{x}/\mathrm{d}t$ and the output y depend only on the states $\boldsymbol{x}$ and the system input u. The states depend on the history, but not on the present values of the inputs. Typically, in physical systems, the output depends only on the states, i.e. $d = 0$, and the state variables are associated with energy storage. As examples, the state variables can be:
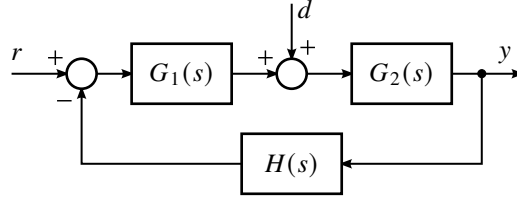
93

Figure A.3: Block diagram of a feedback system.

- current i of an inductor (or its flux linkage $\psi = Li$);
- voltage u of a capacitor (or its charge $q = Cu$);
- speed v of a mass (or its momentum $p = mv$).

The choice of state variables is not unique, as shown in the parenthesis above. For a given linear system, there are infinitely many state-space representations.

Transformation of (A.11) to the frequency domain results in the transfer-function representation

$$G(s) = \frac{y(s)}{u(s)} = \boldsymbol{c}^{\mathrm{T}}(s\boldsymbol{I} - \boldsymbol{A})^{-1}\boldsymbol{b} + d \tag{A.12}$$

where $\boldsymbol{I}$ is the $n \times n$ identity matrix. The transfer function is unique for a given system, i.e., all state variable choices result in the same transfer function. The transformation (A.12) is useful, e.g., in numeric or symbolic calculation of transfer functions of more complicated systems.

The transfer function can be expressed using its numerator polynomial $N(s)$ and denominator polynomial $D(s)$, i.e., $G(s) = N(s)/D(s)$. The denominator $D(s) = \det(s\boldsymbol{I} - \boldsymbol{A})$ is also known as the characteristic polynomial of the system. The solutions $D(s) = 0$ are the poles of the transfer function, but they also equal the eigenvalues of the matrix $\boldsymbol{A}$. The stability can be determined from these poles (eigenvalues). The system is stable if all eigenvalues have negative real parts.

For a nonlinear single-input single-output system, the state-space form is

$$\frac{\mathrm{d}\boldsymbol{x}}{\mathrm{d}t} = \boldsymbol{f}(\boldsymbol{x}, u) \tag{A.13a}$$

$$y = h(\boldsymbol{x}, u) \tag{A.13b}$$

where $\boldsymbol{f}$ and h are nonlinear functions of the states and the input, respectively. The form (A.13) is useful in numerical simulation of nonlinear systems. For analysis purposes, a nonlinear system (A.13) can be linearized around an operating point, which results in a linear state-space model (A.11).

A.4 Transfer Functions of Feedback Systems

Consider the generic block diagram in Figure A.3, which consists of two blocks $G_1(s)$ and $G_2(s)$ and a negative feedback loop with a transfer function $H(s)$. When deriving transfer functions, each input can be considered separately such that other inputs are set to zero, which follows from the linearity of the system. The transfer functions from the input $r(s)$ (which is often a reference signal) to

the output $y(s)$ can be derived based on the block diagram, giving

$$\frac{y(s)}{r(s)} = \frac{G_1(s)G_2(s)}{1 + G_1(s)G_2(s)H(s)} \tag{A.14}$$

It can be noticed that the numerator $G_1(s)G_2(s)$ is the product ot the transfer functions between the input and output. In a similar manner, the transfer function from the input $d(s)$ (which is often a disturbance signal) to the output $y(s)$ is

$$\frac{y(s)}{d(s)} = \frac{G_2(s)}{1 + G_1(s)G_2(s)H(s)} \tag{A.15}$$

In both transfer functions, the denominator is the same, containing the product of all the transfer functions of the feedback loop summed with 1.

Appendix B

AC Systems

B.1 Single-Phase Systems

B.1.1 Instantaneous Power

Consider an example system shown in Figure B.1(a), consisting of a voltage source and the inductive-resistive (LR) load. This system could represent, e.g., a single-phase generator (u corresponding to the back-emf) supplying a resistive load. In the time domain, this example system is governed by

$$u = Ri + L\frac{\mathrm{d}i}{\mathrm{d}t} \tag{B.1}$$

Assume that the source voltage varies sinusoidally (see Figure B.2),

$$u = \hat{u}\cos(\omega t + \varphi_u) \tag{B.2}$$

where $\hat{u}$ is the peak value, ω is the angular frequency, and φ_u is the phase angle of the voltage. If the system is linear, the resulting current response is also sinusoidal,

$$i = \hat{i}\cos(\omega t + \varphi_i) \tag{B.3}$$

The instantaneous power fed from the single-phase source in the steady state is

$$\begin{aligned} p = ui &= \hat{u}\cos(\omega t + \varphi_u) \cdot \hat{i}\cos(\omega t + \varphi_i) \\ &= \frac{\hat{u}\hat{i}}{2}\cos\varphi + \frac{\hat{u}\hat{i}}{2}\cos(2\omega t + \varphi_u + \varphi_i) \end{aligned} \tag{B.4}$$

where the power factor is $\cos\varphi = \cos(\varphi_u - \varphi_i)$. The first term

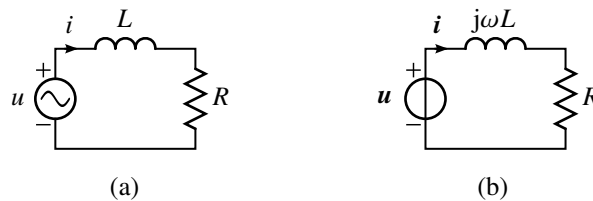$$\overline{p} = \frac{\hat{u}\hat{i}}{2}\cos\varphi \tag{B.5}$$

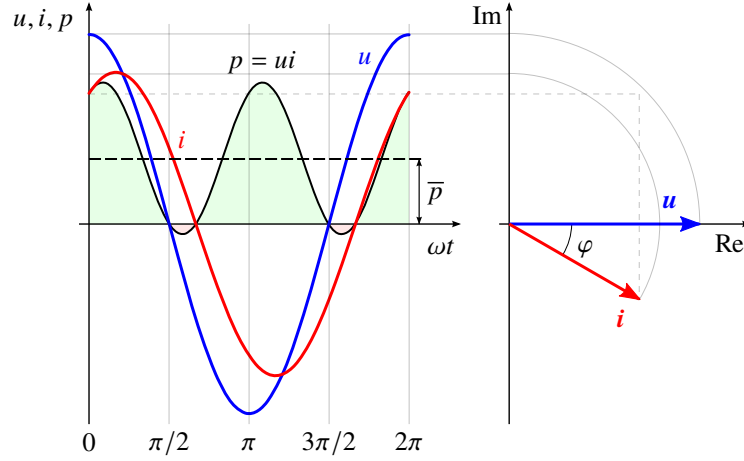Figure B.1: Equivalent circuits: (a) time domain; (b) frequency domain.

Figure B.2: Single-phase sinusoidal waveforms of the voltage u and the current i in the time domain. The instantaneous power $p = ui$ and its average $\overline{p}$ are also shown. The shaded areas are the energy. The corresponding peak-valued phasors are also shown. With no loss of generality, the voltage phase angle is set to $\varphi_u = 0$.

is the average power. The second term in (B.4) reveals that the instantaneous power of a single-phase system oscillates at twice the supply frequency. Figure B.2 shows the waveforms of the voltage, current, and the instantaneous power.

In a general case, the average power over the period T is

$$\overline{p} = \frac{1}{T} \int_0^T p(t) \mathrm{d}t \tag{B.6}$$

Typically, the period of interest is one cycle, $T = 2\pi/\omega$. Another common concept is the root mean square (rms), defined by

$$i_{\mathrm{rms}} = \sqrt{\frac{1}{T} \int_0^T [i(t)]^2 \mathrm{d}t} \tag{B.7}$$

where the current is used as an example, but the definition is valid for other quantities as well. For a sinusoidal signal, the rms value becomes $i_{\mathrm{rms}} = \hat{i}/\sqrt{2}$. Consequently, the average power (B.5) can be expressed as

$$\overline{p} = u_{\mathrm{rms}} i_{\mathrm{rms}} \cos\varphi \tag{B.8}$$

The power factor is $\varphi = 0$ for a resistive load and $\varphi = -\pi/2$ for a purely inductive load. In the latter case, the average power is zero, but the oscillating term in (B.4) still remains.

B.1.2 Complex Phasors

The current could be solved in the time domain using (B.1). However, in the steady-state analysis of AC systems, it is more convenient to apply phasors that are static complex numbers. The phasors corresponding to the example waveforms are (see Figure B.2)

$$\boldsymbol{u} = K\hat{u}\mathrm{e}^{\mathrm{j}\varphi_u} \qquad \boldsymbol{i} = K\hat{i}\mathrm{e}^{\mathrm{j}\varphi_i} \tag{B.9}$$
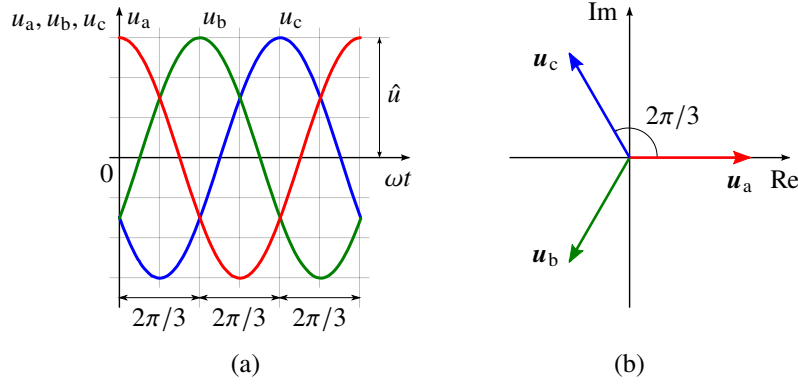
97

Figure B.3: Balanced three-phase voltages: (a) waveforms in the time domain; (b) complex peak-valued phasors. With no loss of generality, $\varphi_u = 0$ is used.

where complex quantities are written in boldface and K is a scaling constant that could be chosen arbitrarily. Feasible choices are $K = 1$, giving peak-valued phasors, and $K = 1/\sqrt{2}$, giving rms-valued phasors. Based on Euler's formula

$$e^{j\vartheta} = \cos\vartheta + j\sin\vartheta \tag{B.10}$$

the time-domain signal can be obtained from the phasor as

$$i = \frac{1}{K}\,\text{Re}\{\boldsymbol{i}e^{j\omega t}\} \tag{B.11}$$

where the current is used as an example.

In the frequency domain, the system model (B.1) becomes

$$\boldsymbol{u} = (R + j\omega L)\boldsymbol{i} = \boldsymbol{Z}(j\omega)\boldsymbol{i} \tag{B.12}$$

where $\boldsymbol{Z}(j\omega) = R + j\omega L$ is a static complex number, known as the impedance. It can be seen that the time derivative appearing in (B.1) has been replaced by multiplication by $j\omega$. Figure B.1(a) shows the corresponding equivalent circuit. The sinusoidal steady state is now relatively easy to solve in a similar manner as in the case of the DC circuits. Using the phasors, the average power is

$$\overline{p} = \frac{1}{2K^2}\,\text{Re}\{\boldsymbol{u}\boldsymbol{i}^*\} \tag{B.13}$$

If the rms-scaled phasors are used, the power expression reduces to $\overline{p} = \text{Re}\{\boldsymbol{u}_{\text{rms}}\boldsymbol{i}_{\text{rms}}^*\}$. Even if the simple RL circuit was used as an example, the above concepts are directly applicable to more complicated circuits and systems.

B.2 Three-Phase Systems

B.2.1 Instantaneous Power

Figure B.3(a) shows the balanced set of three-phase voltages, i.e.,

$$u_a = \hat{u}\cos(\omega t + \varphi_u) \tag{B.14a}$$
$$u_b = \hat{u}\cos(\omega t + \varphi_u - 2\pi/3) \tag{B.14b}$$
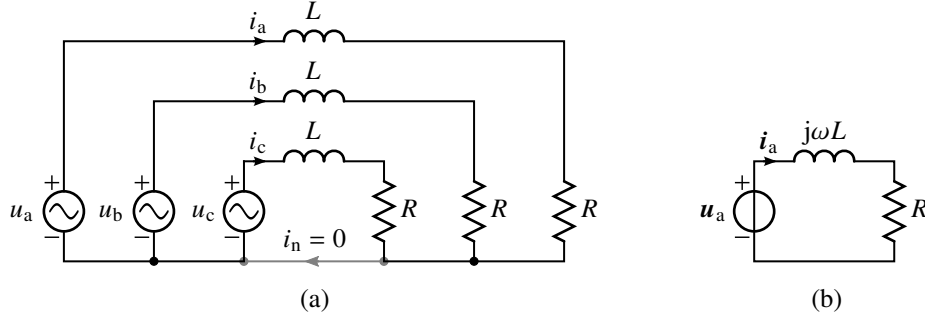$$u_c = \hat{u}\cos(\omega t + \varphi_u - 4\pi/3) \tag{B.14c}$$

Figure B.4: Balanced three-phase system: (a) three-phase circuit in the time domain; (b) per-phase equivalent circuit in the complex domain.

Consider an example system shown in Figure B.4(a). The balanced three-phase voltage source is connected to the balanced three-phase LR load. This system could represent, e.g., a three-phase generator connected to a resistive three-phase load. The system in Figure B.4(a) is equipped with a wye-connected source and a wye-connected load. Delta-connection is also commonly used. Delta-connected components can be transformed to their wye-equivalents for analysis purposes.

In balanced three-phase systems, the current in the neutral wire is zero, $i_n = i_a + i_b + i_c = 0$. Consequently, the neutral wire is unnecessary. Many three-phase systems, including electric machines, are three-wire systems with no neutral wire. In the steady state, the instantaneous power fed from the three-phase source is

$$
\begin{aligned}
p &= u_a i_a + u_b i_b + u_c i_c \\
&= \frac{3\hat{u}\hat{i}}{2}\cos\varphi + \frac{\hat{u}\hat{i}}{2}\left[\cos\phi + \cos(\phi - 2\pi/3) + \cos(\phi - 4\pi/3)\right] \\
&= \frac{3\hat{u}\hat{i}}{2}\cos\varphi
\end{aligned}
\tag{B.15}
$$

where $\phi = 2\omega t + \varphi_u + \varphi_i$. It can be seen that the oscillating components of the phase powers cancel out due to their phase shifts, and the total instantaneous power is constant. Consequently, the electromagnetic torque of three-phase machines is ideally smooth.

B.2.2 Complex Phasors

As illustrated in Figure B.3(b), the balanced three-phase voltages can be represented using complex phasors

$$
\boldsymbol{u}_a = K\hat{u}e^{j\varphi_u} \tag{B.16a}
$$

$$
\boldsymbol{u}_b = K\hat{u}e^{j(\varphi_u - 2\pi/3)} \tag{B.16b}
$$

$$
\boldsymbol{u}_c = K\hat{u}e^{j(\varphi_u - 4\pi/3)} \tag{B.16c}
$$

Balanced three-phase systems can be considered to be composed of three identical single-phase systems. It is sufficient to analyze only one phase of the system. Figure B.4(b) shows the per-phase equivalent circuit of the example three-phase system. The currents in the other two phases are obtained by phase shifting of
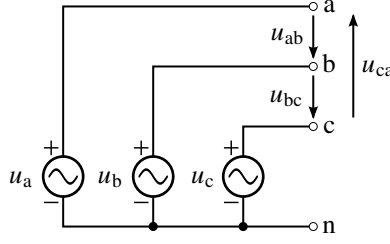
Figure B.5: Three-phase voltage source and the definitions of its line-to-line voltages.
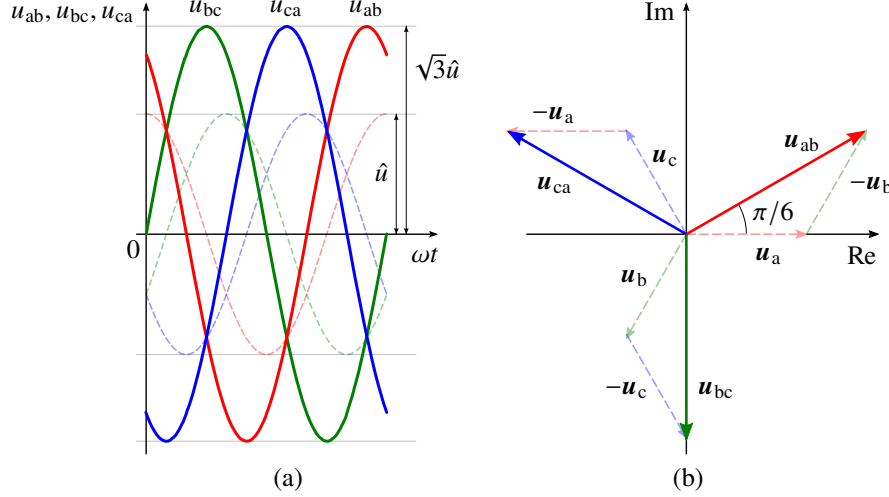

(a)

(b)

Figure B.6: Line-to-line voltages: (a) waveforms in the time domain; (b) complex peak-valued phasors. The waveforms and phasors drawn with dashed lines represent the phase voltages.

$\pm 2\pi/3$. The total power (B.15) fed from the three-phase source is

$$p = \frac{3}{2K^2} \operatorname{Re}\{\boldsymbol{u}_a \boldsymbol{i}_a^*\} \tag{B.17}$$

It is common to use rms-scaled phasors ($K = 1/\sqrt{2}$), in which case the power expression reduces to $p = 3\operatorname{Re}\{\boldsymbol{u}_{a,rms}\boldsymbol{i}_{a,rms}^*\}$.

B.2.3   Zero-Sequence Components

The sum of the balanced three-phase voltages in (B.14) is zero, $u_a + u_b + u_c = 0$. However, the three-phase voltage produced by typical power-electronic converters contains a nonzero average

$$u_0 = \frac{1}{3}\left(u_a + u_b + u_c\right) \tag{B.18}$$

which is called the zero-sequence voltage. Notice that the zero-sequence component may vary as a function of time. In three-wire systems, the zero-sequence current is $i_0 = (i_a + i_b + i_c)/3 = 0$, and the voltage u_0 cannot affect the phase currents or power. Therefore, the zero-sequence components can be omitted in the analysis of three-wire systems.

B.2.4   Line-to-Line Voltages

The term *phase voltage* typically refers to the line-to-neutral voltages u_a, u_b, and u_c, which are measured relative to the neutral, as shown in Figure B.5. Since
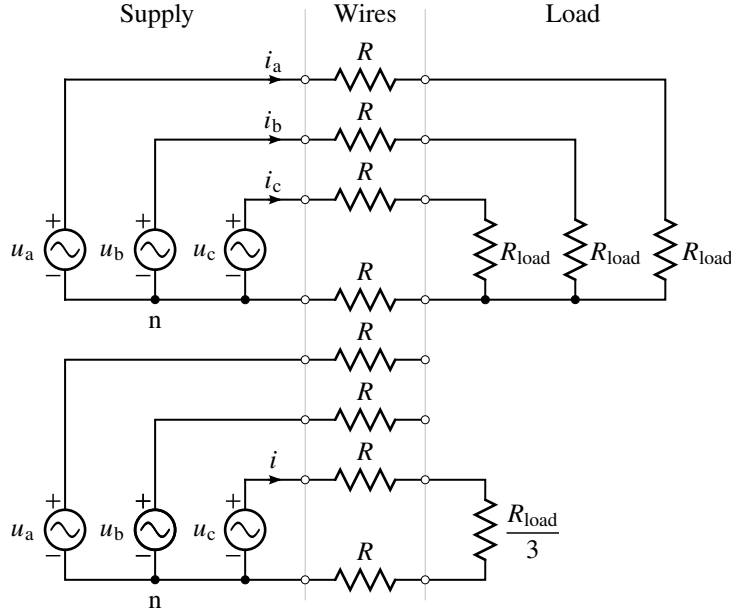
Figure B.7: Two different configurations to feed the same power to the resistive load.

the neutral potential is not often available, the three-phase voltages are typically expressed as line-to-line voltages. They are measured between the phases,

$$u_{\text{ab}} = u_{\text{a}} - u_{\text{b}} = \sqrt{3}\hat{u}\cos(\omega t + \pi/6) \tag{B.19a}$$

$$u_{\text{bc}} = u_{\text{b}} - u_{\text{c}} = \sqrt{3}\hat{u}\cos(\omega t - \pi/2) \tag{B.19b}$$

$$u_{\text{ca}} = u_{\text{c}} - u_{\text{a}} = \sqrt{3}\hat{u}\cos(\omega t + 5\pi/6) \tag{B.19c}$$

where $\varphi_u = 0$ is used for simplicity. The corresponding phasors are

$$\boldsymbol{u}_{\text{ab}} = \boldsymbol{u}_{\text{a}} - \boldsymbol{u}_{\text{b}} = \sqrt{3}K\hat{u}\mathrm{e}^{\mathrm{j}\pi/6} \tag{B.20a}$$

$$\boldsymbol{u}_{\text{bc}} = \boldsymbol{u}_{\text{b}} - \boldsymbol{u}_{\text{c}} = \sqrt{3}K\hat{u}\mathrm{e}^{-\mathrm{j}\pi/2} \tag{B.20b}$$

$$\boldsymbol{u}_{\text{ca}} = \boldsymbol{u}_{\text{c}} - \boldsymbol{u}_{\text{a}} = \sqrt{3}K\hat{u}\mathrm{e}^{\mathrm{j}5\pi/6} \tag{B.20c}$$

Figure B.6 illustrates the voltages in the time and complex domains. The magnitude of the line-to-line voltage is $\sqrt{3}$ times the magnitude of the phase voltages. The phase angles are shifted by 30°.

B.2.5 Transmission Losses

Imbalances in the source, line impedance, or load would produce nonzero current i_{n} in four-wire systems. In power systems, single-phase loads can be connected between the phase and the neutral. Figure B.7 shows two different configurations to supply the resistive load. In the case of the single-phase load, the current in the neutral wire equals the phase current.

Consider that the same power is fed to the single-phase and three-phase loads. Assume that the resistance R of the wires is much smaller than the resistance R_{load} of the load, $R \ll R_{\text{load}}$. Under this assumption, it can be shown that the transmission losses in the balanced three-phase system are only one sixth of those in the single-phase system.

Bibliography

[1] G. R. Slemon, *Electric Machines and Drives*. Addison-Wesley, 1992.

[2] A. Hughes and B. Drury, *Electric Motors and Drives: Fundamentals, Types, and Applications*, 4th ed. Elsevier, 2013.

[3] J. R. Hendershot and T. J. E. Miller, *Design of Brushless Permanent-Magnet Machines*. Motor Design Books LLC, 2010.

[4] N. Mohan, T. M. Undeland, and W. P. Robbins, *Power Electronics: Converters, Applications, and Design*, 2nd ed. John Wiley & Sons, 1995.

[5] J. Kolar, H. Ertl, and F. Zach, "Influence of the modulation method on the conduction and switching losses of a PWM converter system," *IEEE Trans. Ind. Appl.*, vol. 27, no. 6, pp. 1063–1075, Nov./Dec. 1991.

[6] F. P. Incropera, D. P. DeWitt, T. L. Bergman, and A. S. Lavine, *Fundamentals of Heat and Mass Transfer*, 6th ed. John Wiley & Sons, 2007.

[7] J. Pyrhönen, T. Jokinen, and V. Hrabovcová, *Design of Rotating Electrical Machines*. John Wiley & Sons, 2008.

[8] E. Armando, A. Boglietti, F. Mandrile, E. Carpaneto, S. Rubino, and D. G. Nair, "Definition and experimental validation of a second-order thermal model for electrical machines," *IEEE Trans. Ind. Appl.*, vol. 57, no. 6, pp. 5969–5982, Nov./Dec. 2021.

[9] P. Kokotović, H. K. Khalil, and J. O'Reilly, *Singular Perturbation Methods in Control: Analysis and Design*. Academic Press, 1986.

[10] J.-W. Choi and S.-K. Sul, "Inverter output voltage synthesis using novel dead time compensation," *IEEE Trans. Power Electron.*, vol. 11, no. 2, pp. 221–227, Mar. 1996.

[11] S. Buso and P. Mattavelli, *Digital Control in Power Electronics*, 2nd ed. Springer, 2015.

[12] S. Skogestad and I. Postlethwaite, *Multivariable Feedback Control: Analysis and Design*. John Wiley & Sons, 1996.

[13] L. Harnefors and H.-P. Nee, "Model-based current control of AC machines using the internal model control method," *IEEE Trans. Ind. Appl.*, vol. 34, no. 1, pp. 133–141, Jan./Feb. 1998.

[14] F. del Blanco, M. Degner, and R. Lorenz, "Dynamic analysis of current regulators for AC motors using complex vectors," *IEEE Trans. Ind. Appl.*, vol. 35, no. 6, pp. 1424–1432, Nov./Dec. 1999.

[15] H. A. A. Awan, S. E. Saarakkala, and M. Hinkkanen, "Flux-linkage-based current control of saturated synchronous motors," *IEEE Trans. Ind. Appl.*, vol. 55, no. 5, pp. 4762–4769, Sep./Oct. 2019.

[16] L. Harnefors, S. E. Saarakkala, and M. Hinkkanen, "Speed control of electrical drives using classical control methods," *IEEE Trans. Ind. Appl.*, vol. 49, no. 2, pp. 889–898, Mar./Apr. 2013.

[17] J. Holtz, "Pulsewidth modulation for electronic power conversion," *Proc. IEEE*, vol. 82, no. 8, pp. 1194–1214, Aug. 1994.

[18] A. Hava, R. Kerkman, and T. Lipo, "Simple analytical and graphical methods for carrier-based PWM-VSI drives," *IEEE Trans. Power Electron.*, vol. 14, no. 1, pp. 49–61, Jan. 1999.

[19] S. Bolognani and M. Zigliotto, "Novel digital continuous control of SVM inverters in the overmodulation range," *IEEE Trans. Ind. Appl.*, vol. 33, no. 2, pp. 525–530, Mar./Apr. 1997.

[20] H. van der Broeck, H.-C. Skudelny, and G. Stanke, "Analysis and realization of a pulsewidth modulator based on voltage space vectors," *IEEE Trans. Ind. Appl.*, vol. 24, no. 1, pp. 142–150, Jan./Feb. 1988.

[21] A. Hava, S.-K. Sul, R. Kerkman, and T. Lipo, "Dynamic overmodulation characteristics of triangle intersection PWM methods," *IEEE Trans. Ind. Appl.*, vol. 35, no. 4, pp. 896–907, Jul./Aug. 1999.

[22] Y.-H. Lee, D.-H. Kim, and D.-S. Hyun, "Carrier based SVPWM method for multi-level system with reduced HDF," in *Conf. Rec. IEEE-IAS Annu. Meeting*, vol. 3, Rome, Italy, Oct. 2000, pp. 1996–2003.

[23] M. Hinkkanen, S. E. Saarakkala, H. A. A. Awan, E. Mölsä, and T. Tuovinen, "Observers for sensorless synchronous motor drives: Framework for design and analysis," *IEEE Trans. Ind. Appl.*, vol. 54, no. 6, pp. 6090–6100, Nov./Dec. 2018.

[24] L. Harnefors, "Modeling of three-phase dynamic systems using complex transfer functions and transfer matrices," *IEEE Trans. Ind. Electron.*, vol. 54, no. 4, pp. 2239–2248, Aug. 2007.

[25] J.-M. Kim and S.-K. Sul, "Speed control of interior permanent magnet synchronous motor drive for the flux weakening operation," *IEEE Trans. Ind. Appl.*, vol. 33, no. 1, pp. 43–48, Jan./Feb. 1997.

[26] N. Bedetti, S. Calligaro, and R. Petrella, "Analytical design and autotuning of adaptive flux-weakening voltage regulation loop in IPMSM drives with accurate torque regulation," *IEEE Trans. Ind. Appl.*, vol. 56, no. 1, pp. 301–313, Jan./Feb. 2020.

[27] W. L. Soong and T. J. E. Miller, "Field-weakening performance of brushless synchronous AC motor drives," *IEE Proc. Electr. Power Appl.*, vol. 141, no. 6, pp. 331–340, Nov. 1994.

[28] G. F. Franklin, J. D. Powell, and A. Emami-Naeini, *Feedback Control of Dynamic Systems*, 5th ed.   Prentice-Hall, 2006.